Development of Nanofibers for Applications in the Field of Point-of-Care and Environmental Studies

Dissertation zur Erlangung des

Doktorgrades der Naturwissenschaften

(Dr. rer. nat.)

an der Fakultät Chemie und Pharmazie

der Universität Regensburg

Deutschland

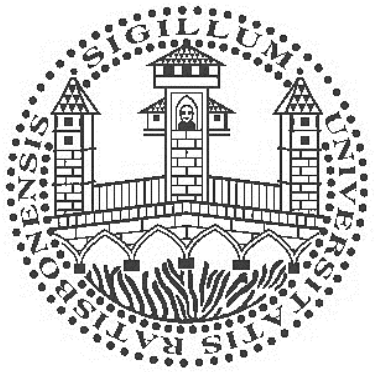

vorgelegt von

Alissa Wieberneit

Regensburg 2024

Die vorliegende Dissertation entstand in der Zeit von Januar 2021 bis Dezember 2024 am Institut für Analytische Chemie, Chemo-und Biosensorik der Universität Regensburg.

Die Arbeit wurde angeleitet von Prof. Dr. Antje J. Bäumner.

Promotionsgesuch eingereicht am: 18.12.2024
Kolloquiums Termin: 24.02.2025

Prüfungsausschuss

Vorsitzende: Prof. Dr. Miriam Breunig

Erstgutachterin: Prof. Dr. Antje J. Baeumner

Zweitgutachter: PD Dr. Axel Dürkop

Drittprüfer: Prof. Dr. Hayo Castrop

Eidesstattliche Erklärung

Hiermit erkläre Ich, dass die vorliegende Arbeit, sowie die digitale Version, identisch sind. Die Arbeit wurde von mir selbstständig verfasst und es wurden keine anderen als die angegebenen Quellen und Hilfsmittel verwendet. Die Arbeit wurde an keiner anderen Hochschule zur Erlangung eines akademischen Grades eingereicht. Von den in § 25 Abs. 5 vorgesehenen Rechtsfolgen habe ich Kenntnis genommen.

Regensburg, den 18.12.2024

_____

Alissa Wieberneit

Acknowledgement

First, I would like to thank **Prof. Antje Baeumner** for the opportunity to do my PhD on such an important and interesting project as well as the trust and freedom to start a new project just based on a PhD students' idea. Thank you for all the productive discussions and of course also for being the head of my committee.
I would also like to thank **Prof. Axel Dürkop** for being not only the second one in the committee but more over for signing all of my Werkstattaufträge and the trust you gave me as a supervisor in Demo.
I would like to thank **Prof. Dr. Hayo Castrop** for being the third in my committee and the support for our microplastic project. Without your trust we could have never started this.
Thank you to **Prof. Dr. Miriam Breunig** for being the chair of my committee.

I would like to especially thank **Dr. Nongnoot Wongkaew**. Even if you can't be part of my committee in my heart you are my "doctor-god-mother". Thanks a lot for all the guidance, extensive talks on long flights and being the leader of the NF club.

I also would like to thank my **collaborators** just to name a few:

- From the KMUTT: **Prof. Dr. Werasak Surareungchai** for letting me work and his group and **Natcha Siriyod** for working together with me in the lab.
- From the IZI-BB: **Dr. Sebastian Kersting** for teaching me how to perform the RPA, **Drik Michel** for helping me with the nano sputter and **Martina Obry** for showing me around in the lab.

A big thank you to the people in the **NF club**. Especially to my colleges:

- **Dr. Antonia Perju** for teaching me electrospinning and good discussion with good Romanian wine
- **Christoph Bruckschlegel** as my coffee mate and running constantly to the SEM
- **Florain Weinzierl** as an honorary member of the 4th floor and my Lästerschwester
- **Barbara Grotz** for being a perfect co-leader of the NF club
- **Michael Lößl** especially for the support during FameLab and the great ChemSlam
- **Michaela Ziebegk** who would have thought in the first class that we would end up together in a chemistry lab?
- **Vivien Fleischmann** as the official meme-maker of the lab and a special birthday in Potsdam
- **Katharina Weiß** for being my first Master student
- **Sarah Dietrich** for all the discussions on our way home and the work you did for the Trio-project
- And all the others that I may have forgotten.

I also want to thank our **Trio-Project**: **Hannah Triebel**, **Sophia Baumann** and **Sarah Dietrich**. It was an honor to work with you and a lot of fun! Here, I want to especially thank Hannah Triebel, what a simple coffee can change. I have learned so much working with you and enjoyed every scientific and non-scientific discussion. It was fun to learn how to translate between different scientific fields.

Thank you to all the people and friends that ever helped me during this long journey of my chemistry studies and making my PhD am memorable time.

A very special thanks goes to **Sophia Baumann**. From the literally first minute of studying chemistry, you have been always there for me and supported me through every crisis. Thanks for being a friend, a college and so much more. I don't know how I should have survived that journey without you!
I would also like to thank my parents **Regina Wieberneit** and **Peter Müllhofer** for supporting me not only financially but even more for listening to endless stories, complaining, and explaining about chemistry. Thanks a lot!
And finally, I would like to thank my fiancé **Dr. Franz Schmidt**. I am grateful of having you on my side. I am glad you have been brave enough to join me on that adventure nearly 10 years ago and came with me to Regensburg. Thank you for all the support, cheerleading and love you have given me ever since!

Declaration of Collaborations

This work was conducted in large degrees of experimental and theoretical work solely by the author. However, at some points collaborations with other researchers were conducted to generate results, which is stated in this chapter in accordance with §8 Abs. 1 Satz 2 Punkt 7 of the "Ordnung zum Erwerb des akademischen Grades eines Doktors der Naturwissenschaften (Dr. rer. nat.) an der Universität Regensburg vom 18. Juni 2009".

New Materials for Nucleic Acid Extraction for Implementation into Sample to Answer Point-of-Care Formats (Chapter 1)

Parts of this chapter is intended as a manuscript for submission as a perspective article. This work focuses material that are development for the extraction of NAs and the integration in sample-to-answer devices in the field of Point-of-Care. The author did the main part in literature search and writing, while Prof. Antje Baeumner lead the preparation of the manuscript as well as the decision of topics.

Novel Electrospun Zwitterionic Nanofibers for point-of-care Nucleic Acid Isolation Strategies under Mild Conditions (Chapter 3)

This chapter has been published. All experiments and experiment design have been conducted by the author. The project was lead by Prof. Antje Baeumner. Manuscript preparation was done by the author and Dr. Nongnoot Wongkaew under the lead of Prof. Antje Baeumner. SEM pictures were provided by Christoph Bruckschlegel.

Integration of Zwitterionic NFs in a Sample-to-Answer Paper-Based Microfluidic System (Chapter 4)

This chapter has not been published. All experiments were conducted by the author. Parts of the experiments about the initial serum studies were supported by Sarah Dietrich under the supervision of the author. Studies regarding the integration of the NFs within the µPAD were performed by in author in the lab of our collaborators at the KMUTT in Bangkok. All experiments regarding the RPA were performed by the author in a research stay at the IZI-BB in Potsdam. Primers and Materials were provided by Dr. Sebastian Kersting. The chapter was written by the author. Prof. Dr. Antje Baumner was leading the project and Dr. Nongnoot Wongkaew contributed with strategic discussions.

Simplified Production of Irregularly-Shaped True-to-Life Microplastics with Embedded Optical Labels for the Realistic Assessment of their Biotoxicity *in vivo* (Chapter 5)

Parts of this chapter are considered to be published in Journal Advanced Functional Materials. Sophia Baumann, Hannah Triebel and the author contributed equally to this work. The NFs were developed and prepared by the author, the preparation of the microplastic by ball milling was performed from Hannah Triebel and the author, while the Ultraturrax study was done by the author alone. Particles were characterized by the author. Sophia Baumann prepared and characterized the UCNPs and conducted measurements involving UCNPs. Hannah Triebel performed all studies involving tissue and made the images with the fluorescent microscope. Sarah Dietrich supported the team by performing parts of the electrospinning and milling. SEM pictures were provided by Christoph Bruckschlegel. The project was led by Prof. Antje Baeumner together with Prof. Hayo Castrop. Manuscript preparation was done by the three main authors supported by Prof. Antje Baumner and Prof. Hayo Castrop. Dr. Nongnoot Wongkaew supported the project with strategic discussions.

Table of Contents

Used Abbreviations and Symbols

In the following all used symbols and abbreviations, besides commonly used ones, are listed.

Abbreviation	Meaning
Au-NP	Gold Nanoparticle
BM	Ball milling
BSA	Bovine serum albumin
CLSM	Confocal Laser Scanning Microscope
DLS	Dynamic Light Scattering
DMF	Dimethylformamide
DNA	Deoxyribonucleic Acid
DPA	9,10-Diphenylanthracen
EDTA	Ethylenediaminetetraacetic Acid
EOF	Electroosmotic Flow
FA	Formic acid
FTA Card	Fast Technology for Analysis of nucleic acids
HPV	Human Papillomavirus
ICP-OES	Inductively Coupled Plasma Optical Emission Spectroscopy
IFAST	Immiscible Filtration Assisted by Surface Tension
IHC	Immunohistochemical
LAMP	Loop-mediated isothermal amplification
LFA	Lateral Flow Assay
IL	Ionic Liquid
LOD	Limit of Detection
MgOAc	Magensium acetate
MIPK	Mouse Isolated Perfused Kidney
MOF	Metal Organic Framework
MP	Microplastic
MTP	Microtiter Plate
MW	Molecular Weight
NA	Nucleic Acid
NaCl	Sodium Chloride
NAT	Nucleic Acid Testing
NF	Nanofibers
NIR	Near-Infrared
Nylon	Polyamide 6,6

PAA	Poly (acrylic acid)
PAH	Poly (allylamine hydrochloride)
PANI	Polyaniline
PB	Polybrene
PBS	Phosphate Buffered Saline
PCR	Polymerase Chain Reaction
PFA	Paraformaldehyde
PLA	Polylactic Acid
POC	Point-of-Care
PS	Polystyrene
PSS	Polystyrene Sulfonate
PVP	Polyvinylpyrrolidone
RE	Rare Erth
RH	Relative Humidity
RNA	Ribonucleic Acid
RPA	Recombinase polymerase amplification
RT	Room Temperature
SEM	Scanning electron microscope
SPE	Solid Phase Extraction
S2A	Sample-to-Answer
TE	Tris-EDTA
TEM	Transmission Electron Microscopy
THF	Tetrahydrofuran
UCNP	Upconversion Nanoparticle
UT	Ultraturrax
WHO	World Health Organization
µPAD	Microfluidic paper-based analytical device

Symbol	Meaning
c	Concentration ($mol \cdot l^{-1}$)
m	Mass
M	Molar ($mol \cdot l^{-1}$)
t	Time
T	Temperature (T)
Y	Yield (%)

List of Figures

List of Figures (Supporting Information)

List of Tables

List of Tables (Supporting Information)

1 New Materials for Nucleic Acid Extraction for Implementation into Sample-to-Answer Point-of-Care Formats

1.1 Abstract

Nucleic acid (NA) extraction is the critical first step in nucleic acid testing (NAT), essential for isolating NAs from interfering substances in downstream analysis. Traditional laboratory-based methods are unsuitable for point-of-care (POC) applications due to the extensive manual input and laboratory equipment required. Therefore, new materials have been developed for NA extraction in POC settings, including porous materials such as paper-based systems, silica membranes and emerging nanomaterials, or particles like magnetic particles with different surface coatings or metal-organic frameworks and ionic liquids. The integration of these materials into sample-to-answer (S2A) devices should then follow the WHO's ASSURED criteria. Various strategies, including paper-based, microfluidic, and magnetofluidic devices, have been explored for automation and reduction of user input. Future developments should focus on testing new materials in the presence of biological samples, reducing user input, and improving the integration of NA extraction into S2A devices. These advances hold promise for improving POC diagnostics, particularly in resource-limited settings and near-patient testing.

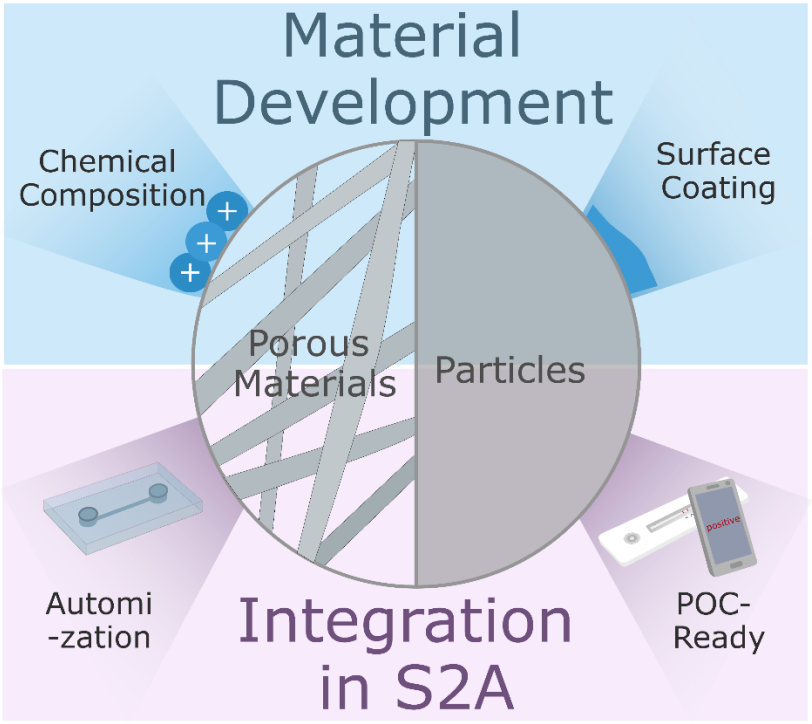

Figure 1.1: Table of contents

This chapter is considered to be published

Author contributions:
Literature review was done by Alissa Wieberneit. Manuscript preparation was done by the author with the help and under the lead of Prof. Antje Baeumner.

1.2 Introduction

Nucleic acid extraction is the first and critical step in nucleic acid testing (NAT) to isolate NA from substances interfering with downstream analysis [1]. Efficient, rapid, and reliable NA extraction methods are essential, especially in the field of point-of-care (POC), such as resource-limited settings or near-patient testing. This can increase testing capacities, leading to faster diagnosis times and more efficient disease control [2,3].

Laboratory-based isolation of NAs often relies on spin columns filled with silica particles, which require manual input and laboratory equipment, making them less suitable for POC applications [1,4]. Therefore, recent advances have focused on the development of new materials and methods to improve NA extraction efficiency particularly in POC settings. Two mechanisms are used for NA adsorption, i.e. interactions with silica-modified surfaces (Figure 1.2A) or electrostatic interactions with cationic charged groups (Figure 1.2B). As silica is negatively charged above pH 3 high salt concentrations are required during adsorption to shield electrostatic interactions and compress the electrostatic bilayer to allow for effective NA adsorption. [5,6]. Chaotropic salts used indeed enhance binding but are toxic and often inhibit amplification, requiring ethanol washing [7,8]. Cationic materials offer positively charged groups for electrostatic interactions at low salt concentrations, avoiding chaotropic salts or ethanol. Elution is often triggered by pH changes or high salt concentrations, that latter of which is again unfavorable for downstream amplification [1,9,10].

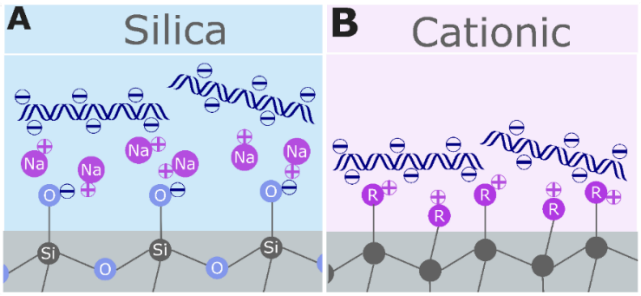

Figure 1.2: Extraction mechanisms for NAs based on silica (A) or cationic materials (B). With R being an (organic) residue having as indicated a cationic functional group.

The most prominent commercially available materials for POC NA isolations are paper-based substrates, glass fiber membranes, and magnetic particles with a silica or charge-switch coating, which is based on electrostatic interactions [1]. Additionally, a brought variety of different materials have been developed in recent years, which can be divided into two main types: porous materials and particles or particle coatings. Porous materials often extract NAs in a flow-through manner and are used in paper-based methods, while particles, often with magnetic properties, are mainly used in microfluidic setups [1,11].

To achieve a complete NAT system for the POC, tests should be designed according to the WHO definition of the ASSURED principle, being affordable, sensitive, specific, user friendly, rapid and robust, equipment free, deliverable to end users [12]. This is often realized by sample-to-answer (S2A) devices, integrating potentially all four steps of NAT within one device, i.e. sample lysis, NA isolation, NA amplification and detection (Figure 1.3) [13].

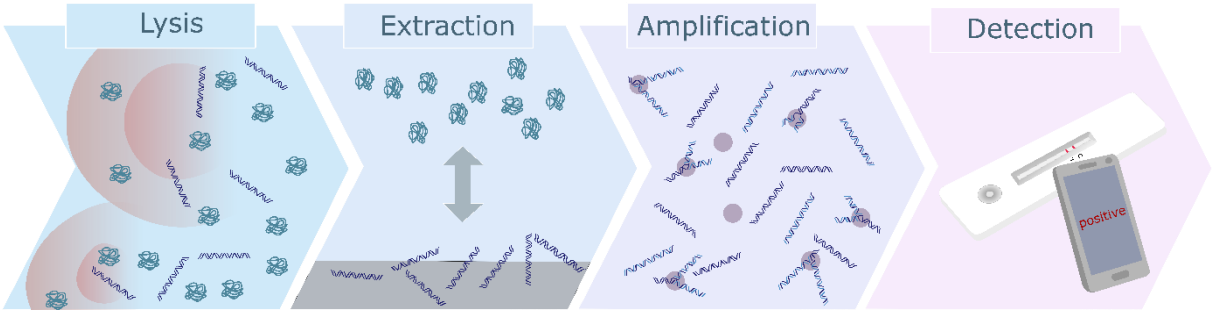

Figure 1.3: Schematic Scheme of a S2A process, including Sample lysis, NA extraction, amplification and in the end detection.

Strategies to integrate sample preparation into S2A devices obviously differ depending on the application, such as resource-limited settings or near-patient testing, and include paper-based assays, microfluidic or magnetofluidic devices [14–16]. Advances made during the COVID-19 pandemic led to the commercialization of near-patient testing systems, but none of those are truly applicable to the POC due to high costs per test, long S2A times, and limited sample types [17,18].

In the following, the most relevant types of materials for NA isolation in the field of POC are compared, and opportunities for future optimizations are addressed. Furthermore, integration strategies in different types of S2A devices are presented and their applicability for resource-limited or near patient testing is discussed.

1.3 Development of Novel Porous Materials for the Extraction of Nucleic Acids

Porous materials, typically used in the form of membranes, can be made from a variety of materials such as paper, silica, or polymers (Figure 1.4). With the right chemical modification, they can be used for NA extraction, where the solution flows through the membrane, ideal for integration in paper-based devices. When applied as a lysed sample, NA will adsorb and remain on the membrane during washing steps. Subsequently, NAs either must be released or amplified directly within the membrane's pores. Since all steps can be done without pumps, and simply executed by the addition of solutions, such process lends itself very well to the POC. While originally nitrocellulose membranes dominated lateral-flow assays, the onset of broader paper-based systems sparked studies of a larger range of materials, including other traditional papers, silica membranes and nanomaterials. Associated chemical and physical material properties have a major influence on their performance in POCTs and on NA extraction. [19].

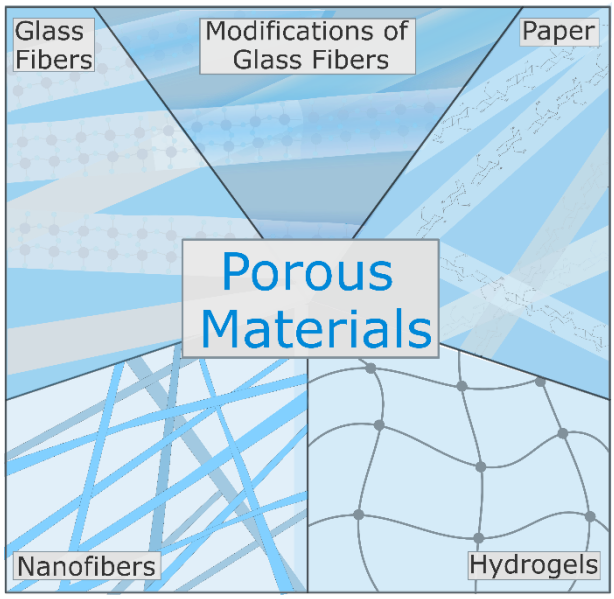

Figure 1.4: Schematic Scheme of types of porous materials developed for POC NA extraction

1.3.1 Paper-Based

Paper-based NA extraction takes advantage of high and irregular porosity, easy, high water adsorption, adjustable paper thickness and variable chemical moieties for chemical interactions. Also, paper allows for simple sample storage and transport. Cellulose materials have dominated early studies and provide very good performance due to the easy electrostatic interactions between the hydroxyl groups of cellulose fibers and phosphate backbone of the NAs [19]. In fact, fast technology for analysis of nucleic acids (FTA) cards are the gold standard as they outperform other membranes in terms of extraction efficiency and purity of the NAs [19]. Interesting developments in recent years focus on a reduction of required washing steps, reduction of costs and overall streamlining of the extraction process. For example, Malpartida et al. tested the use of simple filter paper treated only with the surfactant Ipegal to extract NAs from whole blood [20]. They were able to achieve a comparable extraction efficiency, while reducing the time effort and price drastically. Sullivan et al. and Chen et al. integrated isotachoporesis for separation by applying a direct current between two buffer reservoirs [21,22]. Through different ion mobilities NAs are concentrated along the membrane and simultaneously separated from interfering substances. The studies focused on whole blood and serum using either Fusion 5 membranes or nylon threads as a substrate, where the nylon thread could reduce the extraction time from 30 to 20 min [21–23]. The practicality of the approach still needs to be demonstrated since both upstream lysis and downstream amplification were done off-paper.

1.3.2 Silica Membranes

Silica in the form of membranes or glass fibers is commonly used, due to its high binding affinity to NAs under high salt conditions, which matches the conditions found in many cell lysis protocols. In most cases, just as with the paper-based approaches, already lysed samples are added to the silica materials. Washing uses ethanol-based solutions followed by elution with low ionic strength buffers which may be used in the subsequent amplification reaction directly [8]. The same principle can also be found in ubiquitously used silica spin columns [24]. To avoid an ethanol-based wash step, silica membranes have been functionalized with amino-groups, poly(β-amino ester) or chito oligosaccharides [25–27]. As the adsorption is based on electrostatic interaction, ethanol was not required for washing. These groups demonstrated the purity of their NA extraction by also performing off-membrane amplification reactions. Duan et al suggested a practical pipetting approach rather than a lateral-flow strategy by placing the silica fibers between two pipette tips, realizing a convenient extraction through simple up-and-down pipetting [25]. Afterwards, NA were released in a LAMP mixture and readout by a color change. Wang et al. proposed an almost sample-to-answer device by adding the amplification cocktail to the sample port of their device subsequent to the NA extraction. [27].

1.3.3 Emerging Porous Nanomaterials

Due to their high surface-to-volume ratio and tunable functionality nanomaterials hold great promise for the extraction of NAs for POC application. Nanofibers and hydrogels stand out because they offer a high surface-to-volume ratio especially when compared to. paper-based materials or glass fibers, are lightweight, and often cheap materials. In addition, they can be easily tailored to the desired applications by chemical modification of the surface functionalities. Nanofibers, typically made from polymers, are fibers in the nanometer range. They can be produced for example by electrospinning, often in the form of non-woven fiber mats composed from randomly orientated fibers. Such mats offer high porosity with typically small pore sizes in the micro- to nanometer range, while the surface chemistry is dominated by the chosen polymer(s) and can be modified prior or post synthesis [28]. This versatility of surface moieties has not been fully explored in literature, but NA extraction via electrostatic interactions and modulation with varying pH values has been demonstrated already [29–31]. For instance, zwitterionic NFs were recently developed by our group in which the nanofibers' surface exhibits a positive net charge at low pH and negative one at high pH, allowing for a pH dependent extraction process [30]. Xu et al. used nanofibers with cationic amino groups as a precursor for aerogels [31]. The researchers have demonstrated adsorption, elution and avoidance of interfering substances, but have not applied it to real biological matrices yet.

Hydrogels, which are porous and possess three-dimensional networks of hydrophilic polymers, can store significant amounts of water or buffers. In their swollen state, they offer a nano-porous structure, capable of interacting with various molecules and making them suitable for the extraction of NAs [32]. Tang et al. take advantage of this and developed a pH dependent swelling hydrogel through a functionalization with carboxyl groups [33]. Therefore, the basic lysis buffer

could be stored within the gel. When in contact with neutral samples, such as saliva, the gel is swelling. By compressing the gel in a syringe, the NAs are extracted and released to a filter paper to be added directly to an amplification mixture. This method prevents an off-chip sample lysis and is inexpensive, but further optimization is necessary based on the poor extraction efficiency of about 20 %. Salazar et al. aimed for an elution-free extraction [34]. Their soluble central membrane can adsorb NAs from samples. Afterwards the membrane is dissolved in the RPA amplification mixture, eliminating the need for an elution step. They showed acceptable extraction efficiency from blood samples (60 - 70 %). The integration into a sample-to-answer solution is still missing, as the hydrogel must be manually transferred to the RPA mixture, a direct readout option is also not available.

A porous nanofilter based on silicon nitride was fabricated through photolithography and nanoimprinting [35]. With a pore size of approximately 220 nm, the membrane can be used to filter NA from samples by electrokinetic extraction. In principle, when a direct current is applied, only NA are transported through the nanopores, due to their ion mobility and size exclusion properties. While this method does not require any washing and elution step, unfortunately lysis and amplification are performed off-chip, limiting the applicability for POC applications.

Emerging porous nanomaterials, including nanofibers and hydrogels, present significant potential for nucleic acid (NA) extraction in point-of-care (POC) applications due to their high surface-to-volume ratio and tunable functionalities. Nanofibers, with their customizable surface chemistries and high porosity, have demonstrated effective NA extraction through electrostatic interactions and pH modulation. However, their application in real biological matrices remains limited, necessitating further research to validate their performance in practical settings. Similarly, hydrogels offer unique advantages such as significant water or buffer storage and pH-dependent swelling, which can facilitate NA extraction. Yet, their current extraction efficiencies are suboptimal.

1.4 Development of New Particles and Coatings for the Extraction of Nucleic Acids

Particles offer a high surface-to-volume ratio and, with the right surface chemistry, can effectively adsorb NAs from various biological matrices. However, control of the particles can be difficult as classical applications require a centrifugation step, either by sedimentation of the particles directly or integration into spin-columns [36]. Magnetic particles circumvent such mechanical steps as they can be easily controlled in magnetic fields and have been employed for sample preparation since the 1990s [37]. Such magnetic or other particles can be coated with materials relevant for NA extraction. Alternatively, entirely new particles are designed such as those based on metal-organic-frameworks (Figure 1.5).

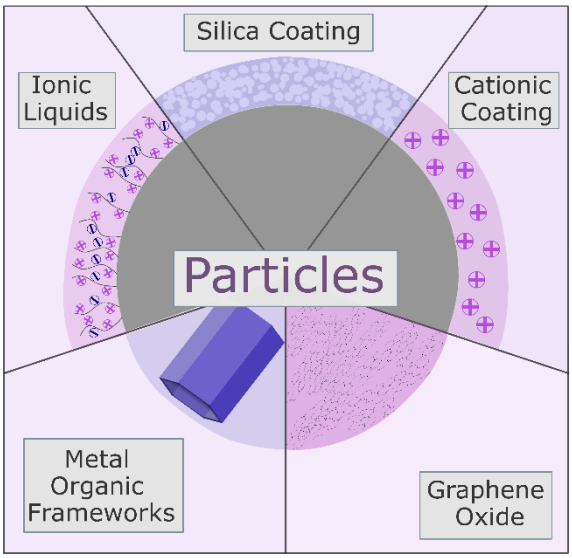

Figure 1.5: Schematic of particle types and coatings developed for POC NA extraction.

1.4.1 Development of Magnetic Particles and Emerging Surface Coatings

Based on the magnetic properties, much research has been done towards the optimization of magnetic particles. Therefore, a lot of options are commercially available both with silica or charge-switch surface coatings. However, there is still a lot of interest in the optimization of synthesis protocols to fine-tune particle properties or developing new of surface coatings as alternative for silica or to enhance the extraction efficiency for fragile RNA samples. Typically, the price can be reduced compared to commercial options material test [38,39].

Optimized synthesis routes for silica-coated magnetic particles can lead to fine-tuned and optimized properties of the particles, such as faster response times to magnetic fields by an optimized magnetization [40] or enhanced adsorption efficiency by adjustments in ζ-potential [39]. As RNA is prone to rapid degradation, custom synthesized particles have shown enhanced RNA extraction efficiency with higher purities compared to commercial particles [38,41,42]. Further research needs to investigate reproducibility and address possibilities for up-scaling of in-house synthesis routes.

Cationic coatings offer an alternative binding mechanism based on electrostatic interactions. Commercially available are the charge-switch particles, where adsorption and elution is triggered by the change in pH, avoiding the use of chaotropic salts for adsorption or ethanol for

washing. Despite their high efficiency, these kits are usually more expensive, do not include or offer sample lysis solutions, and tend to result in lower purities because inhibitors are less efficiently removed [43]. Also, many cationic coatings, e.g. silica-particles functionalized with triethylene glycol spaced glycosyl imidazole or a polyethyleneimine coating, show very good adsorption yields, but then suffer from low elution efficiencies and require harsh conditions like high salt concentrations, elevated temperatures or long incubation times [39,44]. This does not only reduce POC suitability, but can potentially inhibit downstream amplification. Here, Chitosan has been explored as an alternative surface coating, combining heat lysis with an pH dependent extraction mechanism [45]. Purity of the extracted NAs from cell-lysates or serum was proven by off-chip amplification with LAMP or rt-PCR.

1.4.2 Metal Organic Frameworks, Graphene Oxide and Ionic Liquids

Beside the use and development of magnetic particles, also other materials have been evaluated for NA extraction to overcome current challenges of magnetic particles and their surface coating as discussed before. With their unique features such as tunable porosity and versatile surface chemistry metal organic frameworks (MOFs), ionic liquids (IL), and graphene oxide are great candidates to improve extraction efficiency or purity of the NAs.

MOFs consist of metal ions coordinated to an organic ligand. They are interesting for NA isolation as they offer an adjustable surface chemistry and large surface areas, with often tunable porosity. MOFs are suitable for binding NAs because metal ions can interact with the phosphate backbone, similar to silica surfaces, and additionally the organic ligands and the bases can form hydrophobic interactions [46]. Sun et al. took advantage of the high porosity of the MOF Co-IRMOF-74-IV MOFs to specifically extract RNA from blood samples as protection of nucleases could be enhanced because the RNA can be hidden within the pores [47]. However, their method relied on centrifugation, which is less suitable for POC. Therefore, Pan et al. coupled Zr-based MOFs to the surface of magnetic particles by EDC-NHS [48]. As a result, they were able to extract HPV viral DNA from cervical samples or cell-free DNA from human plasma samples using a POC-friendly IFAST-LAMP setup. The extraction efficiency was comparable to classical methods with 57.6% from human serum and as high as 86.5% from swab preservative.

ILs are defined as organic salts in the liquid state, which are generally non-volatile and inflammable. They are typically based on an organic cation and an inorganic anion, and are therefore capable of adsorbing NAs through electrostatic interactions [49]. With their tunable charges and denaturing function, IL can be modified to lyse biological samples and isolate NAs[50]. Based on the water immiscibility of the cationic IL 1-butyl-3-methylimidazolium hexafluorophosphate DNA extraction by a phase transfer was demonstrated [51]. However, only BSA was tested as an interfering agent, and no amplification or detection method was coupled. Therefore, other researchers focused on coupling their cationic IL to silica supports [52,53]. Both tested their IL with bacterial lysate and showed an efficient extraction of DNA. However, NA could only be eluted under high salt conditions (1.5 - 2 M NaCl), which did not allow direct coupling to any amplification method. Although IL

have interesting adsorption functionalities, mild elution conditions still need to be developed to compete with other materials for NA isolation.

Graphene oxide is known to adsorb NA under high salt conditions. Here, ssDNA or RNA is due to the stronger hydrogen bonding instead of van der Waals interactions with dsDNA. Furthermore, it was shown that the access of nucleases on adsorbed NAs is limited, providing a favorable protective function [54,55]. Recently, Cui et al. used graphene oxide to decorate glass microbeads, resulting in a nanostructured surface that provides carboxyl and hydroxyl groups for RNA extraction [56]. With the combination of glass beads, suitable for sample lysis by bead beating, and the strong interaction with ssNAs as well as the protective properties of graphene oxide, these beads were tested to concentrate viral RNA from the stool samples. The RNA is then detected by a hybridization assay. However, these particles may also be of interest for sample lysis in NAT applications based on amplification.

Since metal oxides in general have similar adsorption functionalities to silica due to the high metal oxide content, fly ash has been shown to have a high potential for NA extraction [57]. They were able to demonstrate a reduced extraction time compared to pure SiO2 while also using milder conditions. However, this material has not yet been tested with real samples and still relies on centrifugation, which is less applicable for POC applications.

1.5 Integration Strategies of NA Extraction in S2A formats

The final aim for NA extraction is their subsequent amplification and sensitive detection. The translation of lab-based technology to the POC, can take the ASSURED criteria as a guidance. Therefore, it is advantageous to integrate the entire process from sample lysis to detection in an S2A format, thereby drastically reducing user input. In addition, the use of external equipment should be avoided wherever possible, while maintaining high sensitivity and reliability of the systems. These challenges can be addressed by many different strategies, ranging from paper-based to microfluidic or magnetofluidic systems, and using different materials for NA extraction. While significant progress has been made with the materials and emerging materials developed to-date, they still remain at the proof-of-concept level and none has been integrated into a full S2A design as of yet. Therefore, the following discussion is focused on such possible implementation strategies and demonstrated partial solutions.

1.5.1 Porous Materials and their Integration into S2A Formats

Significant progress has been made in recent years in integrating porous membranes into sample-to-answer formats (Table 1.1). In the field of often paper-based devices, the main challenges, apart from sensitivity and specificity in general, are the reduction of user input, e.g. the realization of automation by simultaneously being device-free.

One of the biggest unresolved challenges is the direct integration of sample lysis with NA extraction, which is currently typically performed off-chip. To address this, Le Thang et al. developed a pressure-driven automated NA extraction cartridge [58]. The 3D-printed device contains pre-stored reagents and a microfluidic chip for NA extraction. While the sample can be added directly, the direct connection to an on-chip amplification and detection is still missing and needs to be addressed in future work. Further strategies for automated fluid flow in S2A devices include capillary forces of paper-based devices [59–61], centrifugal forces [62], microfluidic chips with integrated glass fibers [63], and electrokinetic concentration of NAs using a Nafion-ion-selective membrane [64]. However, all these methods require external laboratory equipment such as centrifuges and pumps, making them unsuitable with respect to the ASSURED concept and only amenable for a small equipment-dependent application in the POC.

In terms of amplification reactions, the development of isothermal amplification methods replacing PCR has dramatically decreased the sophistication needed for heat control in NA amplification. Typically, lyophilized reagents and primers can be stored on chip[59,63] and amplification at a constant temperature can be achieved using a simple heaters [59,60]. Although PCR-based methods are often stated as more sensitive, when comparing the LODs of the S2A device, no difference was found compared to isothermal amplification methods in many cases, such as the low LOD of 1 copy / μL^{-1} was obtained with LAMP [59] and 10 copies / μL^{-1} with RPA [61], comparable to the 5 copies / μL^{-1} by PCR [64] (Table 1.1). Taking this into account, based on a capillary driven LFA combined with RPA, the only external device needed was a battery powered heater with integrated fluorescence readout [60]. Similarly, only a heater is required for the isothermal amplification by LAMP within the COVDIC device, which can be used to detect Covid infections from nasopharyngeal swabs (Figure 1.6) [59]. The only completely device-free system was reported by Sun et al. based on alkaline sample lysis and amplification, both performed at room temperature. However, the need for multiple pipetting steps required in all systems, and off-chip lysis of samples are unresolved issues that need to be addressed in future research.

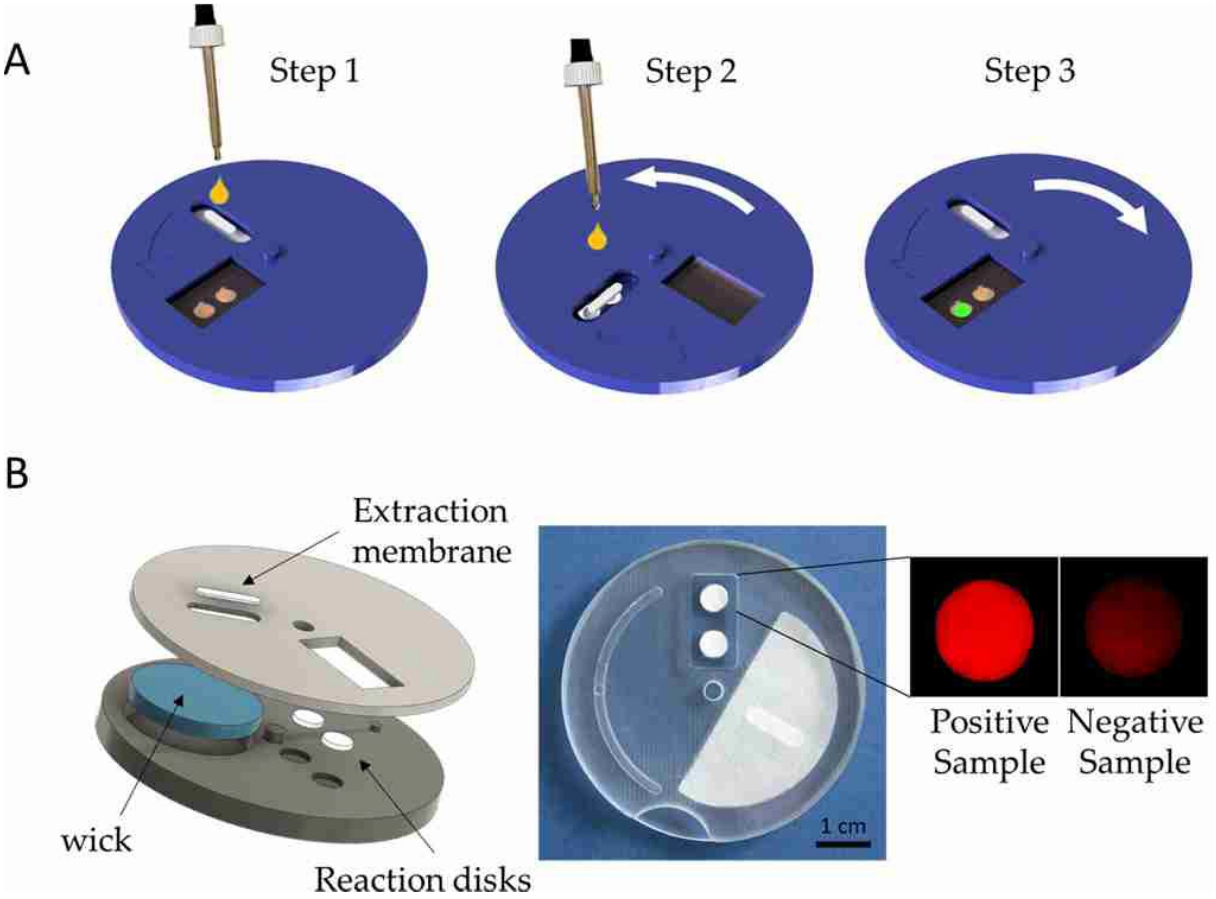

Figure 1.6: From Garneret et al: Description of the COVIDISC. A‑COVIDISC workflow decomposed in three steps (the three steps include the six steps of Fig 1, in the same the workflow): 1 ‑injection, washing (fluids flow through the capture membrane and get absorbed by capillarity in the absorbent wick (in blue)), drying. 2−Disk rotation and elution; 3 ‑Disk counter-rotation, coverage of the reaction zone by a PCR sealing film, heating, amplification and readout. B‑Left: Exploded structure of the device. Center: Picture of a prototype. Right: QUASR readout photograph of a test on RNA extracts of SARS-CoV-2, processed as in Fig 3A; (left) Positive sample; (right) negative sample [59].

Table 1.1: Comparison of sample-to-answer devices based on porous extraction materials

Extraction Material	**Amplification Method**	**Detection Method**	**LOD**	**S2A / min**	**Sample type**	**analyte**	**Ref.**
Glass Fiber	RT-LAMP	fluorescent /visual	1 copy / µL	20 - 60	Nasopharyngeal swabs	SARS-CoV-2	[59]
FTA card	RPA	fluorescent	4×10^2 copies · mL^{-1}	30	Saliva or nasopharyngeal swabs	**SARS-CoV-2 or** Helicobacter pylori	[60]
FTA card	Connective PCR	real-time fluorescent	1.0 TCID50 · mL^{-1}	45	Throat Swabs	Influenza A	[62]
Nafion	PCR	fluorescent	5 copies	Not given	urine, serum	Mycobacterium tuberculosis	[64]
Glass Fibers	RPA	fluorescent	Not given	60	Food samples	bacteria	[63]
Fusion 5	RPA	visual	10 copies · mL^{-1}	23 - 35	Nasopharyngeal swabs	Adenovirus	[61]

1.5.2 Advancements in Magnetic Particle Integration for Automated S2A Systems

S2A systems that seek to integrate sophisticated strategies such as NA extraction, amplification and detection require the development of new supporting technologies not only including new materials to enhance purity of the NAs but also manage precise fluid control, power use minimization, automate manual steps, and the integration of lysis steps and reagents. Without advancements in these areas, user input, costs and portability will never reach the simplicity level required for the POC. Commercially available near-patient devices demonstrate already to-date that reproducible, sensitive and reliable S2A is feasible, , but have long S2A times, high cost per test and are only suitable for a limited variety of sample types [17,18,65,66].

The currently simplest NA extraction protocols are those based on magnetic beads in plastic vessels. Advanced automated, simple solutions for S2A and POC must ensure the same degree of purity of the isolated NAs for downstream amplification reactions [67] and several solutions are described to keep the magnetic separation advantages while translating it into a POC format. For example, to reduce the content of PCR inhibitor in the eluate, Dearaney et al. developed a microfluidic chip, where an EOF was applied while moving the magnetic beads in the opposite direction by a magnet [68]. Kim et al. have focused on the avoidance of power-supplied devices and developed a button-powered microfluidic chip, suitable to directly extract DNA from either blood or bacteria samples within 30 min [69]. Currently, a number of manual off-chip steps are still required in both cases, but such new ideas will continue to move the field forward.

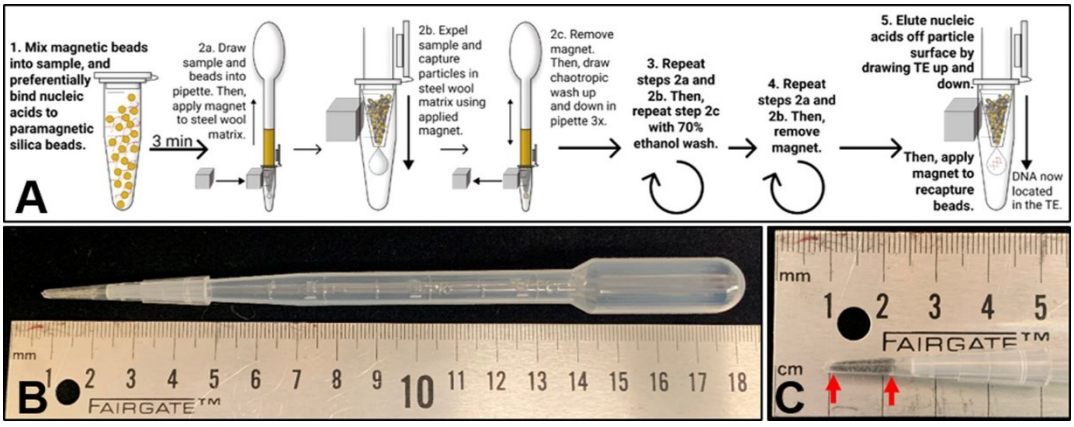

Figure 1.7: Design and detailed workflow of the HGMS-enabled steel wool extraction device. (A) Five processing steps of HGMS-enabled nucleic acid extraction. DNA is adsorbed to silica-coated paramagnetic beads using guanidine-based chemistry. Once bound, the solution is drawn into the transfer pipette, and an external magnet is applied to capture the magnetic beads in the steel wool matrix tip as the fluid flows through. The magnet is then removed to allow for release of the beads, which washes the bead surface and the bound DNA. The magnet is then reapplied to recapture magnetic beads after each wash step. In the final step, the nucleic acids are eluted off the beads while the magnetic beads are retained in the steel wool. (B) HGMS-enabled steel wool separator. (C) Steel wool capture matrix. The matrix is placed between the two graduations on the pipette tip (indicated by red arrows), and the excess is removed from the bottom. From Pearlman et. al [70]

An almost device- and energy-free solution was reported by Pearlman et al., who used a pipette with integrated steel wool to increase the separation efficiency (Figure 1.7) [70]. The extraction process is realized by simply pipetting up and down in the respective buffer reservoir, while particles can be held inside the steel wool by an external magnet, making it a promising solution for POC applications.

Many other researchers focus on achieving precise flow control also in systems with the desire to maintain high reproducibility of the S2A systems (Table 1.2). To avoid the need for pumps the highly controlled, classical microfluidics is achieved through other means including centrifugal forces [71], automated moving stages [72], or fluid release by piercing of sealed vessels [73,74]. Typically, reagents are stored on-chip and still combined with PCR for NA amplification [72–74]. Such solutions are useful already for near-patient testing and compared to commercially available laboratory solutions at least Zhang et al. could show a significant reduction of S2A times with only 30 min [73].

In an alternative microfluidic field, digitization offers the potential to control both fluid and particle movement while avoiding the need for pumps [75]. In particular, samples can be added directly to the chip, reducing user input to a minimum [75,76], magnet movement can be automated [75,77], and potentially they also offer solutions for multiplexing [76]. Although some e.g. Huang et al. are already in clinical evaluation[77], compared to the sample-to-answer times of 45 - 90 min, they could not accelerate this compared to commercial options.

The combination of microfluidics and magnetic particles may hold the most promises for S2A in the POC. In magnetofluidic systems the movement of magnetic particles is controlled precisely through magnetic fields with manually or through external devices. Systems for near-patient testing use automated magnet movements to minimize user input [78–80]. For example, particle motion can be controlled by permanent magnets and servomotors [79,80], or by a combination of a magnetic rod and a magnetic rod sleeve that allow advanced mixing with oscillation[78]. Currently, a direct power connection makes them less portable, but this should be a hurdle that can be overcome easily [78–80].

Manual magnet movement [81–86] provides such portability already such as through immiscible filtration assisted by surface tension (IFAST), a well-established laboratory S2A design based on phase separation of typically water and oil phases (Figure 1.8). Particles are transported through the chambers by precise manual movement of the magnet, multiple solutions are added manually, [84–86], but simplifications are offered through the integration of the magnet into a lid, allowing for an easy transfer of the magnetic beads in the lid [82], and with the LIAMT platform the tube only needs to be lifted and rotated for particle movement (Figure 1.9) [81]. Both platforms offer optical detection, are portable, and work with battery-powered external heaters, making them suitable for POC applications. In a similar device, Trick et al. integrated a servo motor to achieve full automation of particle movement [87]. Only minimal user input is still required for the initial mixing of swab eluates with the particles prior to sample loading into the cartridge, and they demonstrated an outstanding S2A time of only 15 min, which is very promising in the field of POC.

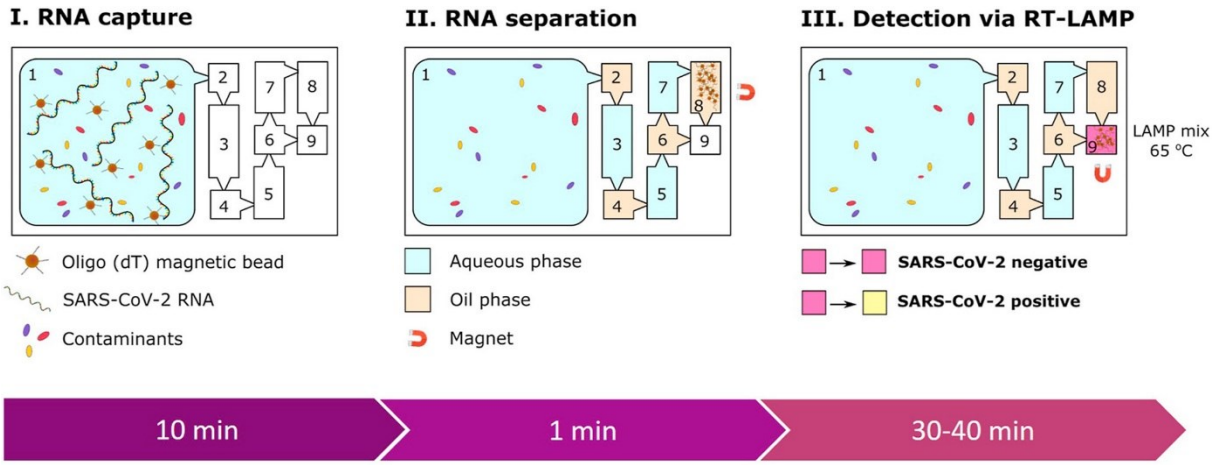

Figure 1.8: Conceptual scheme for the microfluidic IFAST RT-LAMP device for SARS-CoV-2 RNA detection comprising three consecutive steps: (I) RNA extraction via oligo (dT)-functionalized magnetic beads; (II) separation and purification of magnetic bead-captured RNA through a series of immiscible liquids; and (III) colorimetric RT-LAMP for detection of extracted RNA. Visible change of color from pink to yellow indicates SARS-CoV-2 positive. From Rodriguez-Mateos et al. [85].

An important strategy to reduce user input is to store reagents on-chip, including lysis agents, to allow the addition of raw sample to the device, which was demonstrated for devices suitable fonear-patient testing [78–80,83] and also for many POC suitable systems [81,82,87]. As most above described IFAST systems required refilling of the reservoirs prior to use [84,85]. Zhang et al. loaded buffers and lysis reagents into their design [86]. In general, for simple matrices such as swab samples or artificial sputum [81,82,85,86] the raw sample can be added directly to the lysis buffer on the chip. Whole blood, on the other hand, is more challenging, although some groups have used serum or plasma directly [78,81,83]. This issue was addressed by Trick et al. by adding a filtration step of whole blood through a vivid-membrane prior to sample loading on the chip [80]. Similar pre-treatment steps were also required for soil samples, where particles were sedimented after mixing to prevent transfer of particles to the test system [84].

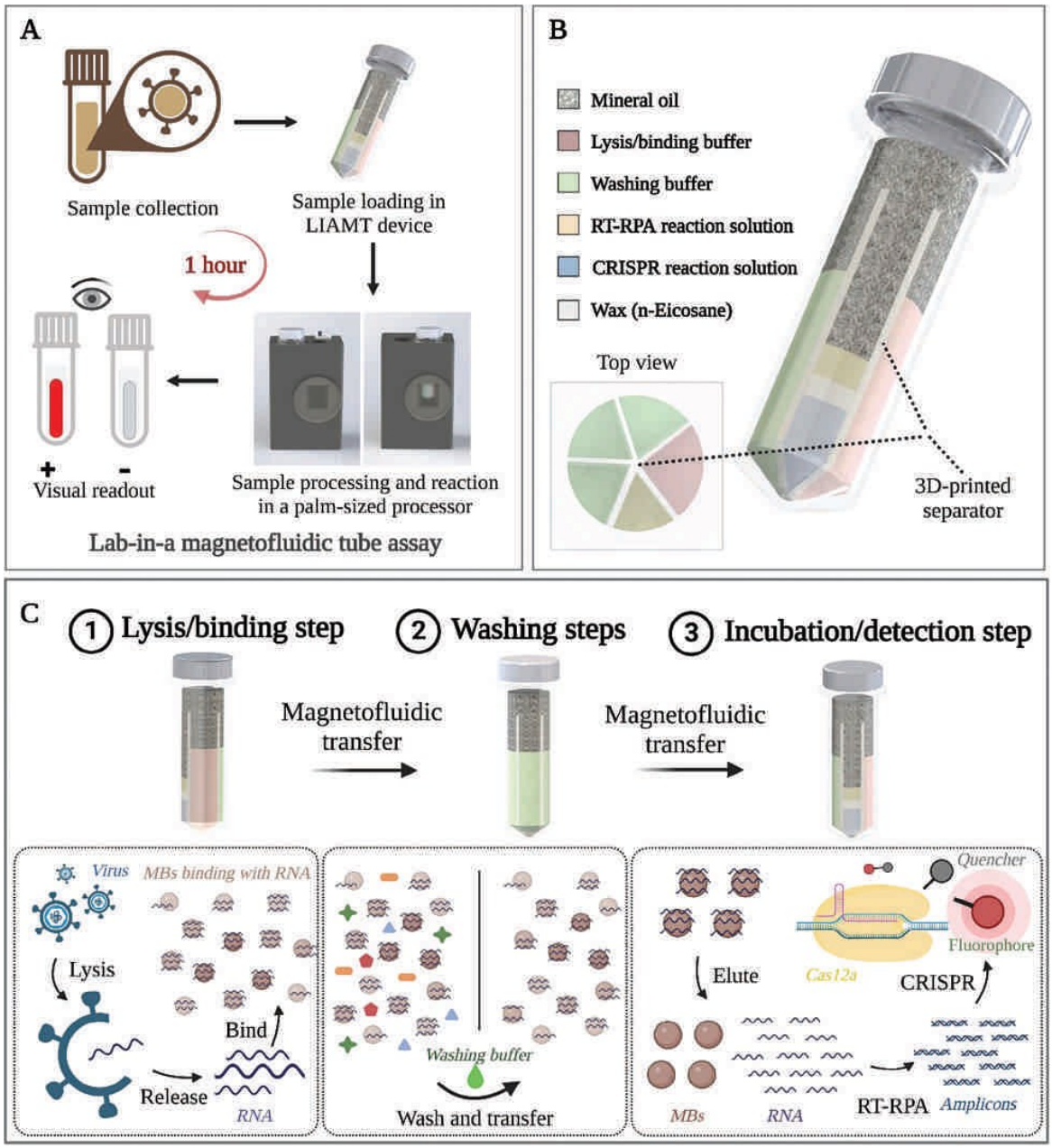

Figure 1.9: Overview of the LIAMT assay. A) Clinical assay workflow of the LIAMT platform. The LIAMT device can accept raw clinical samples. The nucleic acid sample is prepared and transferred bymagnetofluidic operation in the magnetic separation well of the processor. Aftermagnetofluidic-based nucleic acid extraction, the LIAMT device is transferred into the incubation/detection well for isothermal amplification and CRISPR-based fluorescence detection. The endpoint fluorescence signal of the device can be visually observed by the naked eye or recorded by a smartphone. B) Schematic illustration of the LIAMT device. The device contains five independent zones with pre-stored lysis/binding buffer, washing buffer, and RT-RPA/wax/CRISPR reaction solution, respectively. All buffer solutions are covered and sealed by mineral oil. C) Schematic shows the processing of clinical sample detection by the magnetofluidic separation operation in the LIAMT platform. This includes three main steps: 1) adding the clinical sample into the LIAMT device and mixing with lysis/binding buffer containing magnetic beads, 2) washing the magnetic beads bound with nucleic acids in washing buffer zones to purify nucleic acids, and 3) transferring the magnetic beads with nucleic acids into the RT-RPA/wax/CRISPR zone for isothermal amplification and CRISPR detection. From Li et al [81].

Table 1.2: Comparison and overview about sample-to-answer devices based on magnetic particles

Particle Surface coating	Amplification Method	Detection Method	LOD	S2A / min	Sample type	Analyte	Degree of Automatization	Ref.
Microfluidic Systems								
silica	LAMP	fluorescence	102 CFU · mL^{-1}	60	E.coli culture	E. coli	high	[71]
not given	RT-PCR	fluorescence	26 copies / sample	60	nasopharyngeal swab	Influenza A	not fully, loading of reagents and sample required	[72]
not given	real-time connective PCR	fluorescence	1.0 TCID50 · mL^{-1}	50	clinical swabs	Influenza A	not fully (off-chip lysis required)	[74]
not given	real-time PCR	fluorescence	1 copy · mL^{-1}	30	serum	Human Cytomegalovirus	high	[73]
Digital Microfluidic Systems								
not given	LAMP	fluorescence	10 copies · μL^{-1}	60	E.coli culture or diluted reference material	e.coli and SARS-CoV-2	high but manual input required	[75]
not given	RT-PCR	fluorescence	200 copies · mL^{-1} influenca A 229 copies · mL^{-1} Influenza B 217 copies · mL^{-1}	90	swabs	SARS-CoV-2 Influenza A and B	high but manual input required	[77]
not given	dRPA	fluorescence	10 bacterial cells	45	milk	E.coli, Listeria monocytogenes, and Salmonella enterica	very high	[76]

Particle Surface coating	Amplification Method	Detection Method	LOD	S2A / min	Sample type	Analyte	Degree of Automatization	Ref.
Magnetofluidic Systems								
silica	LAMP	color change	0.0375% fresh weight	60	soil	A. rolfsii	manual magnet movement	[84]
not given	RT-PCR	fluorescence	50 IU · mL^{-1}	not given	serum	hepatitis B virus or SARS-COV-2	high	[78]
charge-switch	dPCR	fluorescence	not given	180	polymicrobial samples	Staphylococcus aureus and Escherichia coli	high	[79]
silica	RT-RPA with CRISPR	visual readout	63.9 copies · mL^{-1}	60	nasopharyngeal swabs and plasma	SARS-CoV-2 and HIV	not fully	[81]
not given	dPCR	fluorescence	10 copies · mL^{-1}	30	plasma	SARS-CoV-2	manual magnet movement	[83]
silicon hydroxyl	LAMP	color change	137 copies · mL^{-1}	60	skin swabs	Monkeypox virus	low	[82]
oligo (dT)-coated	RT-LAMP	color change	470 copies	60	artificial sputum	SARS-CoV-2	low	[85]
charge-switch	PCR	fluorescence	10 CFUs	15	penile-meatal swabs	N. gonorrhoeae	high	[87]
silica	qPCR	fluorescence	1000 copies / sample	30	finger pricked blood	HIV	not fully	[80]
silica	RT-LAMP	fluorescence	470 copies · mL^{-1}	45	nasal swab eluates	SARS-CoV-2	manual magnet movement	[86]

1.6 Perspectives on Future Developments

There is a clear potential of NAT in the field of POC, especially due to the higher selectivity and sensitivity. For example, NAT has been proven to be about 1800 times more sensitive compared to antibody or other affinity-based detection strategy [88]. In conclusion, it is crucial to develop new strategies for the POC field to bring NAT to this market.

A reduction of user-input was achieved by fully automated S2A devices by the integration of sample lysis, which was not always feasible for tests in resource limited settings. To overcome complicated lysis protocols, methods like alkali lysis, surfactants, or bead beating have been explored. However, handling complex sample types remains challenging. One example is whole blood, that can be processed in S2A devices but still requires off-chip filtration. Future studies need to address this issue. Due to potential clogging of filtration membranes and to avoid contamination washing or elution buffers should be added via a separate inlet. A solution similar to commercial FTA cards, where the sample can be added, lysed, stored, and transported directly on the membrane, would be ideal. Regardless of the sample matrix, RNA is a problematic analyte due to its instability. Progress has been made with materials such as MOFs or porous silica shells, which have been shown to protect RNA from nucleases.

As an alternative to silica, cationic materials have also been investigated. They have been used as particle coatings or membranes, often showing extremely high adsorption yields but require harsh conditions for elution with lower purity of the NAs. This has been addressed by developing new materials such as chitosan or zwitterionic NFs, which allow milder elution conditions, or elution-free systems, e.g., by dissolving a hydrogel to release the NAs. However, there are many future challenges in this area: First, the impact of real samples on the adsorption has not yet been investigated. This may be especially true for matrices with a high salt content such as urine, which could reduce the electrostatic interaction. Secondly, higher purities of NAs need to be realized, whereas more effective washing solutions need to be developed. Finally, new materials have to be integrated into S2A devices. Ideas are needed to combine nucleic acid extraction with lysis and amplification, and to evaluate whether microfluidic or paper-based systems are more suitable.

To further reduce user impact, devices need to be automated. Comparable degrees of automation for near-patient testing devices have been shown to be effective, but they are not suitable for resource-limited settings as they rely on heavy, large external devices requiring a constant power supply. Transportable options have been developed, thus requiring more manual input. For example, the movement of magnetic particles has been realized in centrifugal tubes, with a magnetic lid or pipette tips. However, automation of paper-based devices remains a challenge. Some innovative solutions include integrating all steps for a S2A device by rotating an external housing or using capillary forces to drive the fluid flow. However, those systems still require manual addition of buffers.

Therefore, storage of reagents within the test is crucial. In microfluidic channels, reagents are typically stored in solution, and their addition has been well established using various options such as valve, button, or pressure-driven methods, or by piercing sealed vessels. On paper-

based devices, reagents such as RPA reagents, primers, or gold nanoparticles are commonly stored in a dry state but buffers must be added manually. This should be addressed in future studies, where solutions could be stored in the test cassette and for example released using a mechanism similar to button-driven microfluids or piercing of reservoirs.

The use of isothermal amplification has proven to be very valuable. With comparable LODs, amplification times have been reduced and only simple heating elements are required. Freeze-dried reagents can be stored directly in the device. However, questions remain about the shelf life and storage conditions of such tests. Since for example commercial lyophilized RPA reagents are typically stored at -20°C, degradation of primers or enzymes will be a major challenge. To fit the requirements of POC testing in resource limited-settings, researchers should aim for portable and battery-powered devices. A readout with the naked eye or a smartphone is favorable. Completely device-free systems are challenging because even isothermal amplification relies on elevated temperatures.

In summary, while significant progress has been made in developing new materials and methods for NAT in POC settings, further work needs to address the discussed challenges to enable NAT in resource-limited settings. The continued development of both materials for nucleic acid isolation and advanced S2A systems holds great promise for making NAT a standard diagnostic technique in the field of POC.

2 Structure and Motivation of the Thesis

Nanofibers (NFs) typically consist of polymers and can be assigned to one-dimensional nanomaterial. The most common production method is electrospinning, which allows the addition of serval doping agents prior to production. NFs are an inexpensive and lightweight materials that can be mass produced. Depending on the used polymers and chemical modifications, the fields of applications are very brought, ranging from biosensors, over medical products, and cell culture experiments to environmental applications. Therefore, this thesis is focusing on the development of NFs for applications in the field of point-of-care (POC) and environmental studies.

POC testing, especially in resource-limited settings, is crucial for ensuring good medical care, particularly in rural areas or developing countries. Therefore, those tests need to be sensitive, reliable, portable, and cheap, which has been realized with multiple dipstick or lateral flow assays. However, to increase the sensitivity and reliability of POC tests, nucleic acid testing (NAT) is an important tool. But NAT involves multiple steps, including nucleic acid (NA) extraction, amplification, and detection, which all need to be integrated in a POC system. Traditional methods for NA extraction often rely on large laboratory devices such as centrifuges and require trained personnel, making them impractical for POC applications. More sophisticated test designs are required to allow the design of sample-to-answer (S2A) devices combining all required steps within one device.

In **Chapter 1** these challenges are addressed discussing the impact of material types used for the isolation of NA in POC applications and methods to integrate NA extraction into S2A devices. Therefore, porous materials and particles developed in this field were systematically investigated. The aim of this work is to identify promising materials and strategies for user-friendly and cost-efficient solutions, to enable testing in resource-limited setting or near-patient testing.

The adsorption mechanism of NA on silica surfaces or by electrostatic interactions are discussed to evaluate their benefits and drawbacks. While most often silica is used in the form of silica-coated magnetic beads or glass fibers, also emerging approaches such as metal-organic frameworks, ionic liquids, or modified nanofibers (NFs) are explored. The focus is here to compare different classes of particle surfaces and types of membranes with each other to identify promising candidates that can compete with commercially available solutions. Furthermore, to fulfill the goal of real-world applications, full S2A devices are compared in terms of their materials used for NA extraction, amplification methods, user input, and limit of detection (LOD). In the end, systems based on membranes and particles are compared towards their current state of development and optimal field of application.

Main goal of this thesis is to develop zwitterionic NFs suitable for NA extraction integrated into S2A device for POC applications. NFs are chosen due to their large surface-to-volume ratio, low production and material costs, and their flexibility in surface modifications. To achieve milder extraction conditions, zwitterionic NFs were developed, where the surface charge of the NFs can be changed depending on the solution pH. This allows binding and elution to occur under mild conditions, avoiding the need for chaotropic salts, charged detergents, or ethanol that could interfere with downstream amplification processes. NA should then be extracted from biological matrices of interest, such as serum. These fibers are integrated into a S2A microfluidic paper-based analytical device (µPAD), and the extraction efficiency is tested in a flow-through setup. The final aim is to realize an S2A device by coupling the extraction of NAs to isothermal amplification via recombinase polymerase amplification (RPA) and detection with gold nanoparticles (Au-NPs) directly within the µPAD.

In Chapter 3, the development of zwitterionic NFs from scratch is discussed. Initially, suitable polymers are identified through a material study. To produce zwitterionic NFs, different electrospinning methods are explored such as layer-by-layer, parallel-one-side, or one-port spinning. Zwitterionic properties are reached by doping a supporting, water-stable polymer with two functional polymers, a weak acid, and a weak base. Then, the the NFs have an overall positive surface charge at acidic conditions for NA binding and a negative surface net charge at basic conditions for NA elution due to electrostatic repulsion. An in-depth study of the material properties revealed the influence of the morphology of the fibers, the chemical composition, and the influence of the fibers' age on the extraction efficiency. Therefore, material properties are optimized and controlled during production. Finally, adsorption and elution parameters such as buffer and incubation times are adjusted, revealing mild extraction parameters and short incubation times. Based on the hydrophilic nature of the nylon-NFs, they are highly interesting for POC applications. BSA was tested in a interference study, leading to the conclusion that further sample matrices such as serum need to be investigated in the future.

Based on the NFs developed in Chapter 3, the goal of **Chapter 4** was to test the extraction efficiency in the presence of serum samples and to integrate the fibers into a S2A µPAD. In comparison to BSA, serum showed an increased impact of interferences, leading to further optimization of the NFs. Here, various doping ratios of the charged polymers are tested, as well as an optimization of the binding conditions such as the pH. Furthermore, different strategies are tested to integrate the NFs into a foldable µPAD The extraction efficiency in solution is compared to the flow-through approach in the µPAD. RPA is tested for amplification of the NAs within the test design. For detection on the test, modified gold nanoparticles are chosen. However, the final development of a S2A device is still pending, as the individual parts still need to be tested in the future, where extraction from serum samples should be directly coupled to amplification and detection within the µPAD design.
A second main investigation of this thesis is to explore the potential of nanofibers as a precursor to produce true-to-life microplastic (MP) in research. Microplastic (MP) in the environment is

of particular interest because of the potential to damage organisms and cells. While the MP particles found in the environment are characterized by irregular fragments and fibers, the commercially available particles for scientific studies are often spherical due to the simpler production method. However, to fully understand the mechanisms of real MP, true-to-life MP particles should be preferably used in studies.

Based on their two dimensions in the nanoscale, NFs are an excellent candidate as MP precursor. Due to the production by electrospinning, NFs can be spun from many relevant polymers and doped with optical labels if necessary. Therefore, the goal of **Chapter 5** is the production of true-to-life MP from electrospun NFs. Different production techniques are explored to tailor the shape of the MP towards irregular or fibrous particles. The MP is then characterized by its shape, size, and production efficiency. Furthermore, optical labels should be integrated in the MP as they are necessary in histology studies to differentiate those particles from the stained tissue. Here, fluorophores and upconverting nanoparticles (UCNPs) are tested and compared in terms of optical properties, integration in the NFs, doping ratio and leaching of the material. Fluorophores are chosen due to their great variability and lower price, while UCNPs are photostable and can be excited in the near-infrared (NIR). MP is then applied to mouse isolated perfused kidney (MIPK) models to prove the detectability of the particles and investigate potential toxicological effects.

Chapter 6 addresses the main findings and remaining challenges of the previous chapters. Future steps and studies are also discussed to provide an outlook on future applications of zwitterionic NFs as well as studies and improvements of microplastic produced from NFs.

3 Novel Electrospun Zwitterionic Nanofibers for point-of-care Nucleic Acid Isolation Strategies under Mild Conditions

3.1 Abstract

Nucleic acid (NA) testing at the point-of-care requires efficient NA extraction followed by post-NA amplification to achieve necessary detection sensitivity. Nanofibers were demonstrated to be an ideal solid surface in an NA extraction process but necessitate harsh conditions that interfere with the subsequent NA amplification process. We demonstrate that novel, pH tunable, zwitterionic nanofibers composed of uncharged nylon doped with the weakly basic, cationic polyallylamine hydrochloride (PAH) and the weakly acidic anionic polycarboxylic acid (PAA) to address the issue. Unlike the other cationic polymers investigated, e.g., polybrene and polyaniline, these polymers allow efficient NA extraction in TE buffer under mild conditions (pH 4.5 containing 0.1 % Tween 20 for adsorption, and pH 10 with 50 mM NaCl for elution). Adsorption and elution yields over 95% and 70%, respectively, were achieved. We also discovered a correlation between material morphologies and the NA extraction suggesting that the combination of polymer chemistries and nanofiber morphologies facilitates efficient NA extraction at low concentrations (ng range) within a short time period (<10 min). Considering the simple protocols and instrument-free operation the as-developed nanofibers are highly attractive for use in sample-to-answer NA testing in point-of-care settings.

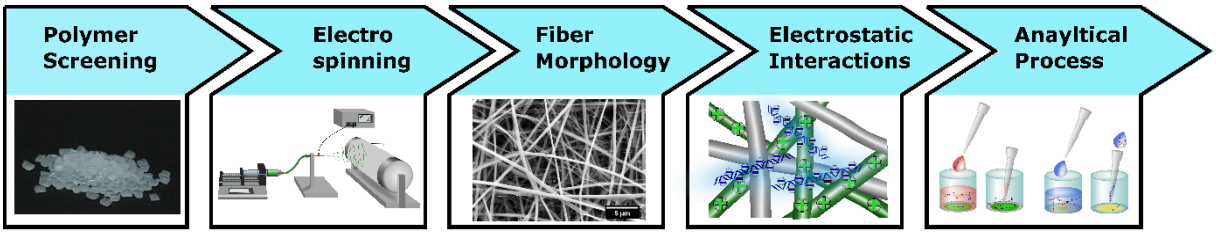

Figure 3.1: Table of Contents

This chapter has been published and formatted to fit in this thesis:
Wieberneit, A. J.; Wongkaew, N.; Baeumner, A. J. Novel Electrospun Zwitterionic Nanofibers for Point‐Of‐Care Nucleic Acid Isolation Strategies Under Mild Conditions. *Adv Materials-Inter* **2024. DOI:** 10.1002/admi.202400329.

Author contributions:
All experiments have been designed and conducted by the author. The project leader was Prof. Antje Baeumner. Manuscript preparation was done by the author and Dr. Nongnoot Wongkaew under the lead of Prof. Antje Baeumner. SEM pictures were provided by Christoph Buckschlegel.

3.2 Introduction

Nucleic acid (NA) tests contained sample preparation, isothermal amplification strategies, and detection modules are of great interest as a viable tool for on-site detection of pathogens [89] with the hope of bridging the gap between lab-based systems, sophisticated cartridge approaches and on-site point-of care (POC) applicability. The superior sensitivity and specificity offered through NA detection combined with rapid and simple amplification and detection procedures makes them an ultimately relevant platform technology. Typically, within the NA test systems, the preceding extraction of the NAs is costly and tedious, and unless incorporated into a sophisticated cartridge, requires trained personnel and external equipment, hindering applicability for POC testing system, especially in resource-limited areas [90]. Thus, an extraction of nucleic acids that is readily integrated into the testing platform while easy to perform is essential [91,92] Such extraction system should also be fast, and suitable for small sample volumes, and importantly only involve non-hazardous chemicals to avoid problems in subsequent the nucleic acid amplification [1,93]. Microfluidic chips, particularly as paper analytical device, will be a viable platform that could fulfill the demands in this endeavor.

In general, a variety of nucleic acid extraction strategies are available, e.g., liquid-liquid or solid-phase extraction (SPE) with various possible materials such as silica, ion exchange, or cellulose [36]. Many commercial systems utilize silica materials in the forms of beads or gel in spin columns due to the high binding affinity of NAs to silica under alkaline conditions [36]. To further POC applicability, researchers study other forms of silica-based materials, such as glass fibers or silica-coated magnetic nanoparticles.[1]

The glass fibers hold great promise for POC applications as they do not rely on equipment and can readily be implemented in paper-based microfluidics [94]. Nonetheless, the need of chaotropic salts to facilitate NA binding and ethanol for washing introduces some critical concerns [89], specifically, in addition to posing the risk to untrained staff and environment due to hazardous nature of chaotropic salts, the latter step can also lead to co-existence of ethanol in the extracted NA and subsequent inhibition of NA amplification, especially when performed in microfluidic channels where complete evaporation of ethanol cannot be guaranteed [1].

NA extraction-based ion exchange strategies offer a solution for these problems as mild conditions prevail and through changes of pH and salinity conditions adsorption and release of NAs can simply be realized. [95]. However, it should also be noted that the current technologies often suffer from very high salinity in the extract which inevitably require a dilution or desalting step prior to amplification [9,10,36,96]

Nanofibers (NFs) are considered an attractive candidate to address these mentioned challenges due to their outstanding surface-to-volume ratio, high porosity, low cost, and tunable chemistries. There are many different fabrication methods available but electrospinning is most commonly used as fiber formation and morphology can be simply controlled by the spinning parameters and industrial up-scaling and production is possible [97–99]. Moreover, NFs can be made from a variety of materials and can even be further modified to tailor the chemical properties to the requirements of specific applications [97,100]. Consequently, NFs are widely

used for SPE applications based on their physical and chemical properties [101]. In particular, due to their high specific surface area, formation of 3D frameworks, and low backpressure as a result of the immense porosity, NFs can be applied to all existing SPE setups such as classical columns or (membrane-)disks [102,103]. The chaotic structure of electrospun nanofibers can also promote efficient passive mixing within microfluidic system [104], thus no operator input is needed for this task, unlike using magnetic beads based separation.

Despite their superior features only two NA extraction systems combining the advantages of ionic extraction of NAs and the advantages of NFs as sorbents in SPE have been reported in the literature. Brandão et al. used an *in situ* polymerization of polyaniline (PANI) on polystyrene (PS) NFs [105] and Xu et al. developed an anion-exchange membrane based on nanofibers for NAs extraction [31]. Here, spin columns and harsh adsorption or elution conditions (pH and charged detergents) and the limit extraction ability only at high NA concentrations make them unsuitable for POC applications, in particular when combined with NA amplification where trace amounts of NAs are typically analyzed.

To overcome such problems, introducing pH-tunable zwitterionic systems into NFs are of great interest. The co-existence of cationic and anionic charge, especially from weak organic bases and weak organic acids, along the NFs can facilitate an efficient control of NA adsorption and elution under mild conditions, and consequently favor the NA amplification process. Nevertheless, due to their intended applications as antifouling matrices or drug carriers, researchers usually strive for pH-stable zwitterionic properties to maintain certain functionality, hampering their extended utility in other areas. Moreover, sophisticated synthesis method is usually required to couple the cationic and anionic functional groups to a single polymer chain [106,107], making it difficult to manipulate or fine tune their functionalities to serve for efficient NA extraction. Therefore, alternative and more flexible approaches in fabricating zwitterionic nanofibers need to be developed.

A synergy of poly(allyamine hydrochloride) (PAH) and poly(acrylic acid) (PAA) is of interest, as the combination of a weak acid and base provides a pH depending surface charge [108,109]. As shown in previous studies, fibers generated from a PAH and PAA mixture can be used to adsorb small cationic ions or molecules such as heavy metals [108,110] or methylene blue [110], in the latter case the fibers were tested as a candidate for drug release. They hence should hold promise also for adsorption and desorption of large biological polyanions such as NAs which are dramatically more challenging when considering their complex chemistries and morphological structures. Furthermore, even though PAH/PAA can be fabricated through electrospinning as demonstrated in the previous studies [108–110] an additional cross-linking step is required to enable water-stable nanofibers as needed for biological reactions. We hence hypothesized that co-electrospinning of PAH and/or PAA with a water-stable uncharged supporting polymer can overcome this issue. Here, Nylon serves as a promising candidate as nano-nets with ultrafine fiber diameters (<20 nm) can be formed along with typical electrospun fibers (diameters in the range of a few hundreds of nanometer)[111] could offer NA extraction at very low concentrations.

The aim of this work is thus to create a NF-based anion exchange membrane readily and suitable for the extraction of NAs even in the POC application field. To fabricate such NF membranes, various polymer combinations and strategies were explored in pursuit of characteristics favored for NA extraction and overall manufacturing. As part of this study, an in-depth material characterization was conducted to unravel the influence of the chemical and physical properties of NFs on NA extraction. Furthermore, NA extraction conditions were thoroughly investigated, ultimately rendering efficient pH-dependent extraction of NAs. High adsorption and elution efficiency within 10 min together with minimally required operator input make the as-developed NF membrane highly suitable for further integration to on-site devices applicable in POC and in-field settings.

3.3 Materials and Methods

Electrospinning of the Nanofibers: Nylon 6,6 NFs were obtained by electrospinning of a 20 wt% polymer solution in concentrated formic acid. All polymers were purchased from Sigma Aldrich, and formic acid was supplied by Carl Roth. The doping ratio of the charged polymers was kept constant at 20 wt% of total polymer content. NFs were electrospun at 22 kV (unless stated otherwise) with a flow rate of 2 µl/min using a 20-G needle at 22 °C and 40% relative humidity and a distance of 20 cm with a rotary drum (Aluminium thin wall, diameter of 80 mm and length of120 mm) system (Starter Kit-Aligned 40kV**,** Linari Engineering srl, Pisa, Italy) where the rotation speed of 150 rpm was used. The fibers were collected for 5 h on grade 1 chromatography paper from Sigma Aldrich. Spinning conditions for all other polymers are summarized in the Supplementary Information in Table S1.
For parallel-one-side spinning, an in-house needle holder was used with a spacing of 2 cm between needles. For layer spinning, a vertical spinning system consisting of two individual spinning chambers was used. One chamber contained nylon-poly(allylamine hydrochloride) (PAH) and the other nylon- poly(acrylic acid) (PAA) setup. In this procedure, the collector was exchanged between chambers after 1 min of collection time, for a total spinning time of 30 min. Until use, the NFs were stored in a vacuum chamber.

Characterization of the Nanofibers: Two 6 mm circles of NFs from two different spots of the NFs mat were placed on a SEM holder. Afterwards the samples were sputtered with a gold palladium mixture. The NFs were characterized by SEM images obtained with a Zeiss/LEO 1530, Germany with 5 - 50 kV with 5 kV. SEM images from at least 8 different spots were taken. For the characterization of the NF diameter images with a magnification of 2500 kX (Image Pixel Size 10.78 nm) and for the nano-nets images with magnification of 5000 kX (Image Pixel Size 5.391 nm). Thickness of the NF mat and knife-coated polymer foil was determined with SEM images from side cuts of the materials. Subsequently, nanofiber and nanonet diameter as well as pore sizes were determined using ImageJ. The pore size was determined with the ferret diameter from automated particle counting function of ImageJ.

Afterwards the number of pores below 400 nm was divided through the total number of pores to determine the nano-pore ratio.
For contact angle measurements, a drop of 5 µL water was placed on a fiber mat and an image taken with an CCD camera on a Dataphysics contact angels system OCA 15EC and analyzed with ImageJ.
Further characterization was performed by determining the dynamic viscosity with a CVO 120 from Bohlin with a cone of 4° and a diameter of 40 mm. Linear extrapolation was used to determine the zero-shear rate from the data set.

Buffers Preparation: All Tris-EDTA (TE) solutions had a TrizimaBase (Sigma Aldrich) concentration of 10 mM and an EDTA (Carl Roth) concentration of 1 mM. The pH was adjusted with NaOH (CarlRoth) or HCl (Sigma Aldrich) with a pH electrode from SCHOTT instruments GmbH Mainz, Germany. The adsorption solution had a pH of 4.5 and contained 0.1% Tween20 (T20) (TE pH 4.5 + T20), and the elution solution contained 50 mM Sodium Chloride with pH of 10. Sodium Chloride and EDTA were delivered from Carl Roth and Tween20 from Sigma Aldrich. Buffers from Citrate and Acetate, both bought from Sigma Aldrich, were made with the same recipe. Buffers were stored at 4 °C until use.

NA Extraction Protocol: NAs from E. coli bacteria was used as a model analyte and was extracted with a GenElute™ Bacterial Genomic DNA Kit from Sigma Aldrich following the protocol and afterwards stored at -20 °According to the manufactured clean, genomic dsDNA should be isolated in the extraction solution.
Before use, NFs were punched into circles of 6 mm diameter using a toggle press (Berg & Schmid GmbH, Germany) and carefully peeled from the filter paper to create free-standing NFs. The resulting fiber mats were placed on the bottom of a 96-well plate. For adsorption, 60 µL of a pre-diluted DNA solution in TE pH 4.5 + T20 was added to the NFs. After the incubation time of 5 min (without agitation), 40 µL of the supernatant was carefully transferred to a new well, and the pH was adjusted to pH 7 with 10 µL diluted NaOH. Here, it was not possible to determine the fluorescence from the NFs directly or within the same well because of the strong backscattering of the porous NFs. Therefore, measurement of the NA remained in the supernatant in a fresh well was chosen, even though this can lead to higher standard deviations. Prior to the elution, the remaining adsorption solution was completely removed without damaging the fibers before adding 60 µL of elution solution. After an incubation for 20 min, 40 µL of the supernatant was again transferred to a fresh well and neutralized with 10 µL HCl. Neutralization prior to the additions of the dye is mandatory to ensure a reliable and stable fluorescent signal since the dye is sensitive to pH. Finally, the NAs concentration was determined with ThermoFisher's OliGreen dye, since this dye is suitable for both double stranded and single stranded NAs. According to the protocol, the dye was freshly pre diluted 200-fold in TE pH 7.5 and then 50 µL of dye solution was added to each well containing the

neutralized NAs solution. After an incubation of 5 min at RT, the fluorescence was measured using an BMG Fluostar MTP (Ex: 485 ± 10 nm, Em: 520 nm, Gain: 1636).

For each measurement, four samples with NAs and four samples without NAs were measured as blanks. Outliers were determined using a Q-test with a confidence level of 95%. To be able to determine the extraction efficiency the NA concentration of the adsorption solution was determined as well.

To process the data, the mean value of the obtained fluorescent signals was determined and corrected by the mean of the related blank measurement. To allow for a quantitative detection, a calibration curve for each solution was measured. Therefore, the concentration of the known NA solution was plotted against the fluorescence signal and linear calibration curve was plotted. From this, the mass per well of NAs in the adsorption solution, madded, the mass NAs remaining in solution after adsorption, mad-sol, and the eluted mass, m_{eluted} , was calculated. Afterwards, the mass of adsorbed NA mad was calculated as shown below:

$$m_{ad} = m_{added} - m_{ad-sol} \quad (1)$$

From this the adsorption yield Y_{Ad} in % was determined:

$$Y_{Ad} = \frac{m_{ad}}{m_{added}} \quad (2)$$

Using the mass of eluted NAs, the elution yield Y_{El} in % was calculated:

$$Y_{El} = \frac{m_{eluted}}{m_{added}} \quad (3)$$

Errors were calculated using the standards deviation and Gaussian error propagation.

For the interference measurements, bovine serum albumin (BSA) was added within the same solution as the NAs. Here, a constant mass of 90 µg/well BSA was added, obtained from Sigma Aldrich. For the measurements similar to the NAs protocol, 5 µL of adsorption or elution solution were transferred to a new well before discarding the remaining supernatant. BSA concentration was determined using ThermoFisher's dye PierceTM Detergent Compatible Bradford Assay Reagent according to the manufacturer's instructions. Here, 200 µL of the dye solution were directly added to the protein solution and incubated for 10 min at RT. The absorbance was measured at 595 nm using a BioTek (Agilent, USA). Adsorption and elution yields were then calculated according to the protocol for NAs.

For the aging study one mat of NFs was stored under ambient conditions and tested over a time period of 16 week. Therefore, on each measurement day NFs were freshly cut and transferred to a microtiter plate with the normal protocol. Adsorption and elution was tested under optimized conditions while the amount of added NAs were kept constant.

3.4 Results and Discussion

3.4.1 Development of Nanofibers

NFs suitable for NA extraction-based ionic exchange require a hydrophilic property and high stability with a pH tunable surface charge. Thus, an initial polymer screening was performed to determine the optimal material (Table S3.2). First, different supporting polymers were assessed, with nylon proving to be the most promising candidate due to its intrinsic hydrophilicity in contrast to polystyrene (PS) and polylactic acid (PLA) (Figure S3.1) and its greater structural integrity compared to polyvinylpyrrolidone (PVP) after exposure to aqueous buffers (Figure S3.2). Zwitterionic moieties intrinsically introduced within polymer chains were not used due to their stable charge state over a wide pH range, which is unsuitable for pH-dependent adsorption and elution [106]. Instead, it was hypothesized that a mixture of individual cationic and anionic polymers can provide such functionality especially since as control over the ratio of positive and negative groups is easily feasible. Poly(allylamine hydrochloride) (PAH), as a weak base with a pk_a of 3.5 [107], was chosen as the cationic polymer because NAs could be efficiently adsorbed onto it at relatively mild acidic conditions , i.e. at a pH of 4.5. This is in contrast to Polyaniline (PANI) [105] where complete adsorption could only be achieved under harsher conditions under which NAs are more prone to degradation (Figure S3.3). Studies with Polybrene (PB) demonstrated an adsorption yield highly comparable to that of PAH (data not shown). However, PB possess a stronger base that does not offer protonatable groups and, in addition, the quintenary amino function is sterically more hindered than the primary one of PAH (Table S3.2), hence elution of adsorbed NA is challenging. Polyacrylic acid (PAA) was chosen as the anionic component because of its lower pK_a compared to polystyrene sulfonate (PSS) ($pK_a \sim 4.5$ and ~ 2, respectively [107]) which could allow the application of milder basic conditions in the elution step. More importantly, in comparison to PSS, PAA provides greater miscibility with PAH and nylon in formic acid, which is vital for homogenous distribution of all components within the as-spun NFs.

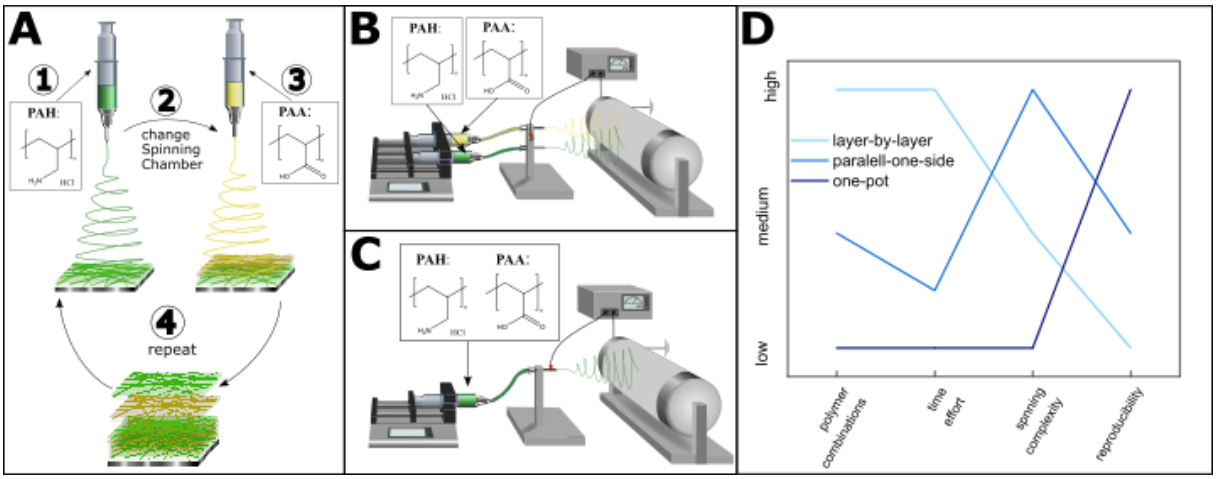

Figure 3.2: Comparison of different approaches for the generation of zwitterionic NFs. A: Layer-by-Layer separately Spinning; B: parallel-one-side Spinning; C: One-Pot Spinning; D: Comparison of the three methods in terms of flexibility, time effort, spinning methods and reproducibility.

Different spinning methods for the preparation of zwitterionic NFs were investigated, including the layering of cationic and anionic layers, parallel-one-side spinning from two separate needles, and a simple one-pot approach (Figure 3.2). The former two strategies allow electrospinning of incompatible anionic and cation polymers. As for the layer-by-layer spinning two spinning chambers are needed, where the two polymer solutions are spun individually this technique permits the effective control over individual fibers, i.e., each polymer is subjected to its optimum spinning conditions as shown in exemplary case of PS and nylon (Figure S3.4). Yet, such a technique is time consuming and needs a lot of input from the operator. Additionally, the static collector makes fiber distribution on the collector inhomogeneous, leading to poor reproducibility within the NF mat (Figure S3.5A and B). Using a rotating drum collector may be a viable option to overcome such issues, but neither for this nor for the parallel-one-side spinning approach a uniform distribution of individual fibers was achievable, where the position of spinnerets had a great impact on the collected location, thus affecting overall NA extraction efficiency as illustrated in Figure S3.6. This necessitated a switching of the spinnerets up and down from time to time to allow homogeneous distribution of both polymers. While this somewhat cumbersome approach results in desirable mats, the one-pot spinning approach, if possible, is highly desirable. Here, a homogenous mixture of the spinning solution was feasible and consisted of PAH, PAA, and nylon in formic acid. This one-pot spinning strategy not only requires minimal personal input but also provides satisfied reproducibility within and between NF batches (Figure S3.6 and Figure S3.7).

3.4.2 Fiber Morphology

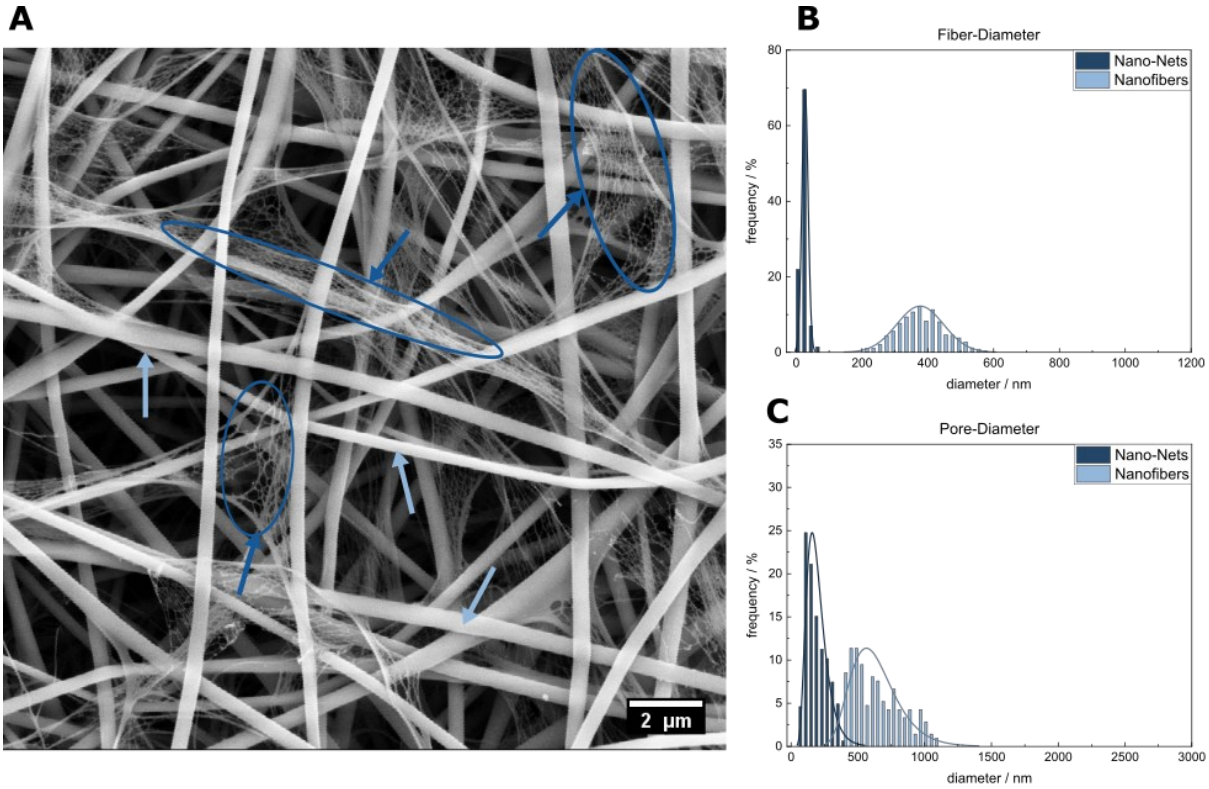

Figure 3.3: A: SEM picture of nylon-PAH-PAA fibers with a magnification of 1000 kX. Nanofibers are marked with light blue arrows, Nano-Nets with dark blue; Size distribution of the nanofibers and nano-nets from the fibers (B) and the pore diameter (C); n > 200

Previous studies have shown that under specific conditions nanonets can be formed within the as-spun nylon NFs, which is considered an attractive feature for boosting NA extraction efficiency [111,112]. The presence of nanonets can be efficiently controlled through the polymer concentration in the spinning solution, type of solvent, and spinning parameters such as an applied voltage. In this study, 20 wt% total polymers consisting of nylon, PAH, and PAA in formic acid were used as a spinning solution, which successfully allowed the simultaneous formation of NFs (diameter of 380 ± 70 nm) and nanonets (diameter of 25 ± 9 nm) with a narrow size distribution (Figure 3.3), showing the same structure as pure nylon-NFs (Figure S3.8). It should be noted that electrospinning of PAA, PAH, and PAA/PAH without supporting polymer did not result in the generation of nanonets as reported in other studies[113–115] Therefore, this material offers not only an increased surface-to-volume ratio, but also very small pore sizes (NFs 600 ± 200 nm; nets 200 ± 80 nm), facilitating efficient interaction between NA and NFs. To unravel the beneficial features of as-spun NF contained nanonets we first attempted to study the parameters that control the formation of nanonets in which an increase voltage plays great role in promoting the formation of nanonets as shown in Figure S3.9 and Figure S3.10 and previously reported in literature [116]. We also investigated the effect of solution viscosity attributed to the presence of HCl in PAH used and stirring time (Figure S3.11). Interestingly, no effect of PAH was detected in terms of fiber morphology or extraction efficiency, confirming the compatibility of PAH with nylon for electrospinning.

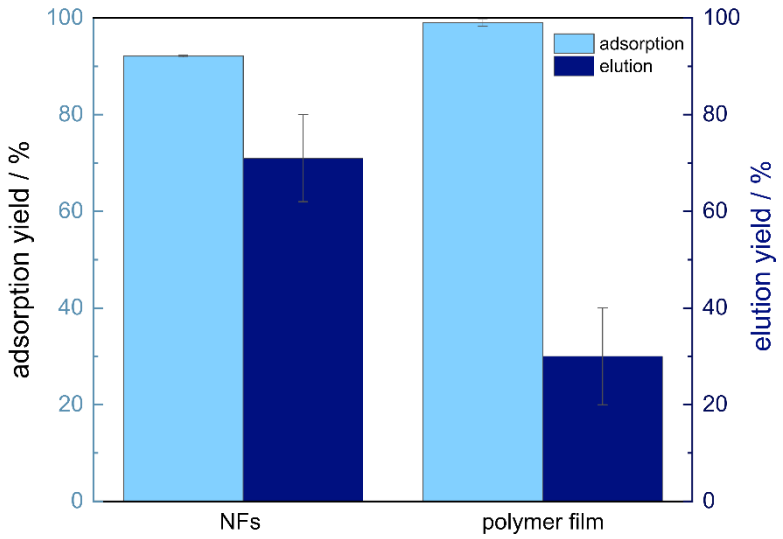

Figure 3.4: Comparison of the extraction efficiency of nylon-PAH-PAA NFs and a polymer film with a similar thickness. The polymer film and NFs were cut into circles with a diameter of 6 mm using the standard protocol as for all NFs samples. Afterwards 7.83 ± 0.01 ng NAs were added to each sample for the adsorption.

We further elucidated the impact of the nanostructures in governing NA adsorption and elution behavior. Here, nylon-PAH-PAA in the form of a knife-coated porous polymer film and nanofibrous membranes of similar thickness were compared. The adsorption of NA was not enhanced by having nanostructures as seen from the highly comparable adsorption yields obtained from the NFs and the polymer film (Figure 3.4). This suggest that the nanostructures are needed to allow a repulsion of NAs during the elution process. We assume that the closer proximity of the cationic and anionic functional groups in the nanofiber mat, especially in the very small nano-pores, is needed to ensure that not only cationic but also anionic functional groups are surrounding the adsorbed NAs. Therefore, the use of nanomaterials does not only provide a high surface-to-volume ratios but also provides functionality in the elution process.

3.4.3 Electrostatic Properties of the NFs

The pH dependency of the NFs is easily realized by a mixture of cationic PAH and anionic PAA. Their ratio was optimized, aiming for leveraging a full adsorption capacity and a maximum elution yield. This study revealed a significant impact of PAH content (Figure 3.5A and Table S3.3). Shifting from 100% to 0%, it was found that pure PAH NFs achieve full NA adsorption but lack an elution capability. Approaching the optimal ratio of 38% PAH yields a substantial increase in elution while maintaining a satisfied adsorption yield. However, a turning point is observed at 35% PAH, leading to more anionic fibers with minimal adsorption yield. Standard deviations of the elution signals are very high as the amount of eluted NAs is close to the LOD and therefore the quantification not precise anymore.

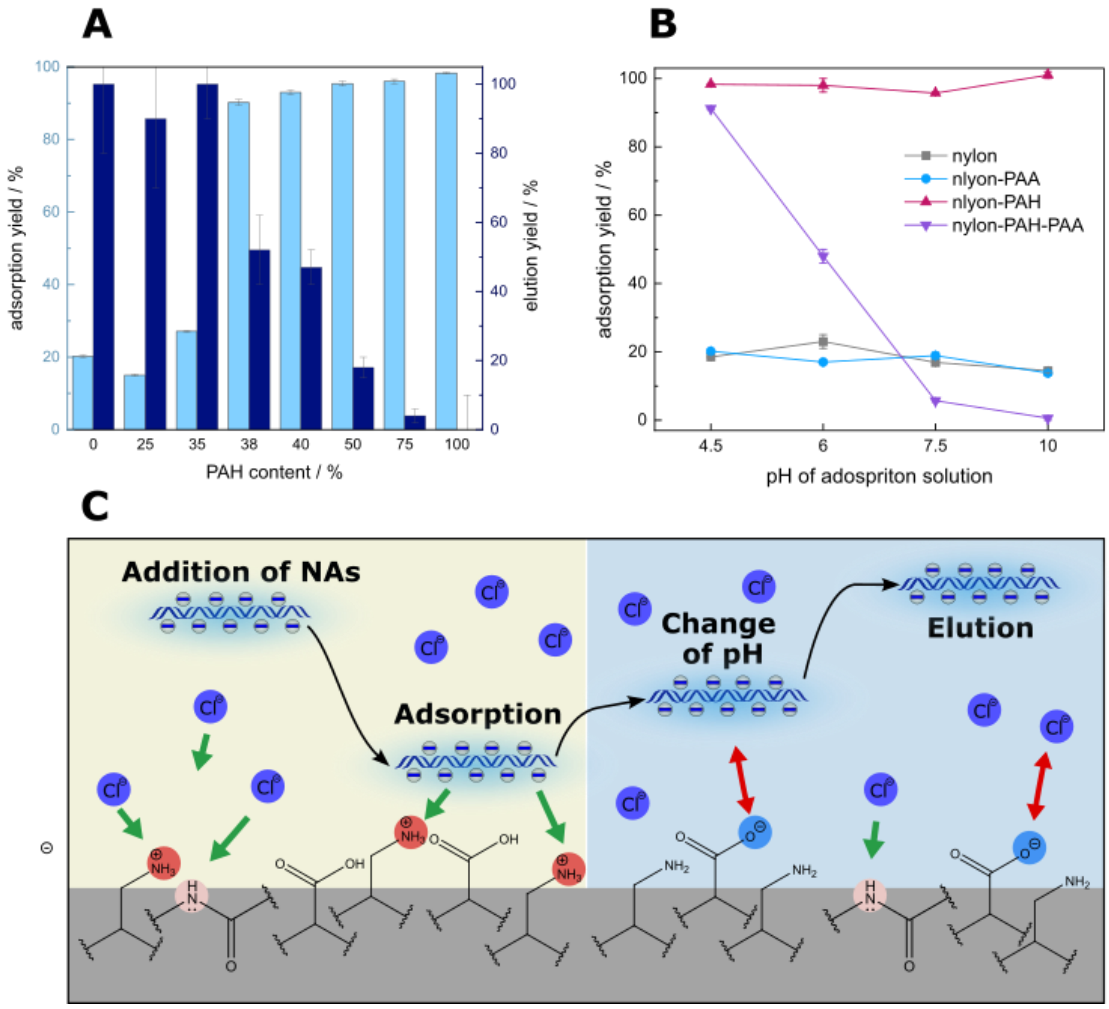

Figure 3.5: pH dependency of nylon-PAH-PAA NF, $n \geq 3$. A: Adsorption and elution yield of nylon-PAH-PAA NFs with varying ratio of PAH and PAA while the absolute mass of added charged polymer remained constant at 16.7 wt%. Adsorption in TE solution pH 4.5 + 0.1% T20, elution in TE pH 12 + 100 mM NaCl; B: Adsorption yield dependency on pH for different non-charged, cationic, or anionic and zwitterionic NFs C: Schematic illustration of the pH dependent NA extraction process from zwitterionic nylon-PAH-PAA NFs.

An in-depth analysis of the fibers' pH dependency demonstrates that the nylon and nylon-PAA fibers show a pH independent and unspecific adsorption of just about 20 % while the nylon-PAH adsorb the NAs completely over the whole pH range investigated. (Figure 3.5B) A strong pH-dependency could only be observed for the zwitterionic nylon-PAH-PAA NFs with a strong NA adsorption at pH 4.5 then decreasing for higher pH-values. The lower adsorption at a basic pH may either be a result of the mixture of PAH and PAA or an experimental mistake. Overall, this pH dependency does fit with the pk_a values reported in literature, as at pH 4.5 and pH 10 mainly the amino and the carboxylic acid groups are presented, respectively [107]. In conclusion, the mixture of PAH and PAA can combine the properties of both polymers, where the fibers are capable of adsorbing NAs at a low pH and eluting NAs due to electrostatic repulsion at a high pH (Figure 3.5C), resulting in zwitterionic NFs with a pH-tunable surface charge.

3.4.4 Optimization of the Analytical Process

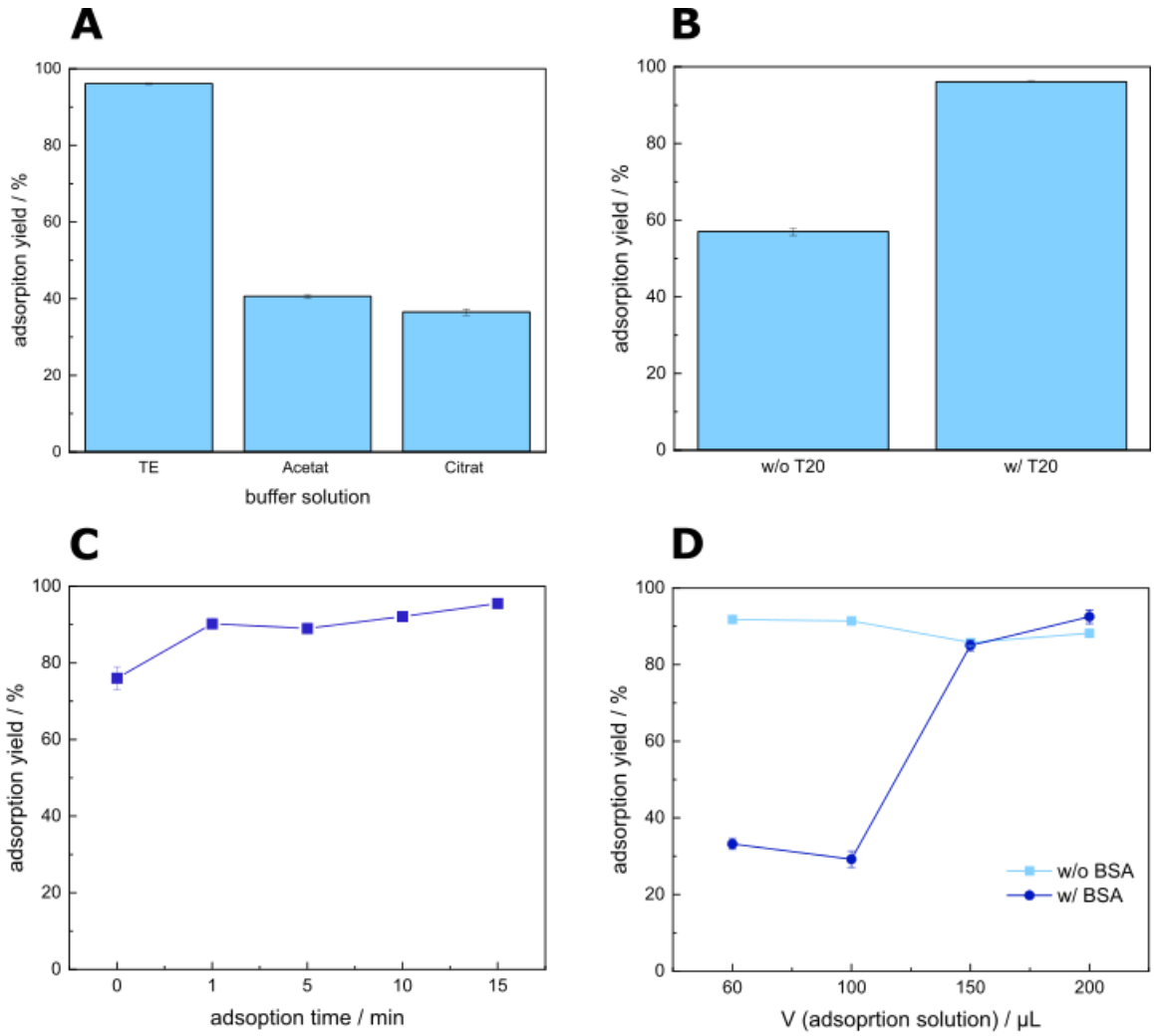

Figure 3.6: Influence on the adsorption yield on nylon-PAH-PAA NF of (A) buffer system while the molarity was kept constant at 11 mM and a pH of 4.5 containing 0.1% T20, (B) the addition of 0.1% T20, (C) adsorption time and (D) the dilution in the presence of BSA. Here, a constant amount of 100 mg BSA and 6 ng NAs were diluted in 60 – 200 µL and the responding adsorption yield was determined; $n \geq 3$

The extraction efficiency of the zwitterionic NFs was further enhanced through the optimization of the extraction conditions. Specifically, adsorption solutions and incubation times were investigated (Figure 3.6), where the TE buffer outperformed the others. The addition of Tween 20 further improved the adsorption yield due to a shortened wetting time. Compared to other studies where complete adsorption was achieved after 9 [105] or 20 min [31], in this work over 70% of NAs were adsorbed immediately and complete adsorption is achieved within 5 min, making this system suitable for flow-through extraction. Furthermore, while the other studies used high NA amounts (µg range), our study focused on low NA amounts, i.e. in the ng range, as this is deemed significantly more relevant for POC application, for example NAs concentration in serum are around 1.8 – 35 ng mL^{-1}, in whole blood about 30 µg mL^{-1} and only

a few copies of pathogen NAs per sample are expected [95,117], emphasizing the beneficial feature of nanonets within the as-developed zwitterionic nanofibers. An interference study with BSA showed no difference in adsorption performance at only 3-fold dilution, even though about 100 µg of BSA and only about 5 ng of NAs were added, which correlates to about 2 – 3 µL of human serum [118]. Nevertheless, human serum does contain more interfering species such as lipids or salts. Due to the low specificity of the electrostatic extraction process more in-depth research is needed here to study the influence of different samples types. However, this simple and promising dilution approach showed that NAs have a high attraction to the NFs due to their negatively charged backbone. Consequently, future studies will investigate the effect of individual sample matrices, such as serum, saliva or urine, and different types of pathogen NAs, such as DNA or RNA, in more detail.

In a final step, the elution process was optimized, focusing again on solution and time parameters. An optimum elution time of 20 min was determined. However, compared to an elution time of 5 min, only a marginal increase was found for longer incubation periods, making this system again also suitable for a flow-through setup (Figure 3.7A). Regarding the solution characteristics, the elution efficiency is primarily affected by the pH due to the NF's pH dependence. A significant increase was observed within the pH range of 7 to 10, with the optimum at pH 10. A higher pH could not increase the elution efficiency and is not recommended as to ensure the NAs' stability (Figure 3.7D). In contrast to other NA extraction-based ion exchange [36], a relatively mild concentration of salt is needed to allow the satisfied elution yields where 50 mM NaCl was optimal (Figure 3.7B). Thus, desalting or dilution is not needed prior to further NA amplification. The required low salt concentration may be attributed to the introduction of anionic moieties, which probably prevent strong binding between the NA and NFs. Unlike NA adsorption shown in Figure 3.7B, the addition of Tween20 in the elution solution had no effect due to the already pre-wetted NFs occupied by adsorbed NA (Figure 3.7C).

When comparing this system to other NF extraction systems reported so far, our zwitterionic NFs show a comparable extraction time of in total 10 min without the need for centrifugation or tedious mixing step. Furthermore, due to the zwitterionic properties, this system does not require extreme pH conditions, high salt concentrations, or charged detergents to elute the NAs, which are preferable for downstream amplification strategies (Table 3.1). Therefore, zwitterionic NFs are able to overcome the current problems of the ionic NA extraction system.

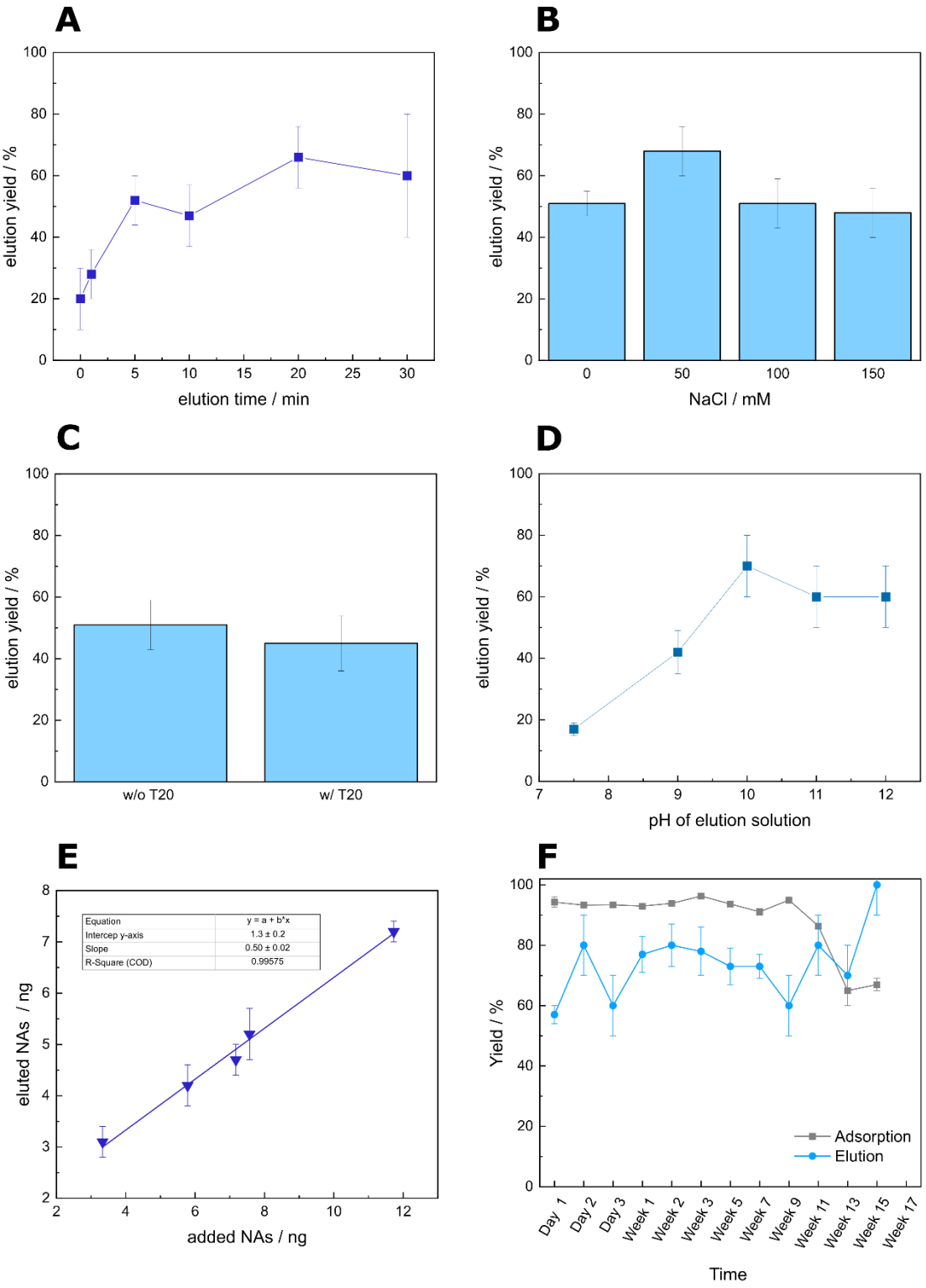

Figure 3.7: Investigation of the elution from nylon-PAH-PAA NFs: Influence of elution parameters on the elution yield with (A) the elution time, (B) the addition of NaCl (C) T20 and (D) the pH. Possibility for (semi-)quantitative detection due to a linear correlation of the added and eluted mass of NAs (E). Aging study on nylon-PAH-PAA NFs. NFs over the storage time and adsorption and elution was measured under optimized conditions (F); $n \geq 3$

Table 3.1: Comparison different nanofiber-based ionic NA extraction systems.

Membrane	Mass of NA	Adsorption time / min	Adsorption pH	Elution time / min	Elution pH	Elution Additives	Equipment demand	Ref.
PS-PANI	µg	9	2.8	10	11.7	SDS	High	[105]
Chitosan aerogel	µg	20 - 30	3 - 4	20	5	1.5 M NaCl	High	[31]
Nylon-PAH-PAA NFs	ng	5	4.5	5	10	0.05 M NaCl	low	This Work

The zwitterionic NFs also offer the possibility of semi-quantitative readout when coupled with an amplification and detection system as a result of the linear correlation between the amount of NAs added and eluted (Figure 3.6E). Finally, the aging of the NFs should be investigated when stored under ambient conditions. The data was generated from a single NF mat the nanofibers showed consistent adsorption and elution for at least 9 weeks (Figure 3.6F). Future studies will study long-term stability also under protective conditions. The aging process itself started with a decrease in adsorption, but not in elution yield, suggesting that primarily PAH are degraded, while PAA and nylon properties might remain intact.

3.5 Conclusion

In this study, novel zwitterionic nylon PAH-PAA NFs fabricated by electrospinning were proposed to enable specific binding and elution of NAs under mild conditions, highly promising for isolation of NAs for POC applications. The one-pot approach, i.e., electrospinning of a spinning solution containing nylon as carrier polymer together with the cationic PAH and the anionic PAA in formic acid, allows facile and reliable fabrication of the nanofibers. The adsorption and elution efficiency of NAs can be simply tuned via adjusting the polymer ratio and assay conditions. The high surface area, the inherent hydrophilic property, and the presence of nano-nets of the nanofibers undoubtedly allows the isolation of extremely low amounts of NAs achievable in a short period of time (within 10 min). The nylon PAH-PAA NFs are thus highly suitable for the extraction of NAs in flow-through systems without the need of additional equipment, making them a promising solution in the POC field, especially when they are integrated within microfluidic channels, µPADs and origami-based assays. Furthermore, with precisely controlled material properties, these fibers offer adaptability for various applications and allow easy customization to specific challenges and needs, such as sample types, while ensuring predictable behavior of the NFs. In conclusion, with their demonstrated efficiency, these zwitterionic NFs can serve as an important tool to overcome current sample preparation challenges.

3.6 Supporting Information

Table S 3.1: Solution recipes, spinning and ambient conditions for all types of investigated supporting polymers.

Parameter	Nylon	PVP	PS	PLA
m (polymer) / g	0.6	0.7	0.45	0.24
Solvent 1	Formic acid	DMF	DMF	Chloroform
Solvent 2	/	Ethanol	THF	Methanol
Ratio of solvents		1:1	1:1	2:1
Total Vol. (solvent) / mL	3	5	3	5
Distance / cm	20	15.5	15	15.5
Flow rate / µl/min	2	10	10	7
Needle / G	20	19	18	19
Voltage / kV	22	7	11	15
Temperature / °C	22	23	23	22
RH / %	40	40	30	30

Table S 3.2: Possible polymers for the formation of zwitterionic NFs

Supporting-Polymers	Cationic-Polymers	Anionic-Polymers
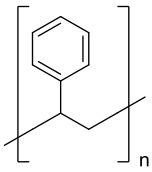 polystyrene (PS)	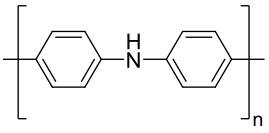 PANI	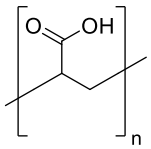 poly (acrylic acid) (PAA)
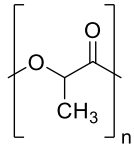 polylactic acid (PLA)	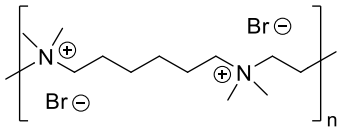 polybrene (PB)	
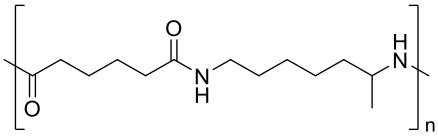 polyamide 6,6 (nylon)	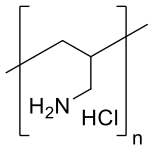 poly (allyamine hydrochloride) (PAH)	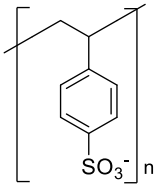 polystyrene sulfonate (PSS)
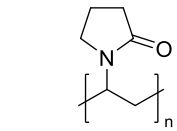 polyvinyl pyrrolidon (PVP)		

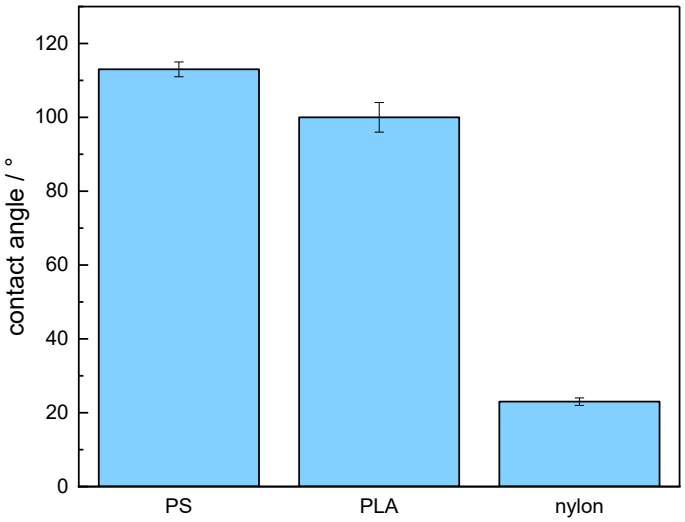

Figure S 3.1: Contact Angle measurements of PS-, PLA and nylon-NFs; n ≥ 3

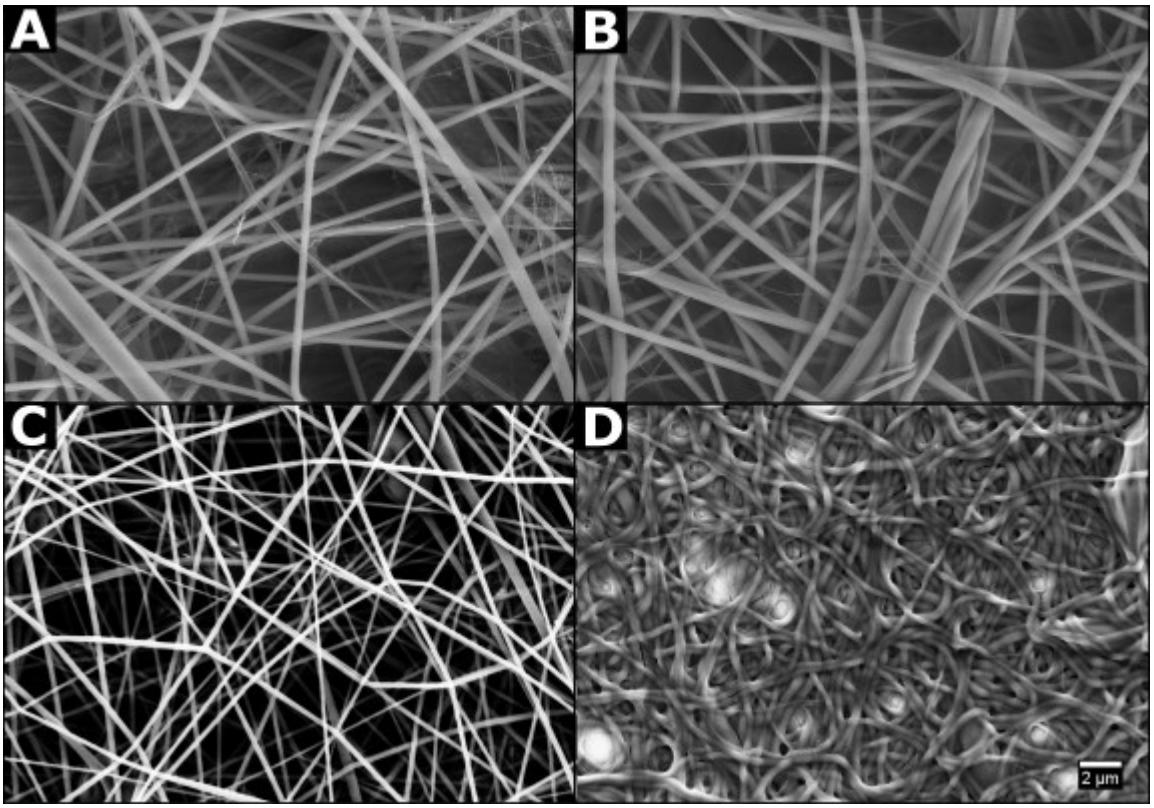

Figure S 3.2: SEM picture of nylon-PAH fibers (A +B) and PVP fibers (C+D) before the lysis buffer was added (A + C) and after the lysis buffer was added (B + D) with a magnitude of 10 000 kX. Lysis Buffer contained 4 M Guanidium HCl and 0.1 % SDS in Citrate Buffer pH 4.5.

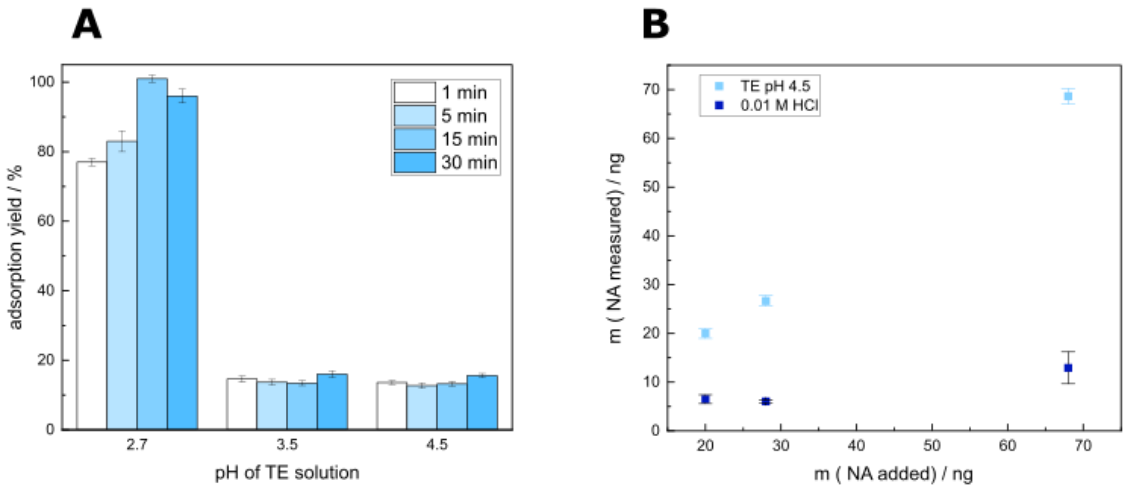

Figure S 3.3: A: Adsorption yield on nylon-PANI NFs in TE solution with varying pH; B: stability of NAs in TE buffer pH 4.5 and 0.01 M HCl acid; $n \geq 3$

Comparison of Electrospinning Methods:

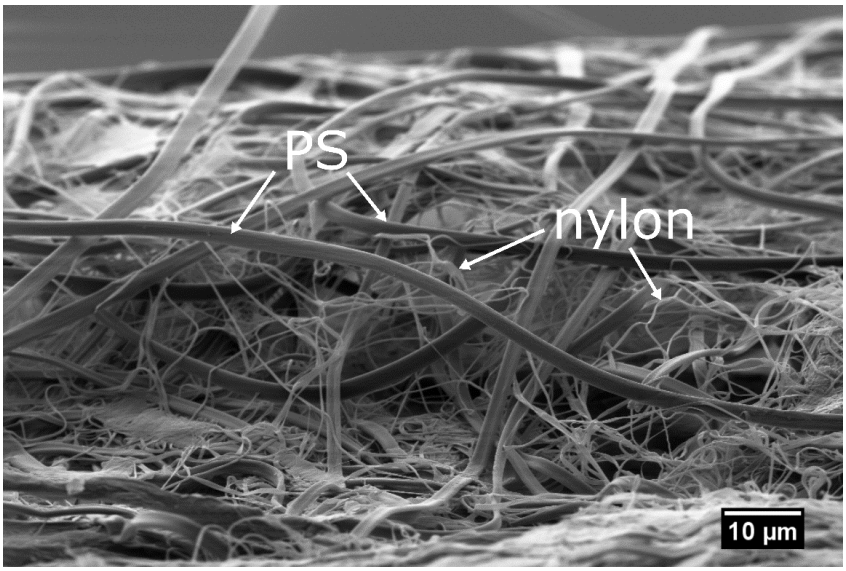

Figure S 3.4: Side cut of layer-by-layer spun PS-nylon fibers

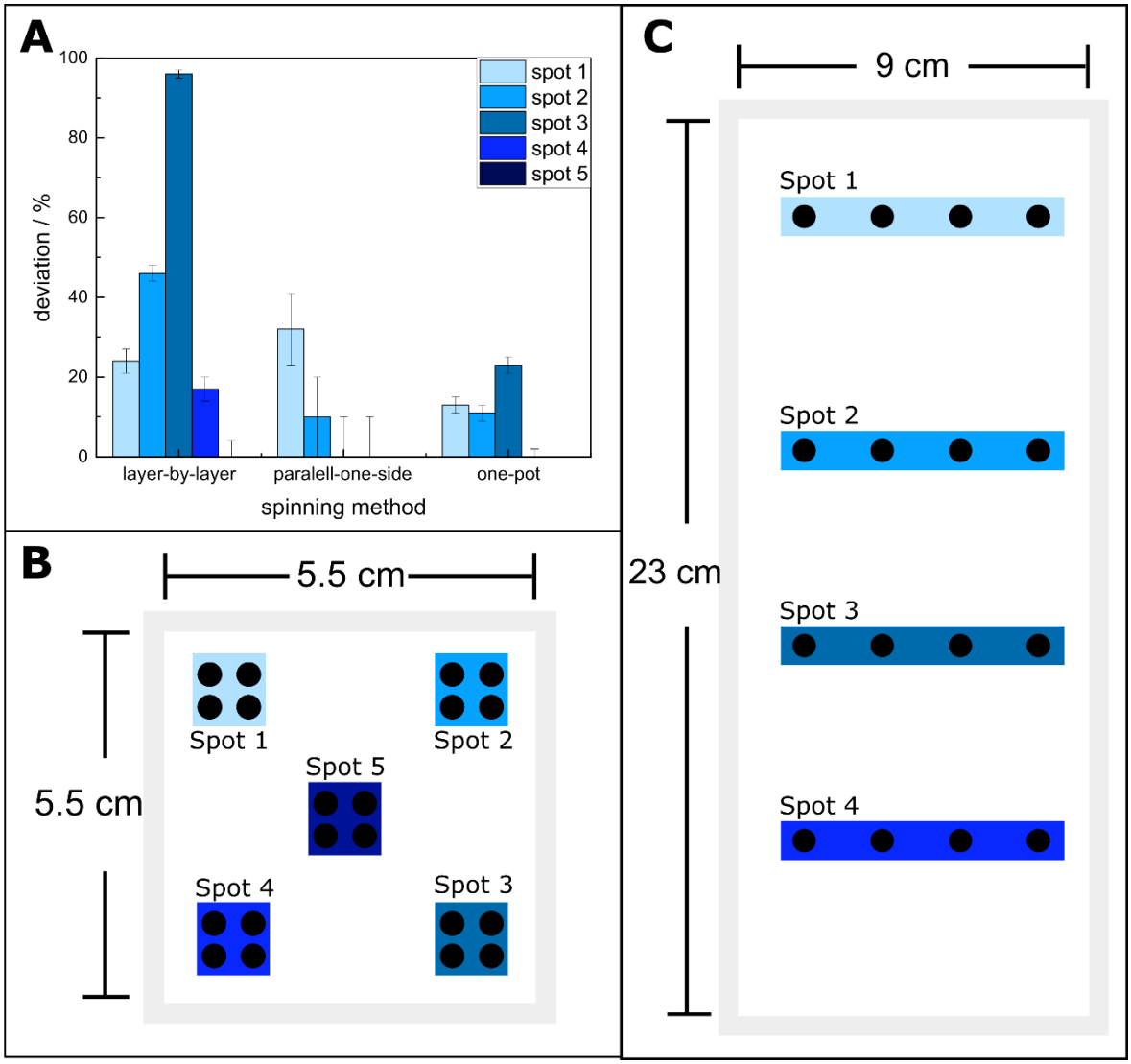

Figure S 3.5: Comparison of the mat homogeneity when nylon-PAH-PAA NFs were produced with different spinning methods. A: Deviation in % from the maximum value of eluted NAs determined within the selected spot (% deviation = $100\times\frac{NA(max,i)-NA(i,n)}{NA(max,i)}$, where *i* and *n* refers to spot number and sampling point within the selected spot, respectively. B: Schematic sampling from the mat produced with layer-by-layer spinning with size specifications. C: Schematic sampling from the mats produced with parallel-one-side and one-pot spinning with size specifications.

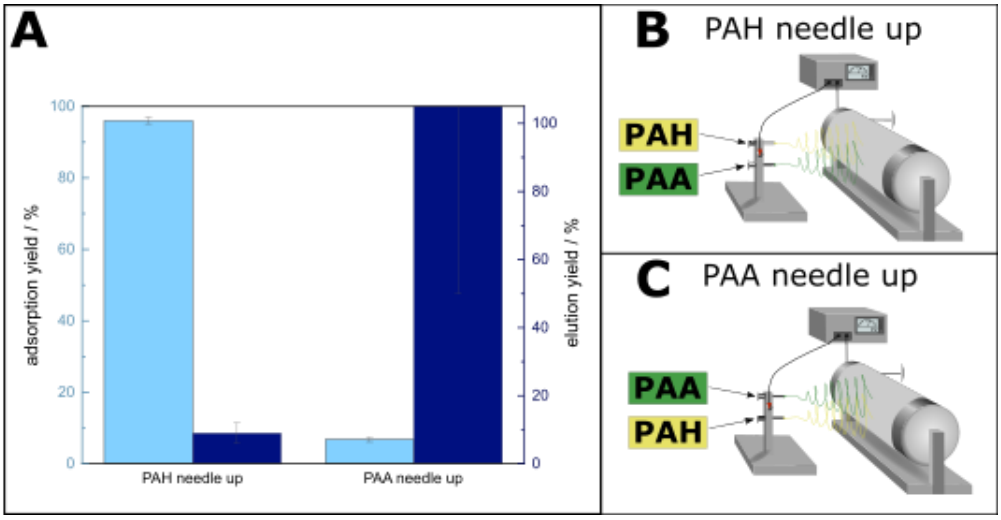

Figure S 3.6: Influence of needle position on the resulting NFs in paralell-one-side spinning (A), when either the PAH needle was kept at the upper (B) or lower (C) position in the needle holder during spinning; n ≥ 3

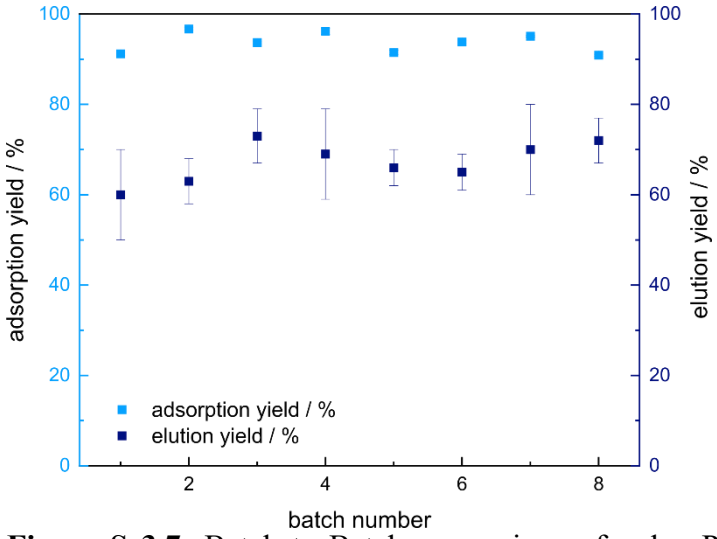

Figure S 3.7: Batch to Batch comparison of nylon-PAH-PAA NFs prepared from one-pot spinning

Fiber Morphology:

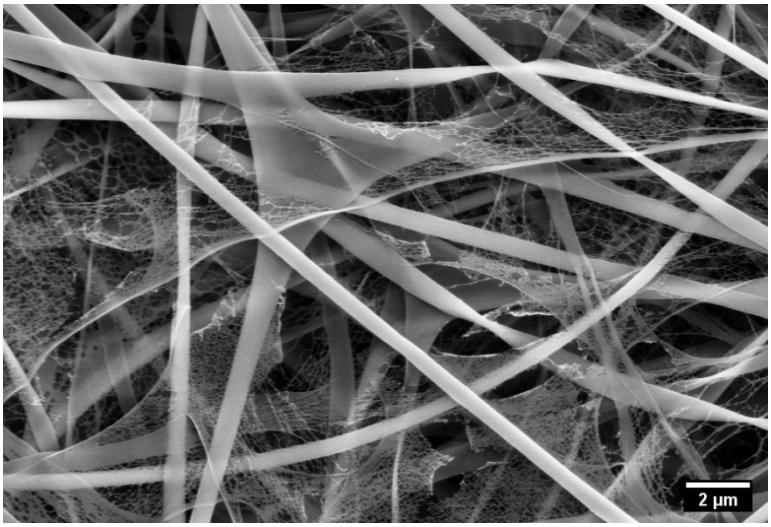

Figure S 3.8: SEM image of pure nylon NFs with a magnification of 1000 kx.

Among many other spinning and solution parameters, sufficient stirring time is also required to ensure a homogeneous spinning solution and subsequently uniform nanofibers [119]. On the other hand, hydrochloric acid (HCl) can degrade nylon over time [120]. Since PAH, and thus the spinning solution, contain HCl, the effect of stirring time in the presence of HCl and PAHs was investigated, with effects on viscosity and NF morphology. Within the first few hours of stirring, a slight increase in viscosity was observed for the HCl-containing samples, while the opposite was true for the pure nylon solution. Then, with even longer stirring times, an increase was observed for all spinning solutions (Fig. S9). An increase in viscosity indicates a decrease in molecular weight of the polymer [119], showing that in addition to the effect of over-stirring the spinning solution, PAH and HCl are also capable of degrading nylon. However, no effect of PAH was detected in terms of fiber morphology or extraction efficiency, confirming the compatibility of PAH with nylon for electrospinning.

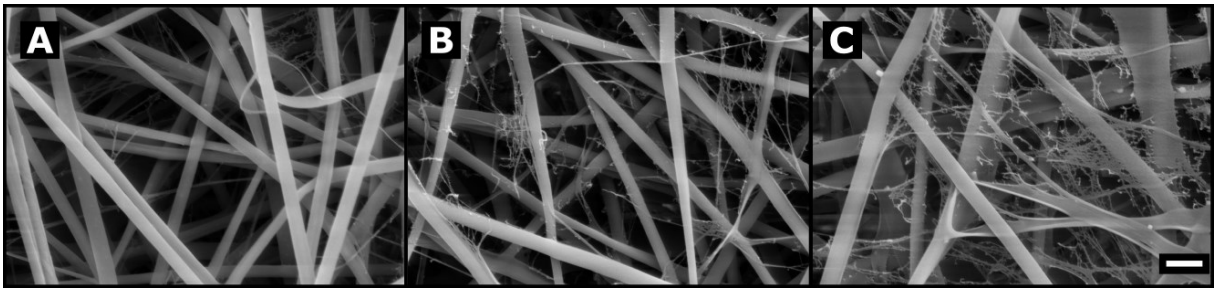

Figure S 3.9: Influence of applied voltage on the fiber morphology. A: 19, B: 22 and C: 15 kV. Scale bar: 1 µm

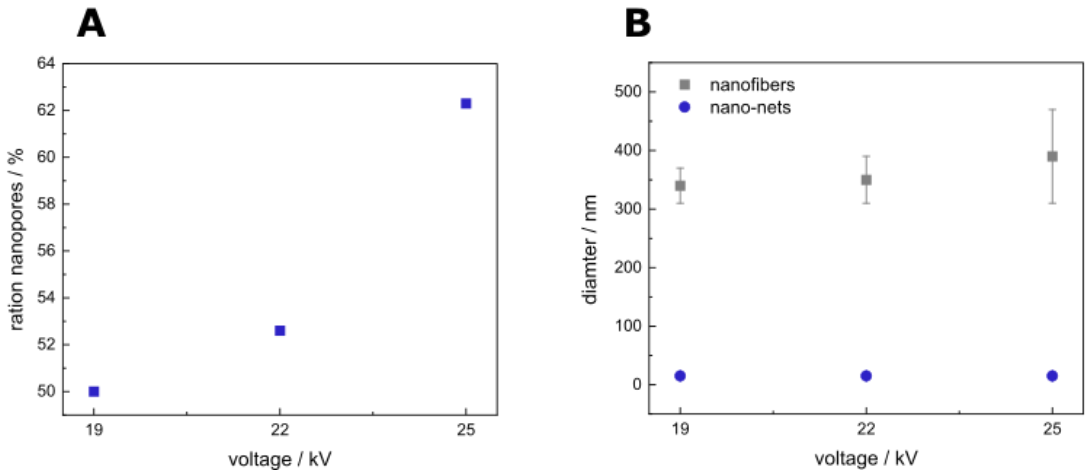

Figure S 3.10: Influence on the applied voltage during spinning. A: ratio of nanopores, B: diameter of nanofibers and nano-nets ; n ≥ 3

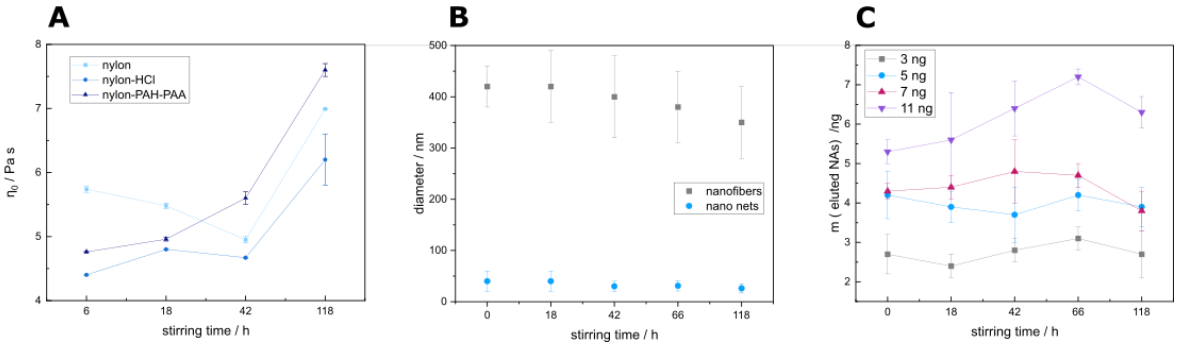

Figure S 3.11: Influence of the stirring time of the spinning solution on the NFs: A: Influence of stirring time on the dynamic viscosity of the spinning solution. Spinning solution of 20 wt % nylon solution in FA was tested. The pure solution or either an addition PAH-PAA or mol-equivalent HCl was tested. B: Influence of stirring time on the fiber morphology of the NFs and the nano-nets. C: Influence of stirring time on the elution yield for different amount of added NAs; n ≥ 3

Electrostatic Properties of the NFs:

Table S 3.3: Influence of PAH content to the mass of adsorbed and eluted NAs from nylon-PAH-PAA NFs; $n \geq 3$

PAH content / %	m (added NAs) / ng	m (adsorbed NAs) / ng	m (eluted NAs) / ng
0	7.93 ± 0.01	1.6 ± 0.03	1.6 ± 0.2
25	8.69 ± 0.01	1.33 ± 0.04	1.3 ± 0.3
35	8.54 ± 0.01	2.37 ± 0.03	2.6 ± 0.4
38	6.31 ± 0.01	5.73 ± 0.03	3.1 ± 0.7
40	7.83 ± 0.01	7.34 ± 0.01	3.3 ± 0.5
50	8.69 ± 0.01	8.49 ± 0.01	1.7 ± 0.3
75	8.69 ± 0.01	8.54 ± 0.01	0.4 ± 0.2
100	6.31 ± 0.01	6.16 ± 0.01	0 ± 0.5

4 Integration of Zwitterionic NFs in a Sample-to-Answer Paper-Based Microfluidic System

4.1 Abstract

Reliable on-site testing in point-of-care (POC) applications is a critical challenge to enhance treatment outcomes and reduce the need for centralized labs. Nucleic acid testing (NAT) holds immense promise due to its sensitivity and reliability, thus requiring more working steps than antibody or other affinity-based detection strategies. Therefore, this study aims to develop a POC-friendly sample-to-answer (S2A) test design by integrating zwitterionic nanofibers (NFs) into a S2A paper-based microfluidic system (µPAD) and combining it with isothermal amplification. For the extraction of nucleic acids (NAs), previously developed zwitterionic NFs should be optimized for serum samples. As simple dilution was inefficient, further adjustment of the material properties by changing the doping ratio of the charged polymers or lowering the binding pH could enhance adsorption yields. However, further investigations are needed to conclude this problem. Subsequently, NFs were integrated in into a µPAD design. The extraction efficiency within the flow-through setup revealed excellent performance comparable if not better than that to assays in solution. Aiming for a S2A design, the NA extraction should be coupled to a recombinase polymerase amplification (RPA) directly on the µPAD. The RPA showed good performance in under 20 min even at room temperature and the integration into the µPAD was successful. Future studies need to enhance the speed of the flow through the test as well as the intensity of the detection lines, and the connection of the extraction with the amplification and detection.

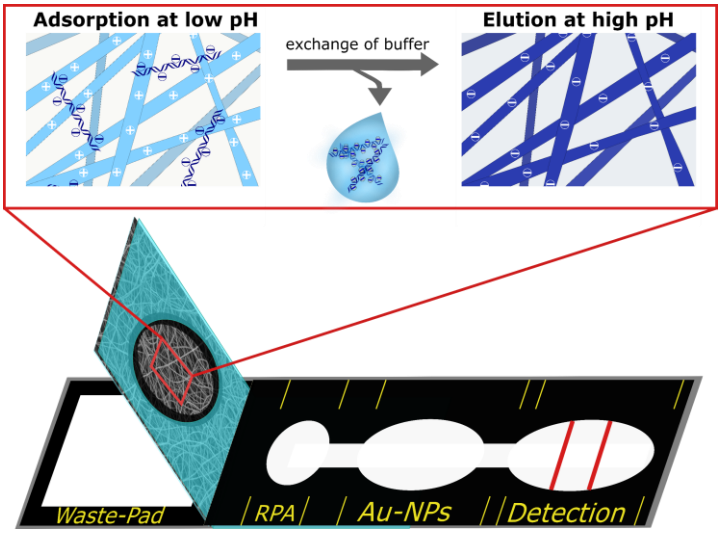

Figure 4.1: Table of Contents

This chapter includes unpublished results.

Author contributions:
All experiments have been designed and conducted by the author. The project leader was Prof. Antje Baeumner and Dr. Nongnoot Wongkaew. The text was written by the author.

4.2 Introduction

Reliable and on-site testing in resource limited settings is a key-challenges nowadays. According to the ASSURED principle defined by the WHO, those testes should affordable, sensitive, specific, user-friendly, rapid and robust, equipment-free, and deliverable to end-users [12]. Here, nucleic acid testing (NAT) is an extremely interesting tool for the detection of several pathogens. Based on its higher sensitive compared to antibody or other affinity-based detection strategies [88], therefore opening up diagnostics for a wide range of targets [89]. However, traditional methods rely on laboratory equipment and trained staff, being unsuitable for point-of-care (POC) applications [90] and therefore making it important to develop POC friendly solutions. But compared to classical lateral flow assays (LFA), NAT requires more working steps such as nucleic acid (NA) extraction, amplification, and detection. Integration into a Sample-to-Answer (S2A) format is a good way of reducing manual user input and meeting the requirements of the POC. [13,91].

Especially in resource limited settings, paper-based systems are promising as they do not require external equipment such as pumps, are portable and lightweight and generally of low costs [91,121]. Over time, paper-based devices have been developed from simple dipsticks to lateral flow assays towards more sophisticated µPADs, where, for example, complex channel designs can be realized by wax printing or vertical flow with origami designs [121,122]. This offers the potential to develop S2A devices for NAT testing on a µPAD [91]. Here, foldable components can help to integrate multiple steps, while more sophisticated channel structures can help to better manipulate the solution flow.

The first step in NAT is the extraction of NAs from a matrix, as the substances within can interfere with downstream amplification. Conventional methods are mainly based on chemical extraction or spin columns, relying on external devices such as centrifuges [36]. For POC application other solutions are necessary, whereas one common example being magnetic particles [3]. They are often used in microfluidic systems, are commercially available with different surface coatings, inexpensive and only require an external magnetic field instead of centrifuges. However, they are not suitable for the use with solid supports such as in paper-based devices [123]. Here, glass fibers are more commonly used. Nevertheless, all silica-based methods require harsh chemical conditions such as chaotropic salts during adsorption and ethanol for washing. Besides being harmful for users this can also disturb downstream amplification if not washed away properly [1,89]. Therefore, it is interesting to develop new classes of materials, capable of extracting NA under mild conditions. Based on our previous work, we developed zwitterionic nanofibers (NFs) that can extract NAs based on a charge switch mechanism [30]. NFs have typically a high surface-to-volume ratio and form porous membranes when spun into non-woven mats [97,99]. With this they are an optimal material for the integration into µPADs as NA can be extracted in a flow-through manner.

After extraction of the NAs, they must be amplified. The classic method is PCR, but this is less suitable for POC applications since it requires precise temperature cycles [91]. More suited are isothermal amplification methods such as loop-mediated isothermal amplification (LAMP) or recombinase polymerase amplification (RPA). The latter is advantageous as it requires only

two primers, has a higher tolerance against many interfering substances, a short reaction time of 5 – 20 min and typically requires lower temperatures (37 - 42 °C) [124,125]. Additionally, there are commercial options available for performing RPA and commercial LFA for detection of the amplicons [126]. Consequently, RPA has already been used for paper-based devices. While some studies performed the RPA in solution [60,63], other groups implemented it on the filter-paper test, where reagents can be stored directly within the test design [127,128].
The aim of this work is to pave the way for a S2A device based on our previously reported zwitterionic NFs. The material should first be tested and optimized on a real sample matrix such as serum by also optimizing the material properties. Subsequently, the NFs were integrated into a µPAD design, while the performance of NA extraction was investigated in a flow-through process. Finally, isothermal amplification with RPA was tested within the µPAD design and performed directly on filter paper to reduce user intervention.

4.3 Materials and Methods

Electrospinning of the Nanofibers: Nylon 6,6 NFs were produced by electrospinning. Accordingly, a spinning solution with a total polymer content of 20 wt% dissolved in concentrated formic acid. All polymers were purchased from Sigma Aldrich, and formic acid from Carl Roth. Poly(allylamine hydrochloride) (PAH) and poly(acrylic acid) (PAA) were doped in the spinning solution with a total doping rate of 20 wt% to nylon. The ratio between cationic PAH and anionic PAA was kept constant at 38 to 62 wt%.
Afterwards the NFs were electrospun with the following parameters: 22 kV, a flow rate of 2 µl·min^{-1}, a 20-G needle, at a distance of 20 cm and the constant ambient conditions of 22 °C and 40% relative humidity using a rotary drum (aluminium thin wall, diameter of 80 mm and length of 120 mm) system (Starter Kit-Aligned 40 kV**,** Linari Engineering srl, Pisa, Italy) with a rotation speed of 150 rpm. The fibers were collected on grade 1 chromatography paper, purchased from Sigma Aldrich, in non-woven fiber mats for 5 h. NFs were stored under dry conditions prior use.

Buffers Preparation: Tris-EDTA (TE) solutions were prepared by dissolving 10 mM TrizimaBase (Sigma Aldrich) and 1 mM EDTA (Carl Roth) in distilled water. Afterwards, the pH was adjusted (pH electrode from SCHOTT instruments GmbH Mainz) using either NaOH (CarlRoth) or HCl (Sigma Aldrich). For the adsorption solution the pH was set to 4.5 and 0.1% Tween20 (T20, Sigma Aldrich) (TE pH 4.5 + T20) was added, while for the elution solution 50 mM sodium chloride (NaCl, Carl Roth) was added and pH was adjusted to 10. All solutions were stored at 4 °C until use. For experiments conducted with RPA, the elution solution did not contain EDTA but instead 280 mM magnesium acetate (MgOAc, Sigma Aldrich) was added.

NA Extraction Protocol: As a model analyte, DNA from E. coli bacteria was extracted with a GenElute™ Bacterial Genomic DNA Kit from Sigma Aldrich. NAs were isolated following the instructions and stored at -20 °C prior to use.

To conduct NA extraction experiments using NFs, they were punched into circles of 6 mm in diameter using a toggle press (Berg & Schmid GmbH, Germany). Afterwards, NFs were carefully peeled of the filter paper by wetting each circle with 4 µL water and placing the free-standing fibers on the bottom of a 96-well plate with a flat bottom profile (Greiner Bio-One GmbH). In the adsorption step, NAs were diluted in the adsorption solution and 60 µL, if not stated different, were added to each well containing NFs, while for the negative controls only buffer was added. For testing of the the influence of serum, the stated amount of serum was pre-diluted in the buffers. The negative control for NA testing did contain serum but not DNA, while the negative control for serum did not contain any serum.

After 5 min incubation, for NA measurements, 40 µL of the supernatant was carefully pipetted in a fresh well, where the pH was adjusted to pH 7 by adding 10 µL diluted NaOH. For protein measurements, 5 µL of the remaining supernatant was transferred to additional fresh wells.

Before the elution solution was added, the remaining solution on the NFs must be completely removed without damaging the fibers. Then, 60 µL of elution solution were added and the samples were incubated for 20 min. Afterwards, the solutions for NA and protein measurements were removed accordingly to the adsorption step but neutralization was now conducted with 10 µL HCl.

After the extraction was finished, the dye for NAs or protein determination was added to the wells containing the supernatants. According to the protocol, OliGreen was thawed and then freshly diluted 200-fold in TE pH 7.5. Then, 50 µL of the dye solution were added and mixed with the neutralized adsorption and elution solutions directly in the wells. After 5 min incubation at RT, fluorescence was measured with the BMG Fluostar MTP (Ex: 485 ± 10 nm, Em: 520 nm, Gain: 1636). To determine the protein content, 200 µL of Pierce™ Detergent Compatible Bradford Assay Reagent (Thermo Scientific, USA) were added to the solution and incubated for 10 min at RT. Here, absorbance was measured with a BioTek reader (Abs: 595 nm, Agilent, USA).

For each measurement, four replicates were measured. Outliers were determined using a Q-test with a confidence level of 95%. To calculate adsorption and elution yields, the NA and proteins content in the adsorption solution was measured as well.

For data evaluation, mean values were calculated, and signals were corrected by the mean of the corresponding blank measurement. For both, NA and protein measurements, calibration curves were measured beforehand, according to the protocol. This allowed the calculation of the mass per well of NAs or proteins. Here, the mass of NAs or proteins in the adsorption solution, m_{added}, the mass of NAs remaining in solution after adsorption, $m_{ad\text{-}sol}$, and the eluted mass, m_{el}, were calculated.
Afterwards, the mass of adsorbed NAs or proteins, m_{ad}, was calculated as followed:

$$m_{ad} = m_{added} - m_{ad-sol} \quad (1)$$

Now the adsorption yield Y_{Ad} in % could be calculated:

$$Y_{Ad} = \frac{m_{ad}}{m_{added}} \quad (2)$$

Finally, the elution yield Y_{El} in % was determined:

$$Y_{El} = \frac{m_{eluted}}{m_{added}} \quad (3)$$

Standards deviation and Gaussian error propagation was used to determine errors of each sample.

Desing of the Extraction Zone: Channels of the µPAD design were wax printed with a ColorQube 8580 (from Xerox) on chromatography filter paper grade 1 CHR purchased from Whatman (Figure S2). To melt the channels on the paper, the sheets were baked in the oven at 140 °C for 3 min and cooled to RT prior use.
To seal the NFs, a wax ring with a diameter of 10 mm and a line-thickness of 2 mm was printed on laser foils (Overhad transparencies colour laser from AVERY Zweckforum). For the connection foils, double sided adhesive tape (from Tesa) was glued to the design, leaving the folding area free. Afterwards, the design was cut with a laser as described in the supporting information. NF mats were placed on the wax ring with the fibers facing towards the wax. This sandwich was placed between two glass slides and baked in the oven for 3 min at 140 °C. Immediately after, the fibers were removed from the glass slides and cooled to RT. The filter paper was wetted with water and peeled off to generate free-standing NFs. Afterwards, the connection foil was aligned on the NFs so that the two holes in the plastic foils are perfectly assembled allowing solutions to flow through the fibers. For the sandwich design, NFs were cut in circles of 6 mm diameter and glued between two layers of filter paper with a wax-ring design to seal it.

Flow-through NA Extraction: To determine the extraction efficiency, 1 µL of Cy5-tagged DNA (provided by collaborators, source unknown) was added directly to the extraction zone within the test design. First, 60 µL of adsorption solution was added, followed by 60 µL TE pH 7.5 as a washing solution, both with the extraction zone facing towards the waste pad. Afterwards, the extraction zone was folded towards the amplification zone and finally 60 µL of elution solution were added, now flowing through the test. To follow the extraction efficiency after each step, a fluorescence mapping was measured with the help of a Biotek (LED int. 10, Int. time 3500 s, gain 10). Data analysis was then performed in ImageJ by integrating the colored pixels area.

Production the µPAD: Self-made adhesive backing foils were produced with laminating foils and double-sided adhesive tapes. To assemble the tests for the free-standing design, the backing foil of the free-standing NFs was placed on the backing card. Then, the µPad design is glued on the connection foil, so the sample spot is aligned with the hole of the free-standing NFs.
Test- and control line were spotted on the µPad with a nanospotter (sciFLEXARRAYER S11 from SCIENION GmbH). Poly-streptavidin (BioTez BerlinBuch GmbH, Lot: K475-M) for the test-line and Donkey anti-Goat IgG for the control line (ImmunoReagents, Inc. #DkxGt-003-E, Lot: #70-53-072619) were diluted in 50 mM Na_2CO_3/$NaHCO_3$ pH 9.6 in a concentration of 2.2 mg·mL^{-1} and 1 mg·mL^{-1}, respectively. For each line, 3 rows of each 30 dots were spotted with about 4.4 – 5.2 nL each using a PDC 90 # 136289 nozzle with a voltage of 87 V and pluses of 49 µs. Tests were stored in the fridge until use.
Au-NPs (Innoca Coat@Gold conjugate kit) were modified with a goat Anti-Fluoresceine antibody (Rockland, Lot #329512951) according to the protocol. Afterwards, 1 µL of the modified Au-NPs were added to the test.

Paper-based RPA: The RPA was performed using the TwistAmp^{TM} nfo Kit from TwistDX (LOT: 115689). For every experiment a fresh master mix was prepared according to Table 4.1. Then, the master mix without MgOAc was added to the lyophilized RPA mixture and resuspended carefully. Sequences of the used primers can be found in the supporting information (Table S4.2).

Table 4.1: Composition of one RPA master mix:

	concentration	**volume / µL**
hydration buffer	/	29.5
forward primer	10 µM	2.1
reverse primer	10 µM	2.1
probe	10 µM	0.6
water	/	2.2
MgOAc	280 mM	2.5

To test the RPA in solution, 10 µL of MgOAc were added to start the reaction and the solution was incubated at RT for 10 min. The success of the reaction was tested with commercially available dip sticks (Milenia GenLine HybriDetcet, LOT: 049). For this, the RPA solution was diluted 10-fold in the buffer delivered with the kit in vial, where the dipstick was added. After 5 min the results were obtained and documented under constant light conditions.
To test the RPA on filter paper, 80 µL of the RPA resuspended in buffer were added to the amplification zone on the µPad and dried. Then, primers and probe were also directly added to the RPA zone. After complete drying, a 1:50 dilution of the amplicons in the elution buffer containing the MgOAc was added to the RPA zone and the test was run for 20 min at RT before signal readout.

4.4 Results and Discussion

4.4.1 Interference of Adsorption with Serum Samples

Zwitterionic NFs have been developed and tested for NA extraction in previous studies [30]. BSA was tested as an interferent and the reduction in adsorption could be minimized by simple dilution in buffer. Nevertheless, for future application real sample matrices need to be tested, which should be done in this study.

Since serum is an interesting sample matrix for many diseases, its interfering potential should be investigated [14].

First attempt was again a simple dilution approach (Figure 4.2A). While the addition of 1 µL serum did not result in a reduction of adsorption, with 2 or 3 µL a drastic drop can be seen. Compared to the amount BSA added in the previous work, this would equal to 2 – 3 µL serum. [30,118]. Thus, the adsorption yield was not reduced for pure BSA, leading to the conclusion that not only the serum proteins but other components such as salts or lipids influence the adsorption efficiency [118].

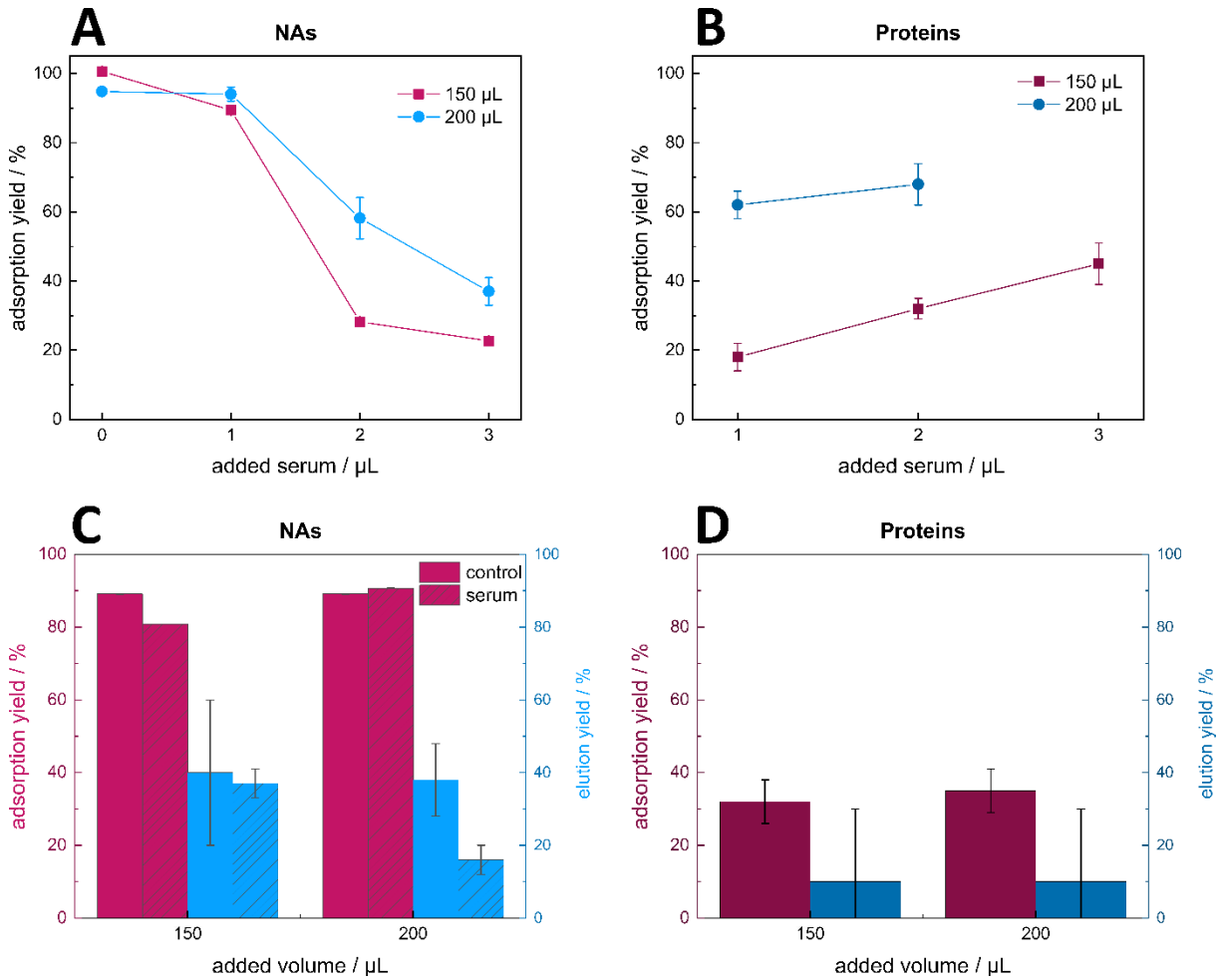

Figure 4.2: Influence of the addition of serum to zwitterionic NFs. Adsorption of NAs (A) and protein (B) on zwitterionic NFs depending on the volume of added serum to 150 or 200 µL of TE buffer, pH 4.5. (C) Comparison of the extraction efficiency of NAs from zwitterionic NFs from 150 or 200 µL buffer with no or 1 µL serum added and the behavior of proteins (D).

For both, NAs and proteins, a higher adsorption yield was found for a dilution in 200 µL. Surprisingly, proteins also showed a higher adsorption when more serum was added, regardless of the volume (Figure 4.2B), which cannot be further explained at the moment.
To test the impact of dilution on the elution yield, the whole extraction was investigated of 1:150 and 1:200 serum to buffer ratios (Figure 4.2C and D). Both samples with a total volume of 150 µL had a comparable extraction efficiency with and without serum and are therefore being optimal for the use of serum (Figure 4.2C). The reduced elution efficiency with 200 µL sample could be due to inefficient mixing based on the larger volume. Serum proteins adsorbed to the NFs with about 30 - 40% but only small amounts of protein were found in the elution solution, which are not expected to interfere with downstream amplification reactions (Figure 4.2D) [129].
However, a dilution factor of 1:150 is very high and further optimization should be done to increase the binding efficiency in the presence of serum samples. It is expected that proteins or other charged substances from the serum matrix compete with the NAs for the positively charged binding sites of PAH. Therefore, increasing the number of binding sites could enhance the extraction efficiency (Figure 4.3A). Here, either the PAH content in the NFs could be increased or the adsorption pH could be decreased as more functional groups should be charged based on the pk_a of PAH [130].
To test the influence of the number of cationic groups on the adsorption efficiency in the presence of serum, the zwitterionic NFs were tested in comparison to the cationic nylon-PAH NFs with increasing amount of serum (Figure 4.3B). While the adsorption yield on the zwitterionic NFs already deceased to about 30% in the presence of 3 µL serum, the adsorption yield of nylon-PAH fibers was still above 80% under the same conditions. While the absolute adsorption of proteins on the two fiber types were similar, the trends were inverse (Figure 4.3D). On the zwitterionic NFs with more added serum the yield of adsorbed proteins increased, while on the cationic fibers the amount was reduced. This could be explained as nylon-PAH NFs have only cationic groups on the surface while zwitterionic NFs at pH 4.5 provide both cationic and anionic groups, so proteins with positive surface potential, such as BSA at pH 4.5, have more possible interaction sites [130,131]. In conclusion, an increase of the PAH content can help to increase adsorption efficiency but for pure cationic NFs no elution could be found as shown in previous studies [30]. Therefore, the ratio between PAH and PAA should be optimized to increase the binding efficiency while also maintaining the elution functionality of the fibers.

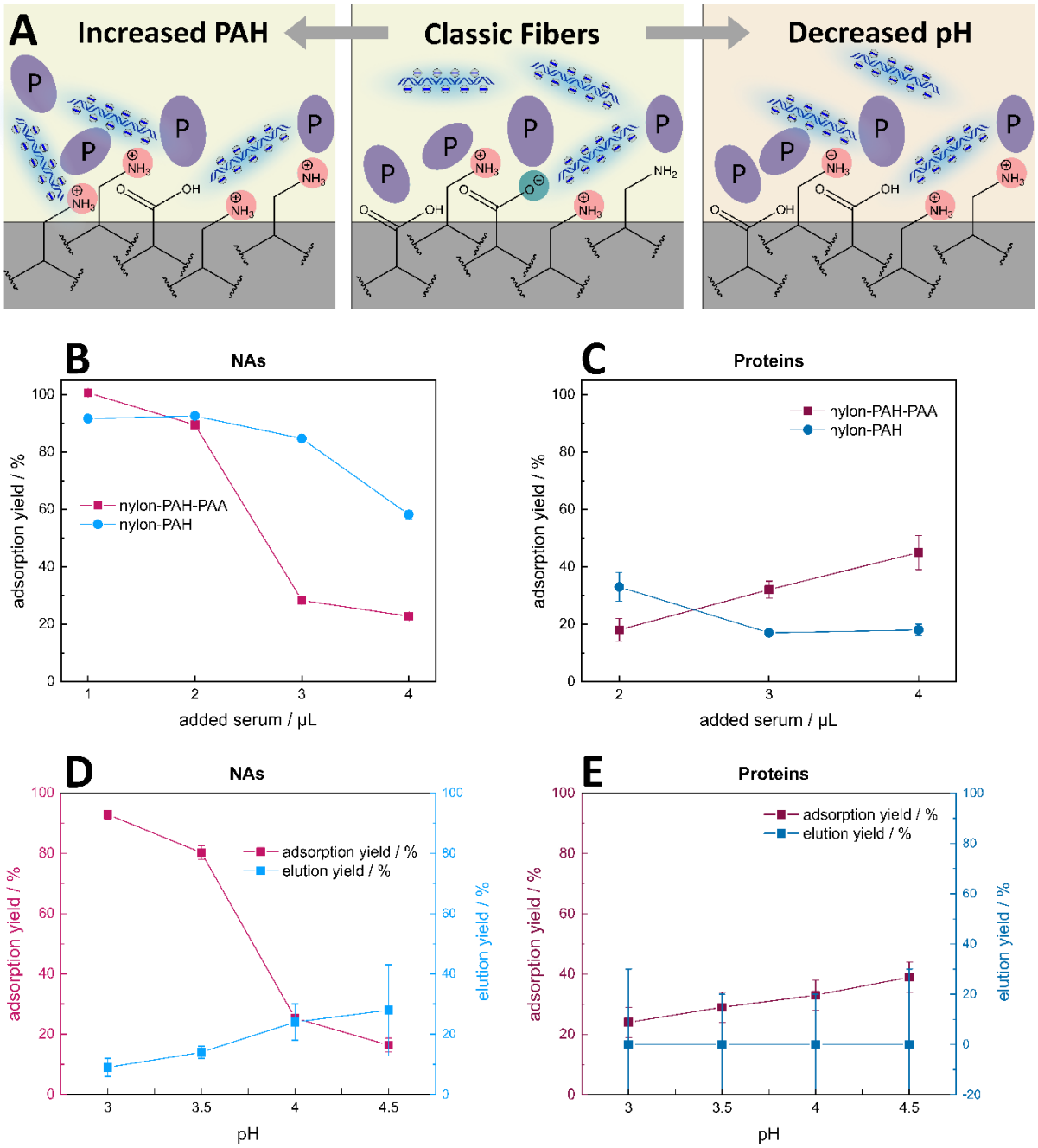

Figure 4.3: Strategies to enhance the binding efficiency of NAs on zwitterionic NFs in the presence of serum. (A) Schematic illustration of possible enhancements of the binding site by either increasing the PAH content or decreasing the adsorption pH . Comparison of the adsorption behavior of NAs (B) and proteins (C) on zwitterionic nylon-PAH-PAA or cationic nylon-PAH NFs in the presence of different amounts of human sera in 200 µL buffer volume. Influence of the adsorption pH on the extraction efficiency of NAs (D) and the behavior of proteins (E)

The second approach was to decrease the adsorption pH (Figure 4.3D and E). As expected, the adsorption yield increased with decreasing pH in the presence of serum. Meanwhile, the adsorption of proteins is reduced as the surface potential of both proteins and the NFs becomes more positive [131]. However, the elution yield of the NAs is also reduced at lower adsorption pH values. A less efficient charge switching of the NFs during the addition of elution solution may be the reason.

In summary, enhancing the number of binding sites can indeed increase the binding efficiency of the NFs but may also reduce the elution efficiency. Future studies should therefore optimize the doping ratio of PAH and PAA and test the performance in the presence of serum. A further step can be the reduction of the adsorption pH, where a higher doping of PAA could maintain the elution efficiency. Therefore, it would be interesting to either increase only the amount of PAH or to increase the overall doping while keeping the ratio of PAH and PAA constant.

4.4.2 Integration of NFs into a µPAD

An envisioned application of the zwitterionic NFs would be their integration into a µPad design. Therefore, a feasible way to integrate and protect the NFs within the test design was necessary. The sandwich method, developed by our collaborators at the KMUTT in Bangkok, consisted of sandwiching the fibers between two layers of filter paper imprinted with a wax pattern to guide the fluid flow only through the fibers (Figure 4.4B). Since the NFs were mainly tested as free-standing NFs, an alternative was developed to allow the use of free-standing NFs. For this, the NFs were sealed by a wax ring and embedded between two layers of plastic foil for protection and stabilization (Figure 4.4A). In addition, the connection foil was used to integrate the extraction part within the µPad. However, bending of this design was difficult due to the stiffness of the plastic film. Therefore, a method was developed to weaken the materials in the desired bending region. Here, engraving dots, lines or ablation of the material with a laser was tested (Figure S4.4). With the shortest engraving time and high bending ability, the engraving laser-ablation was chosen as an optimal bending method and will be used in further experiments.

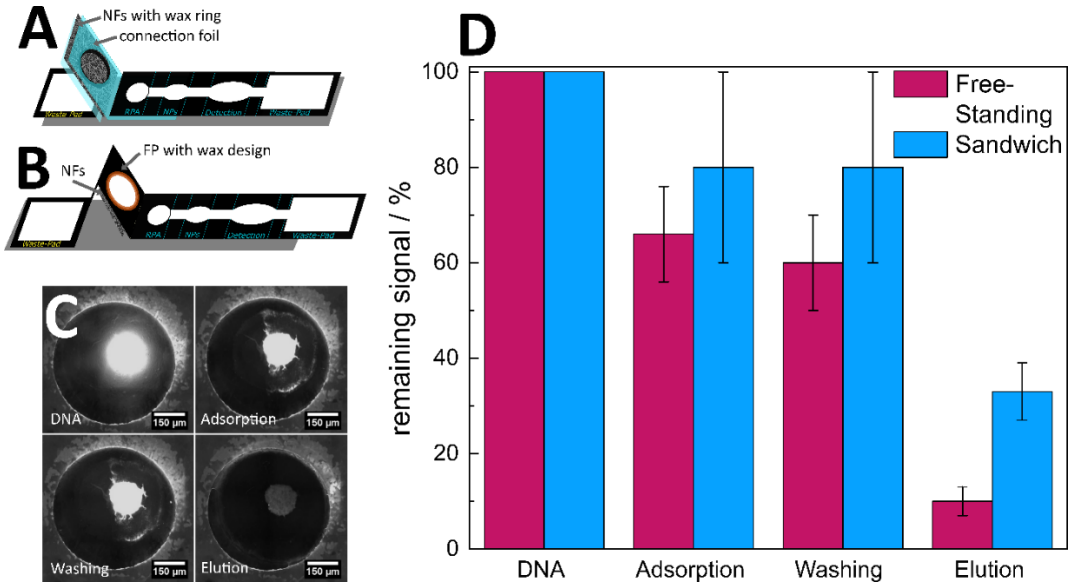

Figure 4.4: Integration of NFs in a paper-based microfluidic system. Schematic illustration of the free-standing design where NFs are sealed with a wax ring and sandwiched between two plastic foils (A) and sandwich design where NFs glued in between two layers of filter paper sealed with wax (B). Flow-through extraction of NAs on the free-standing design followed by fluorescent labeled NAs (C). Comparison of the extraction efficiency of both designs by evaluation of the contrast by ImageJ from the measurements shown in C (D).

Both designs were investigated for efficient extraction of NAs in a flow-through setup. The process was tracked with Cy5 labeled DNA (Figure 4.4C and D). NAs could be efficiently

adsorbed in both designs with no loss of NAs during washing. However, elution of NAs was much more efficient from the free-standing NFs. As also leaking could be reduced with this design, it will be used further. Furthermore, these results may indicate a higher extraction efficiency of the NFs within a flow-through design compared to the extraction within a MTP. While the contact time is reduced, the whole solution is flowing through the membrane allowing a more efficient extraction. However, further testing would be required to prove this theory.

4.4.3 Integration of RPA within the µPAD

Finally, the extraction should be coupled to RPA as an isothermal amplification method as lower temperature is required for amplification and it can be performed directly on filter paper [124,125].

Therefore, RPA with established primers was first tested only with commercially available dipstick assays to optimize the reaction conditions (Figure S4.4). Here, an incubation time of 10 min, even at RT, was sufficient for a strong signal.

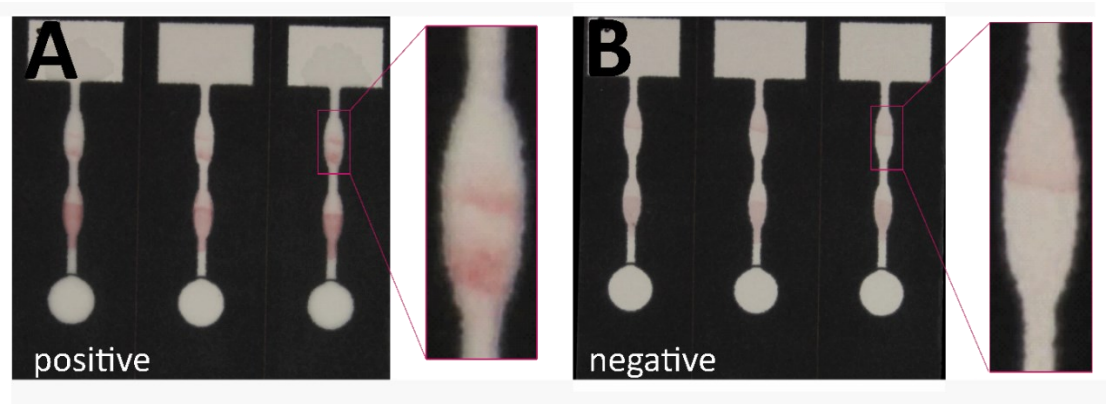

Figure 4.5: Results of the optimized RPA run on the µpad at RT with the addition of DNA (A) and the negative control (B).

For a S2A device, RPA should be performed directly on the filter paper in the µPAD design, which have been already proven in literature [126]. Consequently, the RPA mixture, primers and Au-NPs were pre-dried directly on the test. To reduce primer noise, MgOAc was separated from the RPA mixture and added directly to the elution solution [127]. Subsequently, target NAs diluted in this elution solution were added to the test, where the signal could be read out in 20 min. In Figure 4.5, two developing lines could be seen for the positive tests, while only one line was visible in the negative control, indicating a successful RPA directly within the µPAD. However, the transport of the Au-NPs through the test was not efficient, which is shown by a remaining red color below the readout area. This might be also the reason why the signals are very weak. Further optimization is needed to prevent this. In addition, the flow through the test was very slow. This could be solved in the future by sealing the test with adhesive tape to prevent evaporation.

4.5 Conclusion and Outlook

This study demonstrated that NAs can be extracted with our zwitterionic NFs from the real sample matrix serum, but the NFs need to be further optimized to increase binding in the presence of higher serum concentrations. This could be done by a combination of optimizing the PAH and PAA content in the fibers while lowering the adsorption pH.

Meanwhile, efficient extraction in flow-through setups has been demonstrated, especially when using free-standing NFs. Here, a layering approach with an imprinted wax-ring was developed to protect the NFs, while defining the contact area with the solution. A bending line for easier folding of the plastic foil was developed by laser ablation.

The µPAD design itself is produced using a wax printer. A test and control line were successfully nanospotted on the paper-based design. RPA was also performed on the test by drying the reagents directly on the test-design. Future studies need to optimize the flow of the Au-NPs within the µPAD to improve the visibility of the lines. Also, extraction and amplification have not yet been tested together. The goal would be to extract target NAs from serum samples and detect them, all directly in the µPAD.

4.6 Supporting Information

Production the µPAD:

The designs of the wax-printed and laser-cut parts of the µPAD were done as vector graphics with CorelDraw suite 24.0 (Figure S4.1 and S4.2). Here, a color code was used, where black are the wax printed areas, red was used for cutting the material and green for laser ablation. The color profile was set to RGB (Table S4.1). The lines for laser cutting were drawn as hairlines without defined thickness, so the laser cutter could work in vector mode.

To produce the extraction section of the µPAD design, first the wax rings were printed onto the plastic foil (Figure S4.1 A). For the connection foil, double sided adhesive tape was placed on the foil, leaving the folding area free (green). Afterwards, the prints were placed in the laser cutter and carefully positioned in alignment with the center of the printed circle or the folding area.

Then the designs were cut with a laser cutter (Figure S4.1 B and C). This was done by using a VLS 2.0 laser engraving system based on a 10600 nm infrared laser with a maximum power output of 30 W. Laser settings for the different color codes can be found in Table S 4.1.

Table S 4.1: Color coding for laser settings:

Color	function	Speed / %	Power / %	Color in RGB
Red	cutting	76	90	255:0:0
Green	laser ablation	90	7.5	0:255:0
Black	Wax printing	/	/	0:0:0

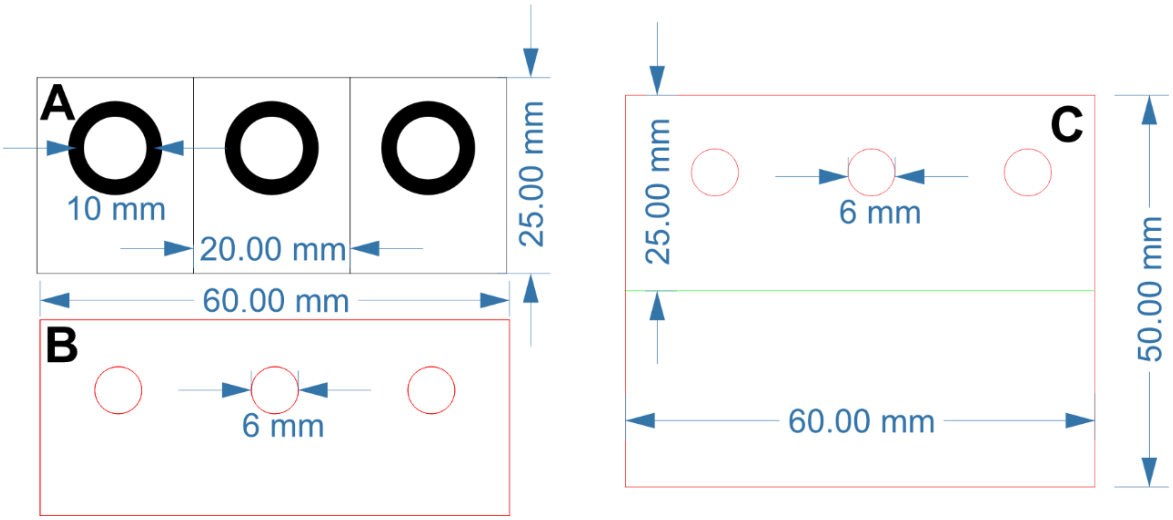

Figure S 4.1: Dimensions of the NF extraction zone for the free-standing design to produce triplicates. (A) Scheme for wax-printing with (B) the corresponding design for laser cutting. (C) Scheme for laser cutting of the connection foil. Color-code: Black: Wax-printing, Red: Cutting, Green: Laser ablation.

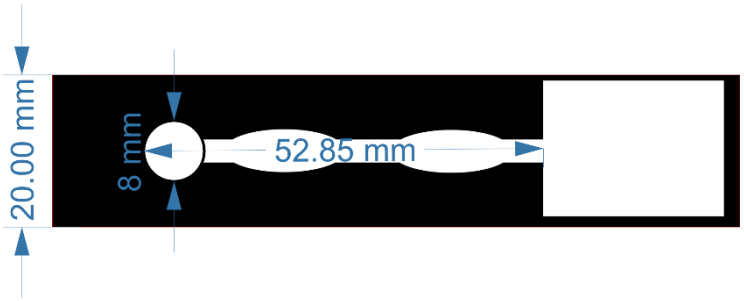

Figure S 4.2: Scheme of the µPad for wax-printing (with dimensions).

Paper-based RPA:

Table S 4.2: Sequence of the primer used for the target pBlue (e.Coli), designed and provided by Dr. Sebastian Kersting, IZI-BB Fraunhofer Institute in Potsdam.

Primer	Sequence	Origin
Forward Primer	5'-cagcaacgcgggcctt-3'	Biomeres.net
Reverse Primer	5'attaatgaatggcggt-3'	Biomeres.net
Probe	5'-tcttccgcttggctgc-3'	Biomeres.net

Results and discussion

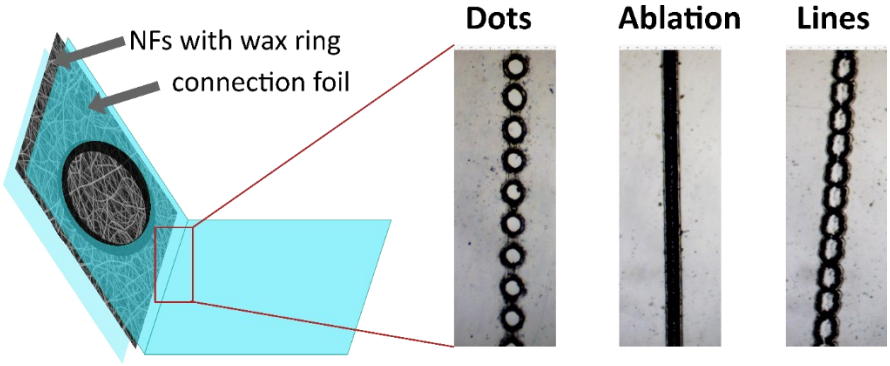

Figure S 4.3: Microscope images of different options to enhance the foldability of the plastic foil.

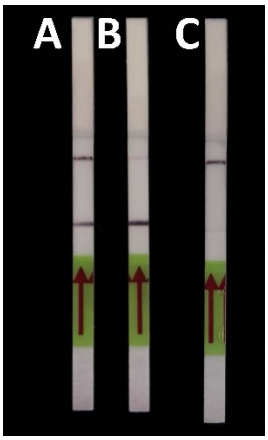

Figure S 4.4: Results of the RPA on commercial dipsticks. (A): Amplification 10 min @RT; (B): 20 min @ 40 °C; (C): negative control 10 min @RT.

5 Simplified Production of Irregularly-Shaped True-to-Life Microplastics with Embedded Optical Labels for the Realistic Assessment of their Biotoxicity *in vivo*

5.1 Abstract

The ubiquity of microplastic and the lack of understanding of its biotoxicity drives the desire to develop model systems with which this complex issue can be addressed. The vast variety of physical structure of microplastic is typically not given justice in most toxicity studies. Here, we propose that using electrospun polystyrene nanofibers (NFs) can provide the desired mostly irregularly shaped and sized particles, and can easily be translated to other polymers. Upon mechanical disruption of the NFs, microparticles of sizes of (4 ± 3) µm for ball milling, and lengths of (20 ± 20) µm for shear force exfoliation processing are obtained. Compared to literature, about 10-times faster and simpler MP production is achieved. Using organic dyes and inorganic upconverting nanoparticles as dopants, imaging under standard or NIR exposure conditions is provided. Minimal leaching over the time course of 35 days (DPA: 0.0023 wt%, and UCNPs: 0.2 wt%) indicates stable embedment.

Finally, *ex vivo* application in murine kidneys serves as example for imaging studies, where the particles deposit in small renal vessels and glomerular capillaries. Overall, this rugged and irregularly shaped material is very easy to produce, which may make it an excellent candidate for future environmental and biological studies.

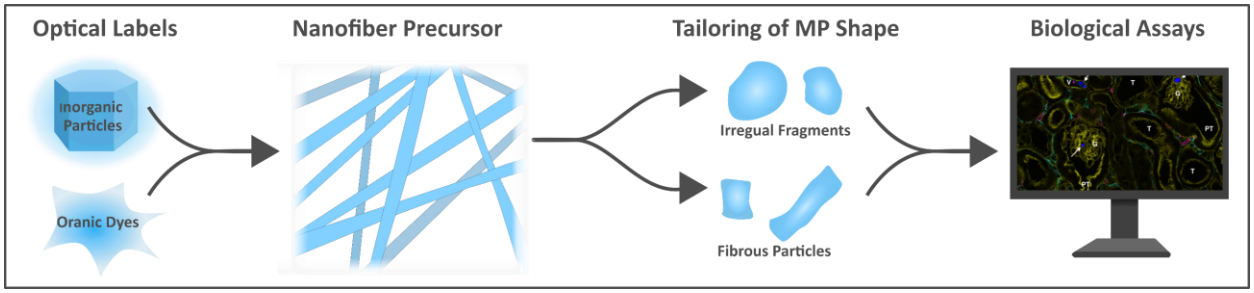

Figure 5.1: Table of Contents

This chapter is considered to be published in Advanced Functional Materials

Author contributions:

All experiments have been designed have been designed and condutced by the three main authors Hannah Triebel, Sophia Baumann and Alissa Wieberneit. Sarah Dietrich supported the team with lab work regarding the production of NFs and MP. The project was lead by Prof. Antje Baeumner and Prof. Hayo Castrop. Manuscript preparation was done by the three main authors under the lead of Prof. Antje Baeumner and Prof. Hayo Castrop. Dr. Nongnoot Wongkaew and Dr. Thomas Hirsch supported with strategic discussions SEM pictures were provided by Christoph Buckschlegel and TEM images by Christoph Bühler.

5.2 Introduction

Plastics in general are chemically inert and persist in the environment for prolonged periods. The annual rise in plastic production serves as an indicator of the increasing consumption of plastics by industry and consumers [132]. The degradation of plastic into particles in the environment involves mechanical and radiation-mediated breakdown, which eventually leads to the formation of microplastics (MPs) (< 5 mm) and nanoplastics (< 100 nm) [133]. The majority of MPs in aquatic or terrestrial ecosystem [134,135], and in the human body, consist of fragments and fibers [136,137]. In fact, MPs have been detected in almost all human tissues [133,138–143]. Most of the particles found in the ecosystem are in the size range between 1-100 µm [137]. For detection of MPs, the most common methods are microscopic evaluations (fluorescence, scanning electron) coupled to spectroscopic methods for chemical analysis such as Raman or FT-IR [144–146]. Additionally, attempts were made towards a detection by subsequent fluorescence staining of environmental MPs [146,147]. Current labeling strategies of MPs include carbon dots [148], inorganic particles [149–151], and radioactive labels [152]. However, Fluorophores are most the commonly used optical labels, considering their high quantum yield of nearly 100% under optimal conditions[150,153] and their cost-effectiveness. Nevertheless, fluorophores can suffer from photobleaching, which should be considered regarding sample handling and long-term measurements. Due to their broad absorption and emission bands, fluorophores used for staining of MPs in tissue studies must be carefully selected to avoid spectral overlap, like in the case of Nile Red, a fluorophore commonly used to detect MPs[146]. To avoid the issue of photobleaching, upconversion nanoparticles (UCNPs) are regularly used as alternative optical labels since their composition of stable inorganic material does not change under irradiation [154,155], and first attempts of doping UCNPs into microplastic have been reported[151]. However, the circumvention of photobleaching comes at the cost of lower quantum yields of max. 13% [156]. Nonetheless, UCNPs are attractive for tissue studies due to their excitation in the near-infrared (NIR) as the penetration depth of the excitation light is increased compared to UV/Vis excitation [157–159].

In contrast to the MPs found in the environment, most experimental studies were conducted with spherical PS particles [135,160–162] owing to their commercial availability. Experiments with spherical particles can give indications, but as the shape of the MPs is a relevant factor for the effects of MPS on organisms [135]. To also consider shape factors and not only material and size, studies should aim to use true-to-life MPs, i.e. fragments and fibers. In this sense, researchers face two challenges: selective, stable labeling of MPs and the production of MP fragments or fibers. Current strategies employ retroactive MP staining with dyes dissolved in solvent [163] [164] for a better integration of the label. Other options consisted of simultaneous melting or dissolution of the polymer and dye [165] [166]. To achieve the desired shapes, researchers explored techniques such as lab-based weathering[161] and sonication[167] resulting in particles of 1-3 µm and 0.1-1000 µm, respectively. Furthermore, ball milling (BM), often combined with liquid nitrogen cooling, is frequently used to produce irregular particles [161,168–170], resulting in polystyrene (PS) particles ranging from approximately 5-200 µm in size [160,167,171,172]. First

attempts towards the production of fibrous MPs have been made by sectioning commercial fibers with a cryotome resulting in dimensions of 10x10x40 µm [163].

Recent studies using PS spheres demonstrated a high correlation between the MP particle size and their accumulation in tissues, with 4-20 µm having a higher propensity for tissue accumulation[173,174]. Accordingly, Stock et al. provided evidence for an increased uptake of 4 µm PS spheres in intestinal epithelial caco-2 cells compared to those of 1 µm in diameter, suggesting that the 4 µm particles can be taken up by phagocytosis and pinocytosis instead of phagocytosis only [174]. Given its limited regenerative potential [175], the kidney is of particular interest in toxicity studies. Since it is known that human or rat erythrocytes (biconcave, about 7.5 µm in diameter) can get stuck in glomerular capillaries of mice (erythrocytes about 5 µm in diameter) [176], a MP size of about 5 µm in an irregular shape opens the interesting scenario if they can get stuck in these small vessels because of their shape not their size. Accordingly, the mouse isolated perfused kidney model (MIPK) offers a good opportunity to investigate this, since it comes close to *in vivo* experiments and allows a defined introduction of MPs into an intact kidney without being dependent on intestinal absorption [177].

This study focused on material development of MP for toxicity studies. Specific focus was on the generation of irregularly shaped true-to-life MPs, developing an alternative for uniformly spherical particles. Doping with optical labels enabled imaging and detection in biological assays. Probe selection of both, organic and inorganic labels, considered autofluorescence and general staining strategies to fit into standard protocols for fluorescence microscopy. Potential leaching was addressed by direct embedding of the optical labels into the polymer matrix. The effect of different polymer types was not considered, as this will be part of a subsequent study. However, the applicability of the generated rugged fluorescent MP was demonstrated using MIPK as an ex vivo model. The materials were characterized in terms of size, shape and luminescent properties using scanning electron microscopy (SEM), transmission electron microscopy (TEM), fluorescence and extinction, luminescence measurements and microscopy images, using confocal microscopy also equipped with a 2-photon laser.

5.3 Experimental

5.3.1 Labeling of Microplastic

5.3.1.1 Fluorophores

Knife Coating of Polymer Foils

Knife-coated polymer foils were produced from polymer-solutions according to the same protocol as for electrospinning. To determine the optimal doping concentration and dye, the solutions were doped with different weight percentages of perylene or DPA. To determine influence of solvents on the fluorescence spectra, solutions with either produced with a 1:1 mixture of DMF:THF or pure chloroform while keeping the polymer and dye concentration constant.

The polymer foils with an approximate size of 5.5 x 11.0 cm were produced with an in house build knife coater. The thickness of the coatings was set to 30 µm with the help of spacers. A cleaned mylar support was placed on the coater and 330 µL of the solution were added. By pulling the knife over the foil a uniform film was obtained. The polymer films were dried for 3 – 4 h at 80°C in the oven before use.

To measure the absorbance and fluorescence, the foils were cut with a laser cutter (detailed information can be found in SI) and glued with double sided adhesive tape (Tesa) to the backside of a bottom-less black 96 well plate (Greiner Bio-One). Afterwards, absorbance spectra (300 to 700 nm, step 1 nm) and fluorescence spectra, were measured with a BioTek reader (Agilent, USA) as summarized in Table 1.

Table 5.1: Overview of the measurement parameters of the fluorescence spectra.

Ex / nm	Slit size / nm	Em start / nm	Em end / nm
405	10	430	700
488	10	510	700
561	10	590	700
633	10	660	700

The mean and the standard deviation of the data from eight wells were calculated and plotted. To obtain the maximum fluorescence signal depending on the concentration of the dye, the maximum fluorescence signal was plotted against the concentration.

Photobleaching Study

For the photobleaching studies, the knife coated foils were excited with a Xenon lamp (DPA 385 nm, Perylene 405 nm) with a band width of 16 nm for several hours. The resulting fluorescent signal was continuously measured every 5 s with a AMINCO Bowman Series 2 spectrofluorometer (AB2) with fiber optics (Thermo Spectronics, now Thermo Fisher Scientific). The initial fluorescent signal was normalized to 100%.

5.3.1.2 Upconversion Nanoparticles

Synthesis of Core UCNPs

(Yb,Tm)-doped β-$NaYF_4$ upconversion nanoparticles were prepared according to a modified protocol by Schroter et al.[178]. For a 5 mmol batch size, $YCl_3 \times 6\ H_2O$ (3.72 mmol, 78%), $YbCl_3 \times 6\ H_2O$ (1.25 mmol, 25%), and $TmCl_3 \times 6\ H_2O$ (0.015 mmol, 0.3%) were dispersed in methanol. The solution was transferred to a three-necked round-bottom flask under nitrogen atmosphere. Then, oleic acid (30 mL) and 1-octadecene (50 mL) were slowly added. The mixture was heated to 110 °C, and vacuum was applied for one hour. Afterwards, the reaction solution was cooled to room temperature, and NH_4F (20 mmol), Na-oleate (15.65 mmol), and 1-octadecene (25 mL) were added. Vacuum was applied for 50 min, followed by degassing of the solution three times. The solution was then heated to 315 °C with a heating rate of 16 °C per minute and kept under reflux for 20 min, followed by rapid cooling to room temperature. For purification, the reaction mixture was first collected in centrifuge tubes by precipitation with an excess of ethanol and centrifuged at 3850 *g* (10 min), with a Hettich Universal 320R centrifuge. The resulting pellets were redispersed in a small amount of cyclohexane, precipitated again with excess of ethanol, and collected by centrifugation (3850 *g*, 10 min). This process was repeated twice. Finally, the particles were redispersed in cyclohexane (30 mL) and aggregates were removed by centrifugation (1200 *g*, 5 min). The final particle dispersion was stored at 8 °C until further use.

Core-shell Synthesis

For equipping the core particles with an inert shell, α-$NaYF_4$ were synthesized and used as shell precursor material [178]. In a 10 mmol batch size, $YCl_3 \times 6\ H_2O$ was dissolved methanol and added to a three-necked round-bottom flask under nitrogen atmosphere. Oleic acid (80 mL) and 1-octadecene (150 mL) were slowly added. The mixture was heated to 160 °C, and vacuum was applied for 30 min. After cooling to room temperature, NH_4F (40 mmol) and NaOH (25 mmol, dissolved in MeOH) were added. The solution was heated to 120 °C and kept at this temperature for further 30 min. Afterwards, the reaction mixture was heated to 240 °C (16 °C·min^{-1}) under reflux for 30 min. The solution was rapidly cooled to room temperature and purification was performed, as described for the core particles.

For a shell thickness of approximately 3 nm, core particles dispersed in cyclohexane (1 mmol regarding the total lanthanide content), oleic acid (5 mL), and 1-octadecene (5 mL) were added to a three-necked round bottom flask and heated to 100 °C under constant nitrogen flow. In a second flask, the α-$NaYF_4$ particles (1.7 mmol, regarding the total lanthanide content) dispersed in cyclohexane, oleic acid (8.55 mL), and 1-octadecene (8.55 mL) were also heated to 100 °C. After applying vacuum to both flasks for one hour, the flask containing the core particles was heated to 315 °C (16 °C·min^{-1}) under nitrogen atmosphere. During heating, distinct amounts of precursor solution was added to the reaction mixture with a syringe. The first addition (1 mL) was carried out around 230 °C. At 315 °C, every 8 min, increasing amounts of the precursor solution was added to the core particles to ensure a uniform shell growth. After the last addition,

the reaction was kept at 315 °C for further 8 min, followed by a rapid cooling to room temperature. Purification of the particles was performed as described above.

Surface Modification for Dispersion in DMF:THF

For the embedding of the UCNPs into the nanofibers, the oleate-coated particles have to be stabilized in a mixture of 1:1 (v/v) DMF:THF in the spinning solution, containing also the PS. For this, a ligand removal reaction was carried out following for the core-shell UCNPs a well-established protocol with slight adjustments [179]. For a 100 mg batch size (mass UCNP), the particles dispersed in cyclohexane were added to a round-bottom flask, and DMF (6 mL) was slowly added under constant stirring. The mixture was heated to 30 °C for 10 min. Then, $NOBF_4$ (150 mg) was added, and the temperature was increased to 60 °C. The stirring speed was increased to 1200 rpm and the reaction was held at elevated temperatures for 30 min. Afterwards, the solutions was ultrasonicated for a few minutes. For purification the particles were precipitated from the cyclohexane-DMF mixture by adding an excess of chloroform, followed by centrifugation for 15 min at 2500 *g*. The resulting pellet was redispersed in a 1:1 DMF:THF mixture.

Characterization of UCNPs

Transmission electron microscopy (TEM) was performed on a 120 kV Philips CM12 microscope by FEI GmbH. For sample preparation, the particle dispersions (1 $mg \cdot mL^{-1}$) were dropped on carbon-coated copped grids (400 mesh). NFs were spun directly onto the grid for TEM evaluation. To evaluate the size distribution, several micrographs were taken and analyzed using the software ImageJ (Fiji, v1.54f) with the plugin ParticleSizer by Thorsten Wagner, and Origin (Version 2022b). The determination of particle concentration and composition was performed using inductively coupled plasma optical emission spectroscopy (ICP-OES) from SPECTRO (SPECTROBLUE FMX36). Calibration was carried out using a multielement standard from PerkinElmer. The nanoparticle dispersion (10 µL) was dried and dissolved in concentrated sulfuric acid (0.5 mL). Then, nitric acid (1.5 M, 9.5 mL) was added. Lanthanide concentrations were calculated as the mean value from three subsequent measurements. Colloidal stability was analyzed using the Zetasizer NanoZS from Malvern Panalytical to measure dynamic light scattering (DLS). All samples were measured three times. Luminescence measurements were performed using a home-build set-up, equipped with a 980 nm laser module (200 mW, 156 $W \cdot cm^{-2}$, cw) from Picotronic, and a spectrometer for UV-Vis from Broadcom (Q_{mini}). Spectra were collected from 225 – 1000 nm, with a short pass filter (cut-off 850 nm) and a bandpass excitation filter (cut-off 900 nm) to record upconversion luminescence, using the software *Waves* (RGB Photonics). For luminescence measurements of UCNP in a PS matrix, MP particles ($\beta_{initial}$ = 4 $mg \cdot mL^{-1}$) were stabilized in a 1 wt% soy lecithin solution and further diluted in a 1:10 ratio with bidest. water. Photographs of particle solutions and nanofiber-mats have been taken with a DLSM camera (Canon EOS R6) and a macro lens, including a NIR filter to block the laser.

5.3.2 Production of Nanofibers and Microplastic

5.3.2.1 Production and Characterization of Nanofibers

Electrospinng

PS-NFs were produced by electrospinning. For this purpose, a spinning solution of 15 wt% PS (MW ≈ 28,000) in 1:1 ratio of DMF and THF was stirred overnight in the dark. If not stated different 0.3 wt% DPA relative to the PS mass was added to the solution to obtain fluorescent NFs. The NFs were electrospun with a rotary drum system (Linari NanoTech). The solution was fed with a flow rate of 30 $\mu L \cdot min^{-1}$ through an in house-build four needle holder connected to 18 G needles. The distance between needle and collector was kept at a distance of 15 cm. A voltage of 11 - 12 kV was applied and ambient conditions were kept at 22 °C and relative humidity below 35%. The NFs were collected for 3 h on aluminum foil. The NFs were stored in the dark at ambient conditions until use. Before microplastic production NFs were separated from the aluminum foil. Size evaluation of SEM images was done using ImageJ (Fiji, v1.54f). For the preparation of the polystyrene spinning solution doped with UCNPs, polystyrene (1050 mg; MW: 280,000) was weight and added into a flask. UCNPs in DMF (β = 50 $mg \cdot mL^{-1}$, 3.5 mL) were added under stirring, followed by the addition of THF (3.5 mL). The mixture was stirred at least overnight, to obtain a clear and homogeneous solution. Afterwards, NFs were produced by electrospinning following the same protocol as described above (chapter 2.1.1).

Leaching Study

To investigate the potential leaching of fluorophores or UCNPs from the nanofibers, PS-DPA NFs (515.82 mg) or PS-UCNP NFs (325.1 mg) were stuffed in a dialysis tube (cut-off: 12-14 kDa, Spectrum Labs™ Spectra/Por™) and transferred to a Schott flask (100 mL). Bidest. water (80 mL) was added, and the dialysate was exchanged at day one, two, seven, ten, 14, 28, and 35. Afterwards, the dialysate completely evaporated, and the flasks were either rinsed with 1.5 mL chloroform for PS-DPA NFs, or conc. H_2SO_4 (0.5 mL), followed by the addition of HNO_3 (1.5 M, 9.5 mL) to prepare the samples for ICP-OES measurements in case of PS-UCNP NFs. For the fluorophores, fluorescence spectra were recorded. Afterwards, the percentage of leaching was determined using the integration of the signal between 421 to 441 nm. Based on a calibration curve, the total mass of leached DPA was calculated. In case of PS-UCNP-NFs the mass loss was determined by calculating the ratio between the mass determined with ICP-OES and the theoretical total mass of UCNPs inside the NFs (calculated from the mass used, assuming a homogeneous distribution of the UCNPs within the NFs).

5.3.2.2 Production of Microplastic

Ball Milling

NFs were milled using a planetary ball mill (PM100, Retsch). NFs were filled into a 50 mL grinding jar together with seven 10 mm grinding balls. Due to the high volume of the NFs before milling, several pre-grinding steps were necessary for 30 s at 550 rpm to break the fibers into fragments. After every 30 s step, more NFs were added to the grinding jar and broken down. When the jar was filled to around 1/3 with NF fragments, the main grinding was started. This process consisted of 9 cycles of 2 min milling at 550 rpm, each followed by 1 min of cooling on ice. Intermittent cooling was performed not to exceed the glass transition temperature of polystyrene (around 100°C).

As an alternative to the use of 7 large balls (10 mm in diameter), about 3000 balls of smaller size (2 mm in diameter) were used to increase the frictional force at the expense of a lower impact force. The pre-milling and main milling steps remained the same as for the bigger balls. In a third setup, both milling processes were combined (pre-grinding with bigger balls, 9 cycles bigger balls, 9 cycles smaller balls), leading to the application of impact force followed by frictional force.

Prior to use, the particles were emulsified in a 1 wt% soy lecithin solution by ultrasonication and vortexing.

Cryo Milling

NFs were broken down using cryogenic grinding (CryoMill, Retsch). Specifically, 400 mg NFs were filled into a 50 mL grinding jar together with 8 grinding balls of 12 mm diameter. The material was pre-cooled for 13 min with liquid nitrogen surrounding the grinding jar. The milling process consisted of 9 cycles (2 min, each) milling at 30 Hz plus 1 min of intermitting cooling per cycle.

5.3.2.3 Ultraturrax

20 mL of a 1 wt% soy lecithin solution was added to 240 mg of NFs to keep the hydrophobic PS in solution. Emulsification was conducted using an Ultraturrax (IKA T18 basic). To keep the temperature constant, the solution was kept on ice and shredded for one-minute cycles. Subsequently, the solution was cooled for 5 min in between the shredding cycles. In total, the shredding time was 7 min. Part of the resulting solution was filtered through a 10 µm metal mesh (Puri Select). The filtered and unfiltered samples were characterized by DLS, fluorescence, microscopy pictures and SEM.

5.3.3 Microscopic Evaluation of the Microplastics and Tissue Samples

The microscopic imaging and analysis of the doped nanofibers and their resulting microplastic particles was performed using a confocal laser scanning microscope LSM710 (Zeiss, Oberkochen, Germany) equipped with a Ti: Sapphire Chameleon Ultra Vision II laser (600-1200 nm; Coherent, Santa Clara, CA/USA), an UV Laser diode (405 nm), a multi-line argon laser (458 nm, 488 nm, 514 nm), a DPSS Laser (561 nm), and a HeNe Laser (633 nm). The microscope is controlled by the software ZEN 2.3 SP1 (Zeiss, Oberkochen/Germany). Images were taken with 40x magnification.

The imaging of the UCNP-doped materials was performed under 980 nm irradiation (1200 mW) in the laser scanning mode (41.26 µs·pixel^{-1}). The laser operated at 50% of maximum power for all samples. The emitted light was collected with a shortpass filter for 485 nm (SP485 IR+).

For the visualization of the DPA-doped nanofibers and the resulting microplastics, the multi-line argon laser was used. The laser excited the material at a wavelength of 405 nm using 1.00% laser power in the laser scanning mode (0.66 µs·pixel^{-1}).

The analysis of the tissue samples used all lasers for several excitation wavelengths (405 nm, 488 nm, 543 nm, 647 nm, 980 nm) to display the structure of the tissues as well as the microplastic particles.

Images were processed with ZEN lite, ImageJ (Fiji, v1.5k) and CorelDRAW.

5.3.4 *Ex vivo* Application of Microplastic Particles in Murine Tissue

Isolated Perfused Kidney

The mouse isolated perfused kidney (MIPK) model was used to evaluate the detectability of the produced MP particles in tissue samples. For MIPK experiments, the kidney was perfused via the renal artery with a buffer containing the plastic material of interest. The MIPK was performed according to Schweda et al. [177] with PAX8 / TeO-Cre / Ren1-flox (C57BL/6 background) mice as kidney donors and 0.5 mg of DPA- or 1 mg UNCP-microplastic particles added to the perfusion cycle, respectively. Specifically, the mice were sacrificed by cervical dislocation prior to opening of the abdominal cavity. The aorta was clamped distal to the renal artery, the mesenteric artery was ligated, and a metal perfusion cannula was inserted into the abdominal aorta. Following the removal of the aortic clamp, the cannula was advanced to the origin of the right renal artery and secured in place. After ligation of the aorta proximal to the right renal artery, the perfusion was started. The right kidney was excised, placed in a thermostated moistering chamber and perfused at a constant pressure of 100 mmHg using a modified Krebs-Henseleit solution including physiological amino acids and glucose. The perfusion medium was continuously dialyzed against a larger volume of the same solution to maintain functional preservation. Finally, the kidney was perfused with 3% paraformaldehyde (PFA, pH 7.4) for further histological analysis.

Immunohistochemistry.

The PFA-fixated kidneys were soaked in cryo buffer (200 mL phosphate buffered saline (PBS), 133 mL 4% PFA in PBS, 32 g saccharose) for 24 h before storage in liquid nitrogen.

For fluorescence immunohistology, the kidneys were rapidly thawed at 37 °C and embedded in 3% agarose in PBS before cutting tissue sections of 150 µm using a vibratome (VT1200 S, Leica). After several washing steps with PBS, sections were blocked with 1% bovine serum albumin (BSA) in PBS including 10% horse serum prior to incubation with primary antibodies (CD31 (goat polyclonal, R&D Systems) and F4/80 (rat monoclonal, abcam)) overnight at 4 °C. After washing with PBS, the secondary antibodies (Alexa Fluor 647 donkey anti-rabbit, Alexa Fluor 555 donkey anti-rat; Thermo Fisher) were added and incubated for 3 h at room temperature, followed by several washing steps with PBS. Following another blocking step with 0.5% Triton X in PBS for 1 h, a labeled phalloidin antibody (Phalloidin-iFluor 488 Reagent, abcam) was incubated on the tissue sections for 2 h. Afterwards, the sections were again washed several times using PBS.

After immunohistochemical staining, the sections were mounted between two cover slips using a spacer (0.10 mm iSpacer, Sunjin Lab) for imaging. Kidney sections were analyzed using a confocal laser scanning microscope (LSM 710, Zeiss).

5.4 Results

For the production of luminescent irregularly-shaped MP, a suitable precursor material is required. Using a precursor which is already a nanomaterial in such a top-down approach should enhance production efficiency [180]. It is suggested that NFs are a promising candidate as they have two dimensions in the nanoscale, are non-spherical, and can easily be mass produced from many polymers found in the environment including PS, PMMA, PET or nylon [99,134,181,182]. Furthermore, the above discussed challenges of post-production doping [183] can be avoided by a direct embedding of optical labels in the polymer solutions[184]. To demonstrate such capability, PS as commonly used MP material was chosen as model polymer [135]. A range of optical labels was investigated, the resulting MPs were fully characterized, and finally applied to an *in vitro* kidney model. Ultimately, desired MP characteristics were rugged shape, homogeneous non-leaching optical labels, and a size around 5 µm, the latter of which best addresses the critical size range for MP uptake in intestinal epithelial caco-2 cells in that size[174].

5.4.1 Application-Related Selection of Optical Labels

5.4.1.1 DPA – A Suitable Fluorophore for Labeling Based on its Optical Properties

Aside from general criteria such as high quantum yield, good photostability, relevant is also the solubility within the polymer solution, and an excitation wavelength which will avoid interference with those fluorophores used in standard cell studies. Perylene and 9,10-Diphenylanthracene (DPA) were chosen with quantum yields of minimum 0.82 and 0.95, respectively, high molar absorption coefficients at 405 nm (Table S5.1) and reported high photostability in polymer matrices [153,185]

When comparing absorbance and fluorescence spectra (Figure S5.2A and B, Figure 5.2A), DPA proved more interesting with a narrower peak in both cases. Of special interest here is the fact that DPA was not excited at 488 nm in contrast to perylene (Figure S5.2 C – D and S5.3). This would allow the imaging of MPs in tissue and cells while simultaneously staining cell compartments with the standard secondary antibodies labeled for example with the Alexa488 fluorophore and excitation at 488 nm.

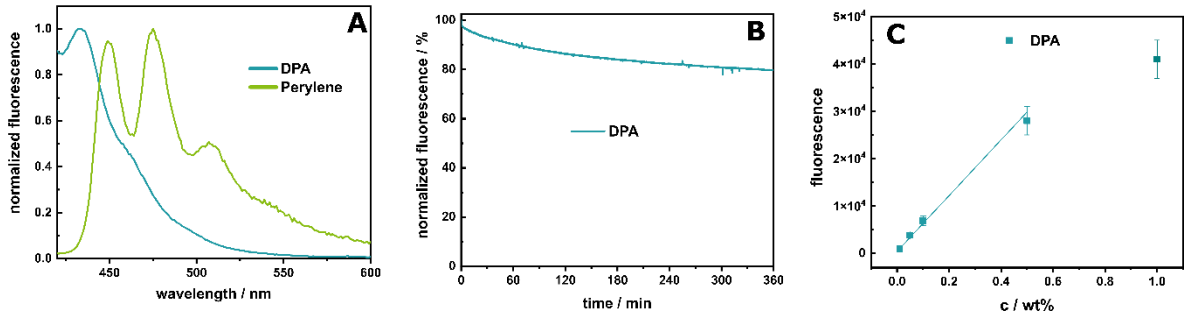

Figure 5.2:(A) Fluorescence spectrum of microplastic particles, dispersed in a 1 wt% soy lecithin solution at a concentration of 2 mg·mL^{-1} (diluted 1:10, Ex: 405 nm). (B) Photobleaching study displaying the percentage decrease in fluorescence of DPA over time. Conducted on the knife-coated PS sheets with a doping concentration of 1 wt% DPA Ex: 385 nm, Em: 410 nm. (C) Dependency of fluorescence signal to the doping concentration of the fluorophore. DPA was excited at 405 nm and the maximum fluorescence signal was plotted against the doping ratio. A linear correlation was revealed (R^2 DPA: 0.996). Measurements done with knife coated polymer sheets (n = 8).

It was found here that when exposing fluorophores embedded in a PS matrix to UV light from a Xenon flash lamp for several hours (Figure 5.2B), DPA can be considered photostable during sample preparation and handling under ambient light. Finally, for an optimal doping ratio, i.e. high signal-to-noise ratios, low concentration to diminish possible leaching effects, and avoidance of self-quenching have to be considered. Therefore, the concentration dependence of DPA's fluorescent signal was investigated (Figure 5.2C and S5.4) and 0.3 wt% of DPA was chosen as best labeling concentration [153].

5.4.1.2 Upconversion Nanoparticles

Inorganic nanoparticles provide another fluorescent detection strategy to overcome blinking, photobleaching and limited range of excitation and emission wavelengths of organic fluorophores as discussed above [154,155]. UCNPs offer the additional benefit of NIR excitation, hence avoiding autofluorescence of the tissue and interferences with standard fluorescent probe detection [157,186,187]. Thereby they also enable deep tissue imaging in the future due to the increased penetration depth of the excitation light [157–159]. Furthermore, they are well suited as model probe as the emission of the UCNPs can be finely tuned by simply changing the lanthanide doping [188], enabling multiplexing without changing the nature of the interaction with the embedding polymer. Their comparably low quantum yields [156] are overcome by generally high doping rates in polymer matrices [189]. Based on previous research, UCNPs with a composition of $NaYF_4$(25%Yb,0.3%Tm) were synthesized and coated with an optically inactive $NaYF_4$ shell, to enhance the optical emission by reducing energy migration to the surface and subsequent surface quenching [190–192] (Figure 5.3A, Figure S5.5 and S5.6). Subsequently, the particles were stabilized in a DMF:THF mixture by a ligand exchange reaction [179] for embedding into PS solutions (Figure S5.5 C, F, I). Characterization of the particles was carried out by TEM, DLS and luminescence measurements, as well as ICP-OES

for the determination of concentration and lanthanide doping of the particles (Figure S5.5 and S5.6). As expected, UCNPs luminescent characteristics did not change upon embedding in a PS-matrix, (Figure 5.3B, Figure S5.6). The peak emerging at around 820 nm is likely attributed to the scattering of the excitation light by the MP particles, while the abrupt cut at 900 nm is a consequence of the selected filter (cut-off at 900 nm to protect the detector from the excitation light).

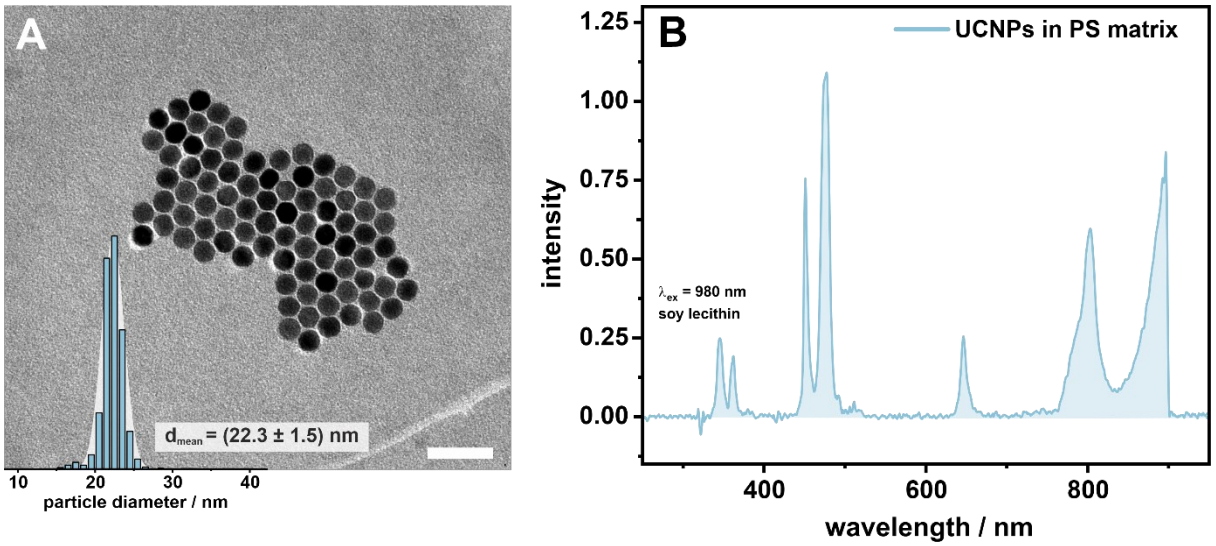

Figure 5.3: Characterization of UCNPs used as dopant in PS matrix. (A) TEM micrograph with corresponding size distribution histogram of $NaYF_4$:Yb,Tm@$NaYF_4$ doped core-shell particles (first batch). TEM analysis results in a diameter of (22.3 ± 1.5) nm, corresponding to a shell thickness of (3.5 ± 0.9) nm. (B) Luminescence measurement of $NaYF_4$:Yb,Tm@$NaYF_4$ UCNPs in PS matrix in 1 wt% soy lecithin ($\beta_{initial}$ = 4 mg·mL^{-1}, 1:10 dilution). Excitation with λ_{ex} = 980 nm, 156 W·cm^{-2}.

5.4.2 Nanofibers as Precursors for the Production of True-to-Life MP

5.4.2.1 Electrospinning Allows Stable Embedding of Optical Labels in the Polymer Matrix

Electrospinning was chosen for the fabrication of luminescent NFs. By mixing DPA or UCNPs into the polymer solution prior to electrospinning, even distribution and full control of dopant concentration is obtained. Considering studies that have shown the leaching of fluorescent dyes from MPs [150,164], this issue was included in the studies in addition to general characterization of nanofiber diameter and luminescent signals.

Thus, upon electrospinning (Figure 5.4A and S5.7B) PS NFs have a narrow size distribution, and the thickness of the fibers is independent of the dopant (DPA: (0.95 ± 0.13) µm and UCNPs: (1.0 ± 0.2) µm) as shown in Figure 5.4A and S5.7B, making this method suitable not only for small molecules but also for larger particles.

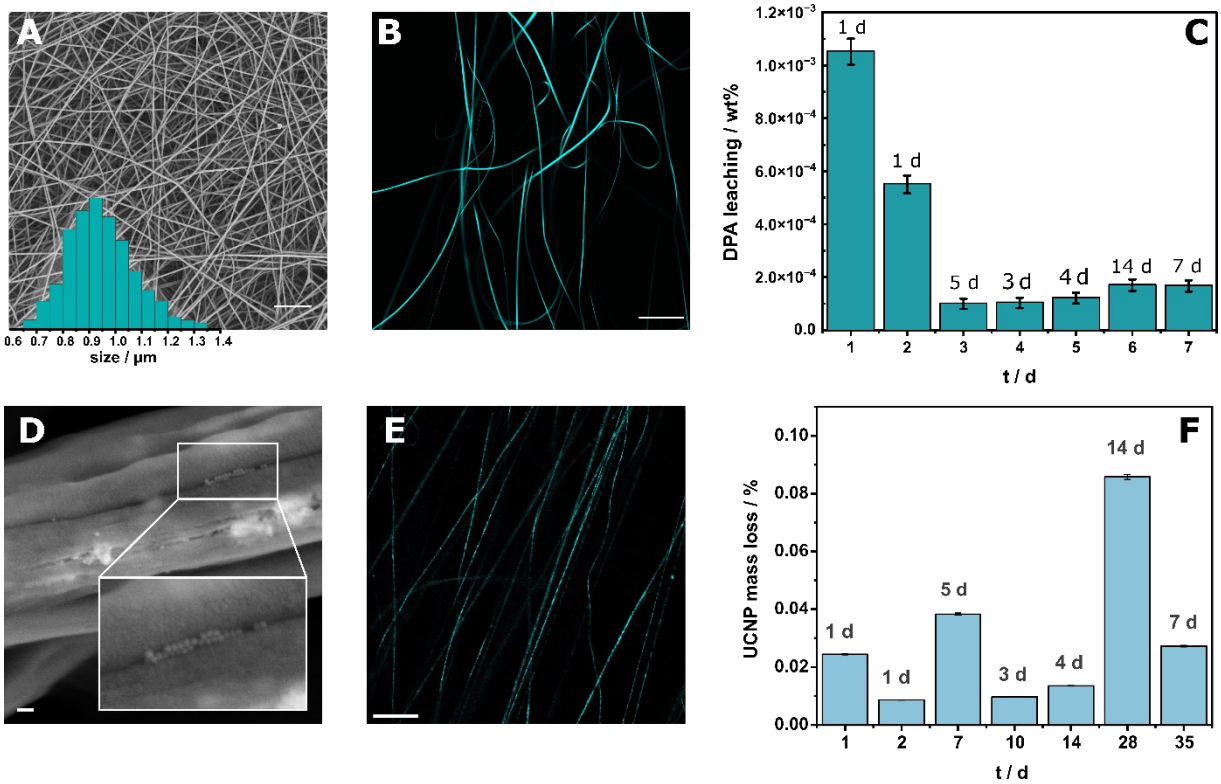

Figure 5.4: PS-Nanofibers doped with 2 wt% DPA (A-C) and 17 wt% UCNPs (D-F). (A) SEM image of the electrospun PS NFs with corresponding size distribution, scale bar 20 µm (B) the same NFs are excited under a fluorescent microscope; scale bar 50 µm. (C) Leaching study investigating the release of fluorophores from the nanofibers into an aqueous solution over a period of 5 weeks, monitored by fluorescence measurements. (D) SEM micrograph of PS-UCNP NFs. One spot where UCNPs can be seen is zoomed out. Scale bar corresponds to 100 nm. (E) Microscopic image of the PS-UCNP NFs. Scale bar 50 µm. Excitation with λ_{ex} = 980 nm, 1200 mW, 50% laser power. (F) Leaching study of $NaYF_4$:Yb,Tm@$NaYF_4$ doped PS-nanofibers. The mass loss of UCNPs leaching out from the NFs is determined by ICP-OES measurements. The numbers above the bars indicate the effective time elapsed during the dialysis.

In earlier research with thin polyvinyl pyrrolidone NFs, UCNP doping distribution in NFs could be evaluated by TEM, [189] but the significantly thicker PS fibers increased electron scattering and phase contrast making a visualization of the particles within the fiber impossible (Figure S5.7 A) [193]. Subsequently, SEM analysis was chosen for the visualization (Figure 5.4D and Figure S5.7 B). The NFs showed a rough surface with occasional fissures, wherein spherical structures could be seen with a diameter that aligns with that of the UCNPs. Finally, to confirm a successful doping, the fibers were further investigated by confocal microscopy, indicating homogenous distribution of the optical labels within the polymer matrix (Figure 5.4B and E, S5.7 D).

To assess the stability of the dopants within the polymer matrix, leaching was performed by soaking the NFs in water over the period of five weeks (Figure 5.4C and F). No reduction in signal intensity is to be expected due to the very low leaching rate of the optical labels (DPA 0.0023 wt%; UCNPs 0.2 wt%). Based on the stable embedding of the labels in the polymer matrix, signal consistency over long term studies can be assured. Considering the released lanthanide and fluoride ions from the UCNPs, the resulting concentrations are below the so far reported cytotoxic concentrations[194–197].

5.4.2.2 Simplified Production with Control of Particle Shape of True-to-Life MPs

MP can be produced from NFs using the typical top-down approaches such as ball- and cryo milling or alternatively shear force exfoliation with an UT. Particle shapes are expected to be highly irregular and possibly even fibrous.

Initial studies showed, that the size of the milling balls affects the milling outcome (Figure 5.5 and S5.7) [198,199]. Larger balls (diameter of 10 mm) break the material down due to impact forces [200] and hence lead to larger flakes with a broad size distribution of (17 ± 9) µm (Figure 5.5A). Smaller balls consequently lead to a reduction in size with a narrower size distribution of (6 ± 4) µm (Figure 5.5B). To avoid the longer cooling times between milling cycles required for heat dissipation in case of the small ball milling process, a combination of both processes was tested. The sample was pre-milled with the large balls for particle formation and then grinded down with the small balls (Figure 5.5C). This approach yielded successfully the smallest particles (4 ± 3) µm, similar to other two-step procedures reported in literature[199]. The size range is of particular interested as discussed above, since such particles can accumulate in the kidneys and liver of aquatic animals and mice [201–204].

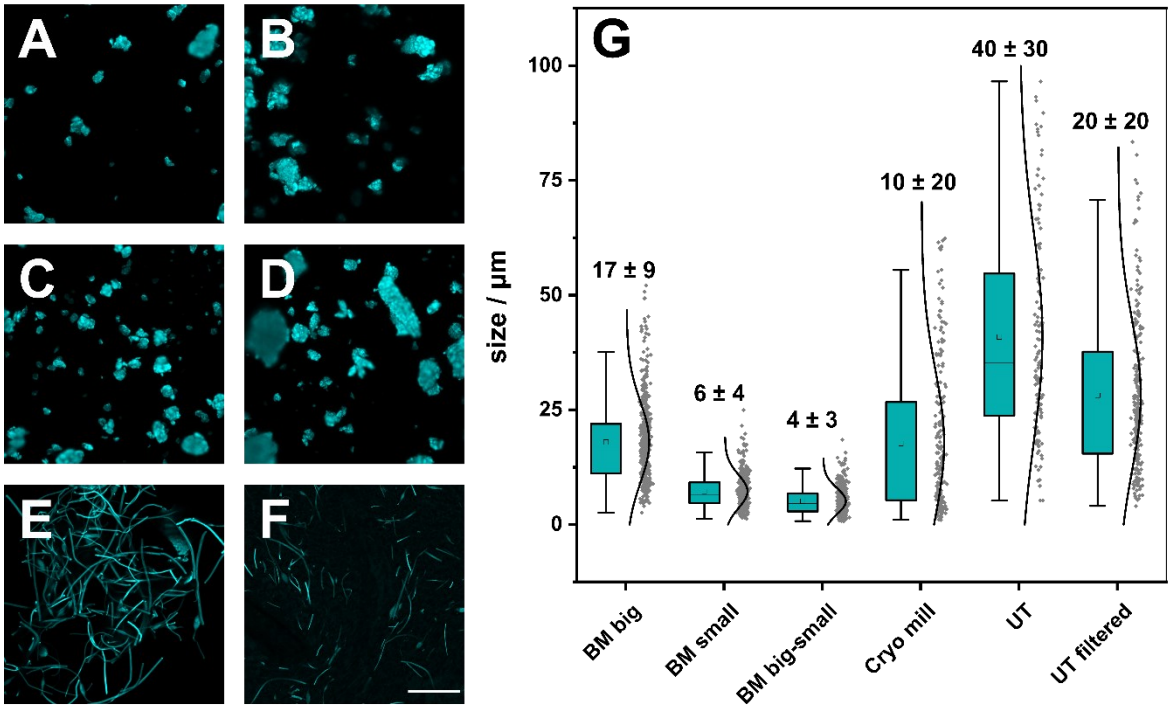

Figure 5.5: Comparison of particle shapes (scale bar 20 µm) and the resulting size distribution after different microplastic production methods. (A) Microplastic generated by a planetary ball mill (50 mL grinding jar; 7x 10 mm grinding balls) after 9 milling steps of 2 min. (B) Microplastic generated by a Planetary Ball Mill (50 mL grinding jar, 3000x 2 mm grinding balls) after 9 milling steps of 2 min. (C) Particles from (A) after a second milling step with 9 cycles of each 2 min with small balls (50 mL grinding jar, about 3000x 2 mm grinding balls). (D) Particles obtained from a cryo mill under liquid nitrogen cooling (50 mL grinding jar, 8x 12 mm grinding balls) after 9 milling cycles of 2 min grinding and 1 min intermediate cooling. (E) Particles produced by an UT in 1 wt% soy lecithin solution with and (F) after filtration through a 20 µm metal sieve. (G) Plot of the size distribution of the different production methods; n > 400.

Cryo milling is a promising technique resulting typically in smaller particle sizes and reducing unwanted side-reactions [205] and has already been tested for making MP[160]. However, in this study only in large particles with a very broad size distribution were obtained (Figure 5.5D). It is assumed that the fluffy nature and hence low density of the NFs prevented effective cryo milling, as reaching the necessary fill level in the grinding jar would require refilling during the process, which is complicated by the formation of ice crystals due to cryo cooling. It may be worthwhile revisiting this method in the future but is deemed unnecessary considering the good MPs produced in the two-step process. Finally, UT was investigated with the promise of maintaining the fibrous nature also in the resulting MPs. This method essentially cuts the NFs into shorter pieces and indeed created the desired shape (Figure 5.5E and F). Since these particles were still too long with (40 ± 30) µm, even after filtration ((20 ± 20) µm), further optimization is necessary to obtain smaller particle sizes, for instance, by extending the shredding time.

SEM images of MP derived from nanofibers and of commercially available spherical MPs demonstrates that irregularly shaped and even fibrous materials can be generated with the proposed procedure (Figure 5.6). Compared to the commercial particles, which display a uniform size, a smooth surface, and a perfectly spherical shape, the MP produced by the top-down approaches exhibit irregular shapes and rough surfaces with edges. They are more comparable to MP found in the environment as described in literature [161,206,207], making them a valuable resource for investigating the biological effects associated with particle shape [208].

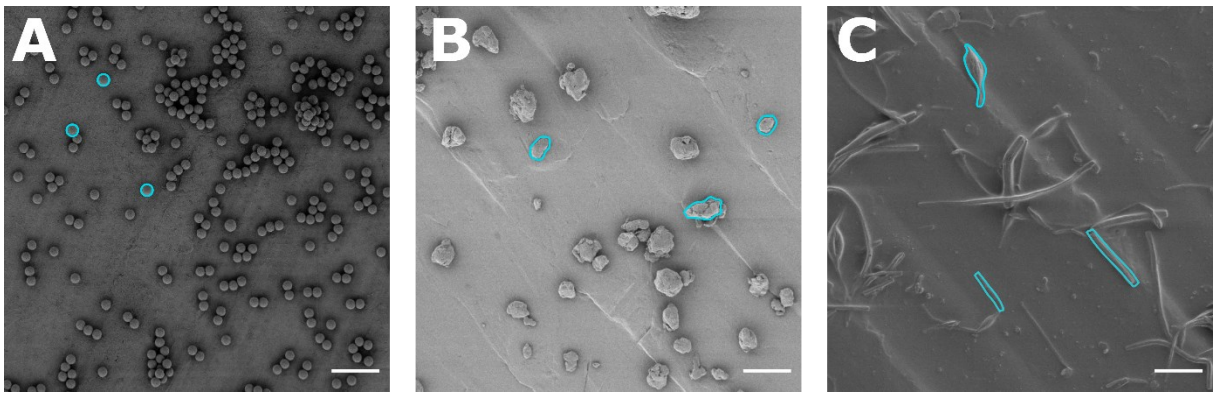

Figure 5.6: Shapes of MPs as determined by SEM with blue edging to emphasize the shape of the particles. (A) Commercially available spherical MP particles from microparticles GmbH. (B) MP produced by ball Milling from PS-NFs doped with 0.3 wt% DPA. (C) Fibrous MP produced by an UT. Scale bar 20 µm.

A variety of techniques have been described in the literature for the production of MPs from PS (Table 5.2). Beside lab-based weathering and sonication [161,167], the majority of reported techniques are based on BM. All reported particles exhibited a rough surface and heterogeneous composition. However, the resulting particle sizes varied considerably, with diameters ranging from 1 to 200 µm (Table 5.2). To address this issue, Choi et al. implemented an additional sieving step, which effectively eliminated larger particles [162]. A reduction of particles sizes was either achieved by milling in wet-media [172], liquid nitrogen cooling [160,171] or extensive milling times [172]. In comparison, using NFs as a precursor, the particle size, size distribution and milling time could be drastically reduced, without the need of liquid nitrogen cooling. Moreover, the production technique allows for the generation of irregular fragments and fibrous particles using the same precursor materials. In addition, this approach enables the direct embedding of optical markers, such as fluorophores and UCNPs into the MP, eliminating the need for an additional production step [160–162]

Table 5.2: Comparison of artificial PS MP by top-down approaches

Material	Final Size / µm	Production method	Medium	T / °C	Production time / h	shape	Label	Ref
Shredded single use products	1-3	Lab-based weathering	Air	ambient	16	Rough surface, heterogenous fragments	none	[161]
Pellets	1-200	Cryo Milling	Air	Liquid nitrogen	3	Rough surface, heterogenous fragments	none	[160]
Polymer Beads	40 - 500	Cryo Milling	Air	Liquid nitrogen	Not given	Rough surface, heterogenous fragments	none	[171]
250 – 500 µm	> 5	Stirred Wet Milling	Denatured ethanol, n-hexane	ambient	22	Not shown	none	[172]
squares (1 cm²)	0.1 - 1000	Sonication	0.25 M KOH	ambient	15	Irregular fragments and films with rough surface	none	[167]
Smashed pellets	5 – 25	Ball Milling and sieving	Air	cooled	2	Rough surface, heterogenous fragments		[209]
NFs 950 nm	20 ± 20	Ultraturrax	Soy lecithin	0 °C	1	fibrous	Fluorophores UCNPs	This work
	4 ± 3	Ball Milling	Air	ambient	1.5	Rough surface, heterogenous fragments		

5.4.3 Application of True-to-life MPs *ex vivo* Revealed Deposition in the Kidney

To evaluate the applicability and detectability of the labeled MPs, the DPA-labeled particles were infused into a murine kidney using the mouse isolated perfused kidney (MIPK) model. This model was chosen since it allows the introduction of the material of interest into an intact organ without being dependent on intestinal absorption. Therefore, the MIPK allows to administer a defined dose to a functional kidney. The fluorescence immunohistochemical (IHC) staining of the DPA-MP perfused kidney included a Phalloidin (label: 488 nm) staining for f-actin, a compound of the brush border of proximal tubules, smooth muscle in renal vessels, and glomeruli [210]. Moreover, the tissue sections were stained for F4/80 (label: 555 nm) as a marker for murine macrophages [211] and CD31 (label: 647 nm) as an endothelial cell marker [212].

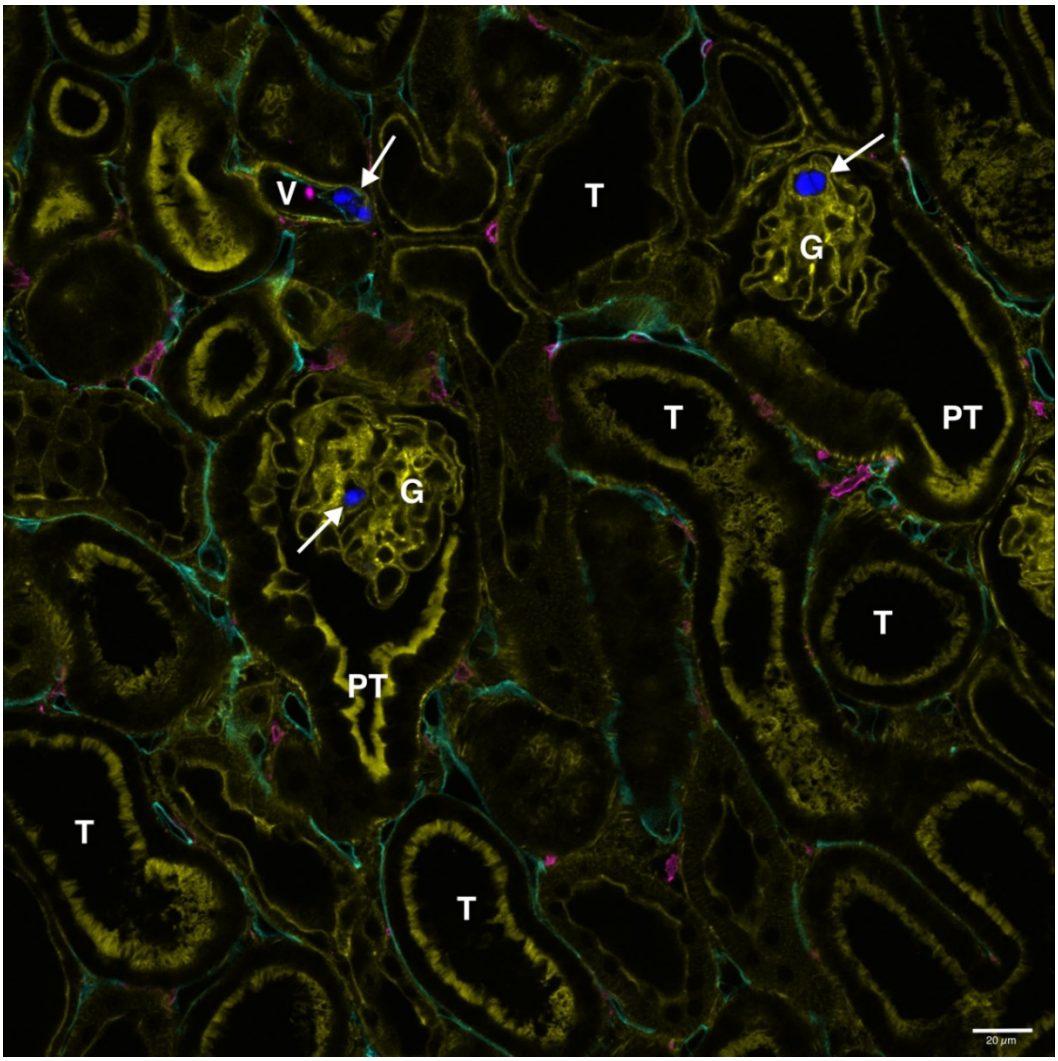

Figure 5.7: Murine kidney tissue (150 µm section) of a MIPK, perfused with 0.5 mg DPA-PS MP (arrows; blue, 405 nm) after fluorescence immunohistochemistry staining for CD31 (endothelial cells; cyan, 647 nm), F4/80 (murine macrophages; magenta, 555 nm), and Phalloidin (f-actin; yellow, 488 nm). Scale bar 20 µm. G – glomerulus, PT – proximal tubule, T – tubule, V – blood vessel.

During microscopic analysis of the MIPK tissue sections, the DPA-doped microplastics were detected using the 405 nm laser setup with low laser power (2.0% max. power). As shown in Figure 5.7, the particles were found in glomeruli and in renal blood vessels with good demarcation from the surrounding tissue. No overlap was seen between any of the fluorescent antibody signals excited with different lasers and the emission signal of the DPA-doped MPs. The low laser power necessary for exciting the DPA-MPs lowers the risk of photobleaching and tissue damage, even after extended exposure times. The parallel usage of several antibody stainings facilitates co-localization studies

It is noteworthy that the irregularly shaped MPs were found to be stuck in smaller renal vessels and in the glomerular capillaries. Consequently, MP fragments in the vasculature may impair renal blood flow and compromise the glomerular filtration.

5.5 Conclusion

The ubiquity of micro- and nanoplastic in the environment, and its presence in every human tissue worries scientists. Intensified research is crucial for understanding of its toxic effect on the environment, flora and fauna. Studies are necessary at all levels, from *in vitro* cell studies to whole organisms to entire ecosystems. This is an immensely complex undertaking considering the various MP sources and materials and the different degradation pathways. Interdisciplinary teams are needed to address specific questions within this task. Here, we have demonstrated that nanofibrous source material can easily deliver irregularly shaped MPs which should more closely resemble MP found in the environment. Through a two-step simple milling process, MP can be produced in the size range at which uptake by cells and in tissue is known. Furthermore, the precursor nanofibers can be easily doped with desirable probes, such as organic and inorganic luminescent labels as done in this study. Those labels do not interfere with necessary staining in cell and histological studies, and MPs from environmental sources can be distinguished. As this study demonstrated the simplicity of the stable embedding of molecules and NPs, this method can be further extended to other labels, such as carbon dots or quantum dots, or differently doped rare earth (RE) NPs. The later offer the opportunity of additional multimodal characterization of MPs. Gd-ions, for example, show magnetic resonance (MR), offering their using in MR imaging applications[213].

The careful design of MP used in biological studies is a mandatory step within the overall study of MP toxicity. Too easily false findings could be obtained, if artificial MP models are used, e.g., those that are only of one shape, one polymer, or those that leach dopants and hence possibly affect the biological system not through MP but through a dopant's presence. Finally, not only precursor material, such as PS in this study, and MP size and shape are important, but also their surface chemistry and coatings. MP found in the environment will have varying coronas that heavily depend on the environmental matrix, the degradation process and also its starting material. Stabilizers added to commercially available MP may be important for the delivery of and workability with the MP, but it may move it even farther away from a realistic MP model.

The more realistic MP developed here is a very good starting point for further studies that also take environmental matrices and environmental degradation processes into consideration and expand the platform to other, environmentally relevant precursors plastic materials.

5.6 Supplementary Information

List of Chemicals

If not stated in the text, chemicals and suppliers are listed in the following:
Agarose (low melting) was purchased from Biozym Scientific GmbH (Hessisch Oldendorf, Germany). Ethanol (EtOH, technical grade) was purchased from CSC Jäklechemie GmbH & Co. KG (Nuremberg, Germany). Dimethylformamide (DMF, ≥ 99.5%), cyclohexane (≥ 99.5%), oleic acid (OA, ≥ 90%), 1-octadecene (ODE, ≥ 90%), chloroform ($CHCl_3$, ≥ 99%), methanol (MeOH, ≥ 99.9%), nitric acid (HNO_3, 65% v/v), sulfuric acid (H_2SO_4, 96% v/v) and tetrahydrofuran (THF, ≥ 99.8%) were purchased from Fisher Chemicals (Schwerte, Germany). Sodium hydroxide (NaOH, p.A.), paraformaldehyde and horse serum were purchased from Merck (Darmstadt, Germany). Thulium(III)-chlorid hexahydrate ($TmCl_3 \times 6\ H_2O$, ≥ 99.99%), sodium oleate (Na-OA, ≥ 82%), ammonium fluoride (NH_4F, ≥ 99.99%), nitrosyl tetrafluoroborate ($NOBF_4$, ≥ 95%), ethanol (EtOH, p.A.), bovine serum albumine (BSA), phosphate buffered saline (PBS), polystyrene (MW ≈ 28,000), perylene, diphenylanthracene (DPA), and soy lecithin were purchased from Sigma Aldrich (St. Louis, USA). Saccharose was purchased from Thermo Fisher (Waltham, USA). Ytterbium(III)-chloride hexahydrate ($YbCl_3 \times 6\ H_2O$, ≥ 99.9%) and yttrium(III)-chloride hexahydrate ($YCl_3 \times 6\ H_2O$, ≥ 99.9%) were purchased from Treibacher Industry AG (Althofen, Austria).

Application-related Selection of Optical Labels

DPA – a Suitable Fluorophore for Labeling Based on its Optical Properties

Table S 5.1: Comparison of possible fluorophores

	DPA[153,185]	Perylene [153,185]
Emission maximum / nm	400 -500	435; 464
Quantum yield	0.95 - 1.05	0.82 – 0.94
Molar absorption coefficient ε	14 000 in Cyclohexane	50 000 in Chloroform
Costs according to Sigma Aldrich / € / g	46.60	103.00

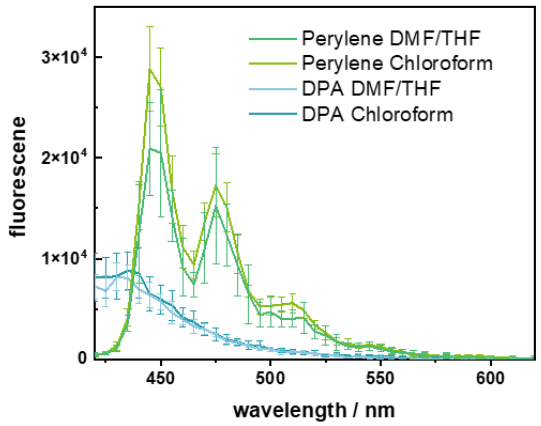

Figure S 5.1: Influence of the solvent on the fluorescence of dried polymer sheets with doping concentration of 1 wt% of the corresponding dye (Ex. 405 nm).

Detailed Information about Laser-Cutting of the Knife-coated foils

In order to laser-cut the foils, the desired designs were drawn vector graphics with CorelDraw suite 24.0. To work in vector mode, all lines need to be defined as hairlines. Engraving was performed with a VLS 2.0 laser engraving systems based on a 10600 nm infrared laser with a maximum power output of 30 W using 5% power and 60% speed for cutting.

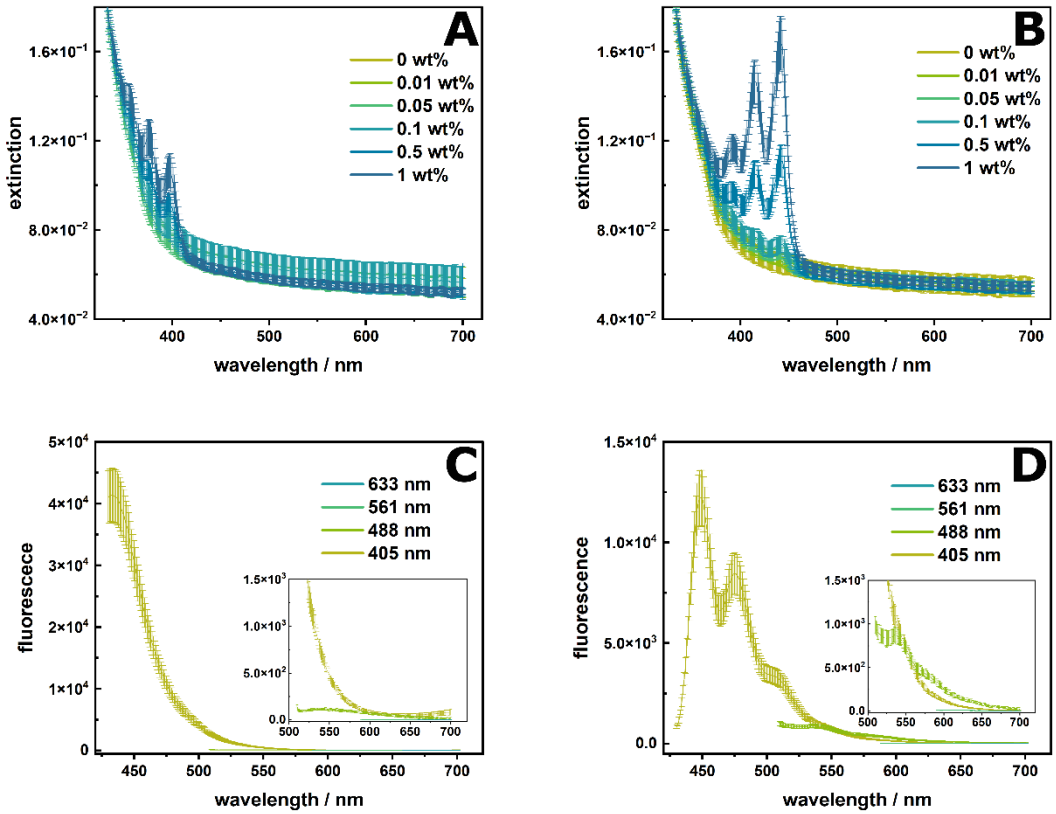

Figure S 5.2: Spectra of polymer sheets are obtained from DPA and (A,C) from perylene polymer foils. (A,B) Extinction spectra in dependency of doping concentration. (C,D) Fluorescence spectra of 1 wt% doping excited with different wavelengths.

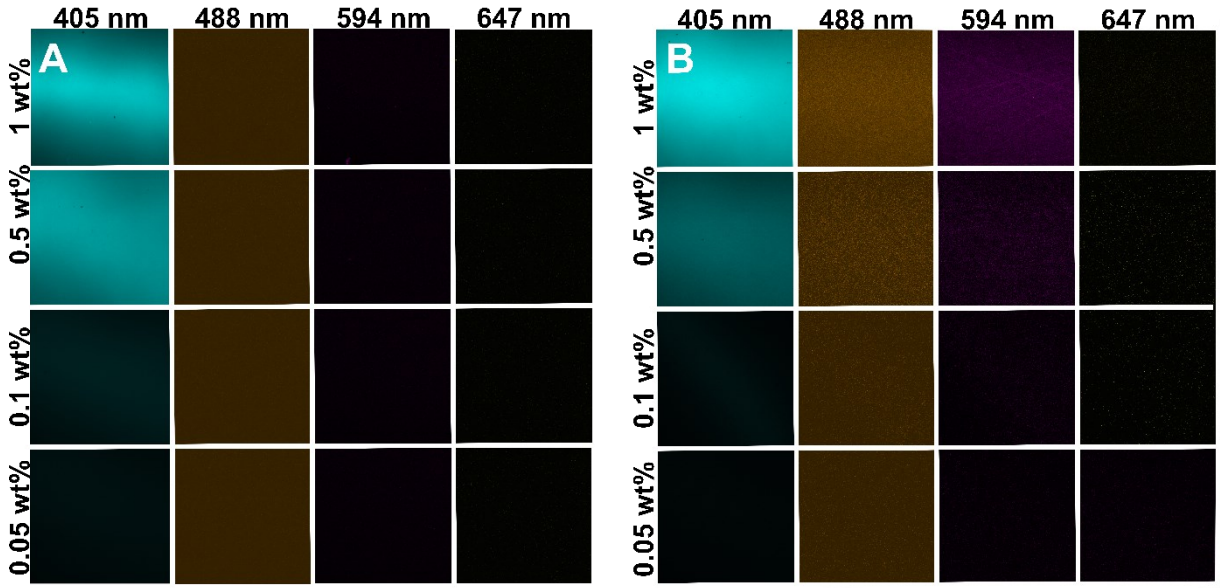

Figure S 5.3: Appearance of knife coated polymer foils with various doping concentration under the fluorescent microscope under all wavelengths used for histological analysis. (A) DPA and (B) perylene. Gain was optimized to highest concentration for each fluorophore individually.

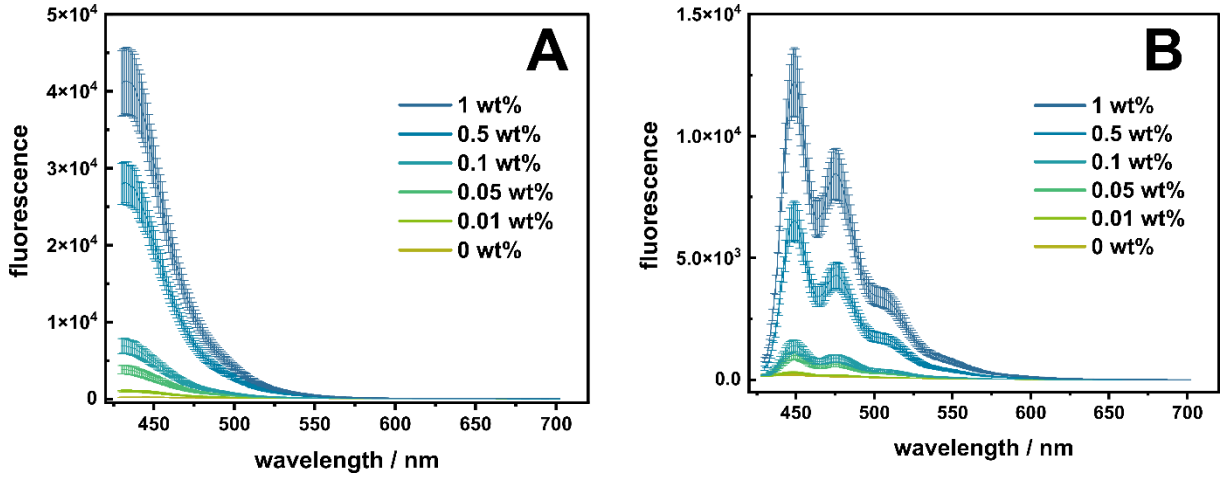

Figure S 5.4: Concentration dependency of doping concentration on the fluorescent spectra of knife coated PS-sheets (Ex. 405 nm). (A) DPA, (B) perylene.

UCNPs – an Option for Deep Tissue Imaging Given their Photophysical Characteristics

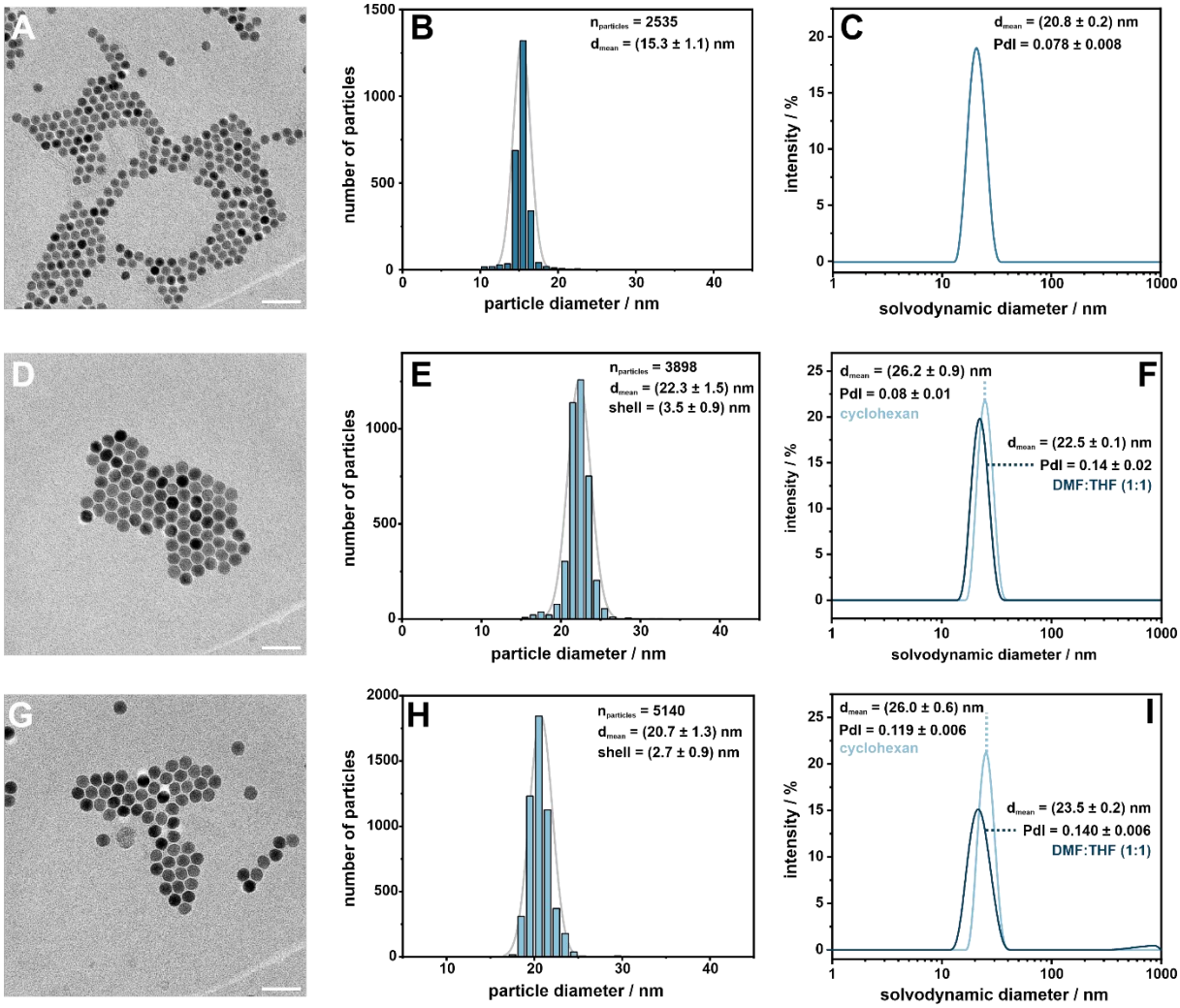

Figure S 5.5: Characterization of UCNPs used as dopant in PS-nanofibers. (A,B,C) TEM micrograph with corresponding size distribution histogram and DLS in cyclohexane of $NaYF_4$:Yb,Tm doped core particles. TEM analysis results in a diameter of (15.3 ± 1.1) nm. The solvodynamic diameter is determined to (20.8 ± 0.2) nm with a PdI of 0.078 ± 0.008 (n=3). (D,E,F) TEM micrograph with corresponding size distribution histogram and DLS in cyclohexane (light blue) and in DMF:THF (dark blue) of $NaYF_4$:Yb,Tm@$NaYF_4$ doped core-shell particles (first batch). TEM analysis results in a diameter of (22.3 ± 1.5) nm, corresponding to a shell thickness of (3.5 ± 0.9) nm. The solvodynamic diameter is determined to (26.2 ± 0.9) nm with a PdI of 0.08 ± 0.01 (n=3). For the particles in DMF:THF the solvodynamic diameter is determined to (22.5 ± 0.1) nm with a PdI of 0.14 ± 0.02 (n = 3). (G,H,I) TEM micrograph with corresponding size distribution histogram and DLS in cyclohexane (light blue) and in DMF:THF (dark blue) of $NaYF_4$:Yb,Tm@$NaYF_4$ doped core-shell particles (second batch). TEM analysis results in a diameter of (20.7 ± 1.3) nm, corresponding to a shell thickness of (2.7 ± 0.9) nm. The solvodynamic diameter in cyclohexane is determined to (26.0 ± 0.6) nm with a PdI of 0.119 ± 0.006 (n = 3). For the particles in DMF:THF the solvodynamic diameter is determined to (23.5 ± 0.2) nm with a PdI of 0.140 ± 0.006 (n = 3). The scale bar in the TEM micrographs corresponds to 100 nm.

TEM measurements show uniform spherical particles with a narrow size distribution for the core, and both core-shell particles batches (Figure S6). The core-shell particles have a shell thickness of about 3 nm and are comparable within the range of the standard deviation. After syntheses, the UCNP were stabilized in cyclohexane, bearing oleic acid as surface-stabilizing ligand. DLS measurements (Figure S6 C, F, I) support the results from TEM measurement, showing a small polydispersity index around 0.1, which indicates high uniformity and colloidal stability of the particles. Previous studies in this group already showed a successful embedding of UCNPs in PVP NFs [189]. In order to make them usable for doping into the PS NFs, the particles need to be transferred into a DMF:THF solvent mixture. This was done by a ligand exchange reaction using nitrosyltetrafluoroborat, which yielded stable particles in DMF[179]. After addition of THF, the particles were still colloidally stable without any formation of agglomerates or a sign of sedimentation as indicated by the small PdI, which is important for a homogeneous distribution of the particles in the NFs (Figure S6 F, I). The reduction in the solvodynamic diameter can be attributed to the removal of the oleic acid ligand, yielding bare, ligand-free nanoparticles.

Luminescence spectra have been recorded to characterize the luminescence properties of the UCNPs. Tm-doped nanoparticles show emissions in the UV, blue, red, and NIR region. By equipping the core particles (Figure S7 A), with an optically silent $NaYF_4$ shell, the overall luminescence intensity can be drastically increase (Figure S7 B,C), and the ratio of the emissions is shifted towards the blue emission.

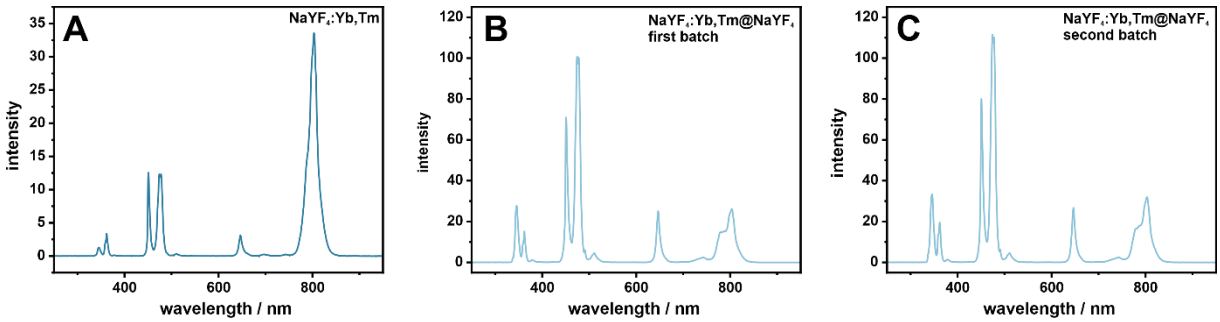

Figure S 5.6: Luminescence characterization of UCNPs used as dopant in PS-nanofibers. (A) Luminescence spectra of $NaYF_4$:Yb,Tm doped core (dark blue) particles in cyclohexane. (B) Luminescence spectra of the first batch of $NaYF_4$:Yb,Tm@$NaYF_4$ doped core-shell (light blue) particles in cyclohexane. (C) Luminescence spectra of the second batch of $NaYF_4$:Yb,Tm@$NaYF_4$ doped core-shell (light blue) particles in cyclohexane. Spectra are normalized to the respective Yb^{3+}-concentration. Excitation with λ_{ex} = 980 nm, 156 W·cm^{-2}.

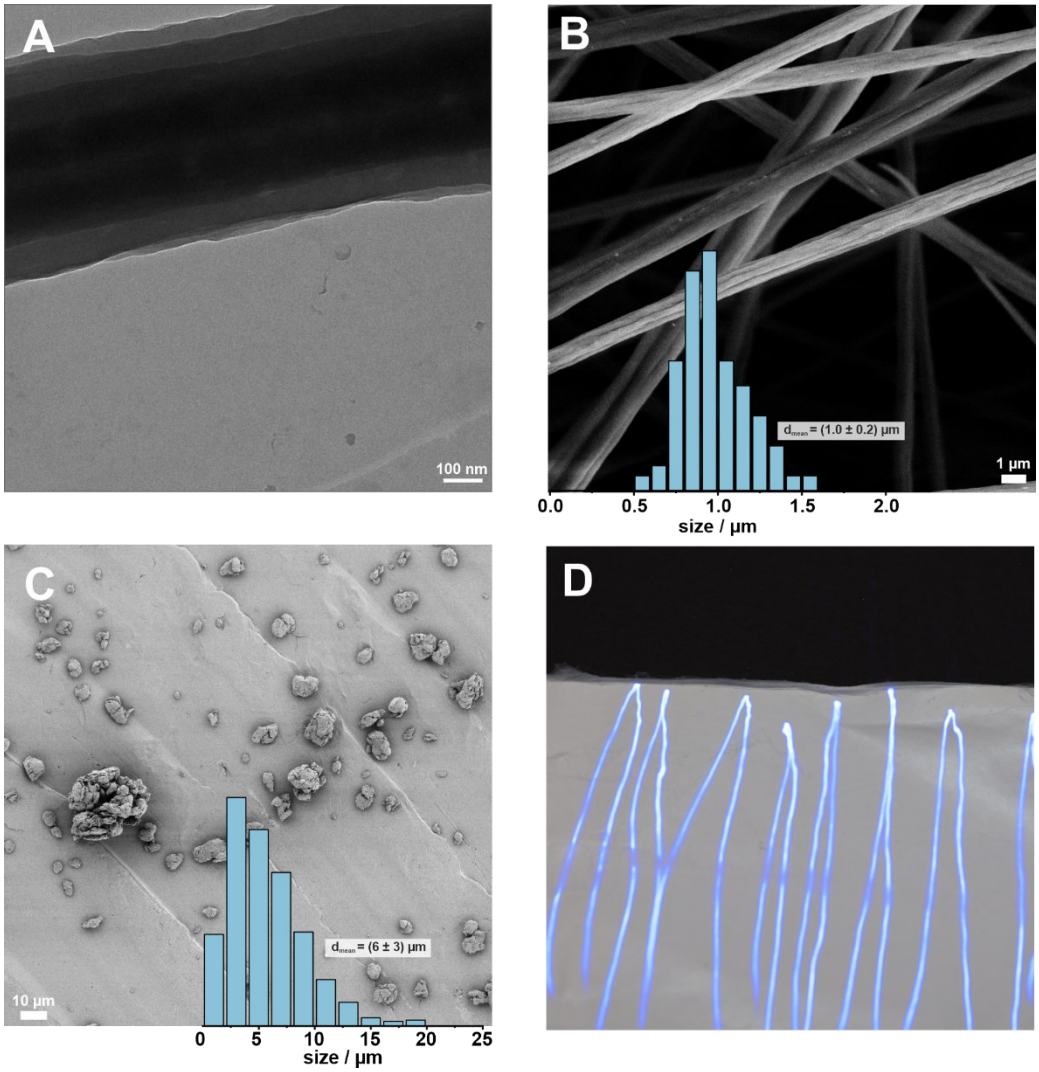

Figure S 5.7: Characterization of PS-nanofibers doped with UCNPs. (A) TEM micrograph of one single fiber. Scale bar corresponds to 100 nm. (B) SEM micrographs showing an overview of the UCNP-doped nanofibers. Fissures are very rare, one spot where nanoparticles in a fissure can be seen is highlighted. SEM analysis results in a diameter of (1.0 ± 0.2) µm, the scale bar corresponds to 1 µm. (C) SEM micrograph of UCNP-doped MP. SEM analysis results in a diameter of (6 ± 3) µm, the scale bar corresponds to 10 µm. (D) Photograph of NF mat doped with UCNPs, excited with a handheld laser module (λ_{ex} = 980 nm, 350 mW, cw).

The distribution of UCNPs in the NFs can normally be evaluated by TEM measurements [189] Unfortunately, no particles were detected in the fiber strand (Figure S7 A), which is likely due to the increased electron scattering and phase contrast caused by the thickness of the fibers [193].

UCNP-NFs were transformed into MP particles using the optimized ball milling method. As shown in the SEM image (Figure S8 C), the particles exhibited a polydisperse nature with a rough surface, with a mean diameter of (6 ± 3) µm. In comparison to the unmilled NFs, no UCNPs can be seen on the surfaces of the MP particles.

Microscopic Evaluation for UCNP-doped Materials

Despite the benefit of an additional antibody staining wavelength due to the change of the excitation wavelength to 980 nm, the visualization of UCNP-doped MPs has some disadvantages. Standard fluorescent microscopes are often not equipped with a NIR or 2-photon laser. Apart from that, common microscopy setups might struggle with the long luminescence lifetime of the UCNPs [214] since some detectors collect light from the entire sample and assign it to the excitation point which could result in a blurred or streaky image. To address these problems a very slow scanning time was used.

Comparison of Fluorophores and UCNPs as Label

Table S 5.2: Comparison of labeling properties and benefits for fluorophores versus UCNPs:

Type of labeling	DPA	Perylene	UCNPs
Excitation / nm	405	405	980
Emission maximum / nm	425	450; 475	variable
Leaching / wt%	0.0023	/	0.2
Photobleaching / %	20	20	/
Price of label / €/g	122.57	55.45	580.88
Price of MP / €/g	86.40	86.31	88.36

Nanofibers as Beneficial Precursor for the Production of true-to-life Microplastics

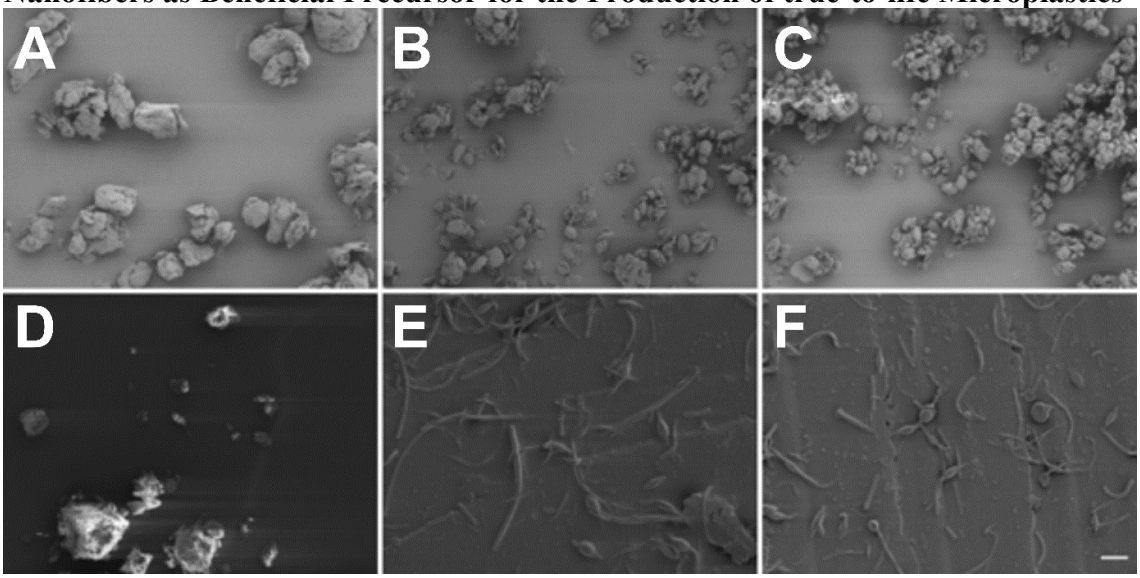

Figure S 5.8: SEM images with a magnification of 1000 of the microplastic produced by different methods, scale bar 20 µm. (A) ball milling with (A) Microplastic generated by a BM (50 mL grinding jar; 7x 10 mm grinding balls) after 9 milling steps of 2 min. (B) Particles from (A) after a second milling step with 9 cycles of each 2 min with smaller balls (50 mL grinding jar, about 3000x 2 mm grinding balls). (C) Microplastic generated by a BM (50 mL grinding jar, about 3000x 2 mm grinding balls) after 9 milling steps of 2 min. (D) Particles obtained from a cryo mill under liquid nitrogen cooling (50 mL grinding jar, 8x 12 mm grinding balls) after 9 milling cycles of 2 min with 30 s cooling steps. (E) Particles produced by an ultraturrax in 1 wt% soy lecithin solution with and (F) after filtration through a 20 µm metal sieve.

6 Conclusion and Future Perspectives

NFs are an interesting material because they can be electrospun from multiple polymers. A they are a one-dimensional nanomaterial , they offer a high surface-to-volume ratio and allow for chemical modifications before or after fabrication [180]. Therefore, the range of possible applications is very wide. In our group, fibers of different polymers and for different applications have been developed in the past [104,189,215,216]. Due to their structure, NFs have been used as mixing agents in microfluidic systems [104], for cell culture [217], for embedding optical detectors [189,216], and as precursors for electrodes [215]. In this thesis, NFs were developed for the use in μPADs for NA extraction and as a precursor with optical labels to produce true-to-life MPs.

As defined by the WHO, POC tests should be affordable, sensitive, specific, user-friendly, rapid, equipment-free and deliverable to end-users [12]. NAT can help to improve the specificity and sensitivity of current techniques such as dipsticks or LFAs, based on the amplification of target analytes [218]. However, the need for multiple steps within a POC setting is a current challenge as the gold standard techniques rely on laboratory equipment and trained staff. New materials and assay designs are needed to meet these goals [90]. In particular, the extraction of NA remains a key challenge, as NA must be separated from interferents present in the sample prior to the amplification reaction [219]. As discussed in Chapter 1, in the field of POC often silica matrices are used for NA extraction in the form of glass fibers or as surface coatings for magnetic NPs. However, silica often requires chaotropic salts, detergents and ethanol during the extraction process, interfering in downstream analysis [89]. Therefore, it is necessary to explore alternative materials for NA extraction.
Due to their high surface-to-volume ratio, NF-based membranes are an emerging substrate and have been modified in the past to adsorb NAs through electrostatic interactions [31,105]. However, they require harsh conditions during elution. Therefore, the aim of this work was to develop NFs capable of extracting NAs under mild conditions, also suitable for POC applications. This was achieved by using zwitterionic NFs, which enable a pH-dependent surface charge, where elution is based on electrostatic repulsion.

First, an extensive materials study identified the best polymers and composition. Nylon was chosen as the carrier polymer because it is hydrophilic but water-insoluble and has an extremely large surface area, by forming nanofibers and nanonets under the right conditions. To achieve the zwitterionic properties, the spinning solution was doped with a mixture of the cationic polymer PAH and the anionic polymer PAA, a weak base and acid, respectively. Different approaches to spin zwitterionic NFs were tested and compared, such as layer-by-layer, one-side-parallel, and one-pot spinning. Although the latter has the lowest degree of freedom to produce NFs, it proved to be the best fabrication technique for this application due to its high reproducibility.
The morphology of the NFs was characterized by SEM images, where also the influence of the applied voltage during spinning and the number of formed nanonets could be shown, which is

also reported in the literature [111,112]. These nanonets not only drastically increase the surface area, but also lead to a smaller average pore size. Furthermore, the NFs are hydrophilic and water stable, as even the nanonetwork structures could be preserved after a complete extraction process.
Chemical composition had the greatest effect on extraction efficiency. Nylon-PAH NFs were shown to bind but not elute NAs, while pure nylon or nylon-PAA NFs were not able to adsorb NAs. However, only the right mixture of PAH and PAA was then able to efficiently adsorb and elute the NAs by changing the pH. According to pKa values, NFs are predominantly positively charged at acidic pH, and negatively charged at basic pH [107]. Therefore, negatively charged NAs can be adsorbed at a low pH and then electrostatically repulsed at a high pH.
Finally, solution parameters and incubation time were optimized resulting in an adsorption efficiency of over 90 % at a pH of 4.5 in the presence of 0.1 % TWEEN 20. With an elution yield of 70% NAs were then released at a pH of 10 and 50 mM NaCl. Compared to elution conditions with high salt concentrations or use of SDS, efficient extraction was achieved under mild conditions.

The as developed NFs were then tested in the serum samples and integrated into a µPAD with the aim of developing a S2A device suitable for POC applications. Compared to BSA, human serum showed a higher interference potential. While a simple dilution was sufficient for BSA, a much higher dilution factor of 1 µL serum in 150 µL buffer was required for serum to achieve comparable extraction efficiencies. As these low sample volumes are less favorable, strategies to increase binding efficiency in the presence of serum by increasing the number of binding sites were explored. Nylon-PAH NFs showed good binding capacities even in the presence of 3 µL serum but did not allow elution of NAs. Reducing the adsorption pH also showed similar results, but elution yields were reduced in this case. Therefore, future studies should aim at increasing the adsorption yield while maintaining efficient elution. A change in the doping ratio could be the solution. Future studies could either increase the PAH content, thereby increasing the adsorption efficiency, but keeping the number of negatively charged groups constant, or keep the ratio between the two polymers constant, thereby increasing the doping of both polymers simultaneously. Furthermore, a reduction of the adsorption pH could also be tested with NFs having a higher doping of PAA to increase the elution yield.
The NFs are then integrated into a µPAD S2A design. Most microfluidic systems made of e.g. PMMA, which require pumps, making them unsuitable for resource limited settings or untrained users. Compared, µPADs made from filter paper are cheaper and do not require for external devices [220]. However, they do suffer from higher user-input, are prone to cross-contamination due to their open channel design and often have a lower throughput [218]. In this work, the NFs are embedded between two layers of plastic foil, by wax printing. NA extraction was then tested within the flow-through design and revealed high extraction yields, comparable to results from MTP experiments. The amplification and detection area were realized by printing a wax pattern on chromatography filter paper.

RPA was then selected as the isothermal amplification method. Good results were obtained at RT with an incubation time of only 10 min. This was successfully implemented in the µPAD design using modified gold nanoparticles for detection. However, the transport of the gold particles through the assay was inefficient, and the flow through the test was therefore hindered and slow. This could be solved by optimizing the amount of gold particles in the test or introducing a separate storage pad for the particles. For a faster flow through the test a different type of substrate could be used for the µPAD, and the channel could be sealed with tape, which could also reduce the risk of cross-contamination [218].
Future studies now need to focus on combining all those parts to achieve a S2A device. First, amplification should be tested with NA isolated with the NFs from buffer and serum. Then, the extraction step can be conducted within the test design, before using a real-application, where LOD and sample-to-answer time could be determined. Also, different storage methods should be investigated, as already the NFs were prone to aging. Here, tests should be stored in a cold and dry environment prior to use.
The overall investigations lead to the conclusion that zwitterionic NFs are suitable for NA extraction under mild conditions yet facing problems with complex biological samples. Therefore, different matrices should be investigated such as sputum, nasopharyngeal swab or water samples. Since binding of the NAs was possible on cationic NFs also in the presence of serum, RPA could be also tested directly on the NFs to avoid an elution step. Furthermore, the beneficial effects of nylon NFs could be also combined with silica adsorption by incorporation of silica nanoparticles in the fibers during the spinning process. These NFs should be then compared to commercially available glass fibers. Also, different strategies to integrate NFs in test systems could be investigated. This could be in microfluidic chip systems, or in lids of squeezable tubes, where currently a project is working on.

Microplastics found in the environment are mainly derived from the degradation of macroscopic plastics used in everyday life with most particles being in the size range between 1-100 µm [133,137]. As a result, MPs have been found in many organs of the human body, but functional consequences for the organism are poorly understood [133,138–143]. The majority of MPs in aquatic or terrestrial ecosystem [134,135], and in the human body, consist of fragments and fibers [136,137].
Since many studies investigate the effect of MP by e.g. histological studies, the implementation of an optical label is crucial. However, commercial suppliers often do not provide much information about the dopants or labels are introduced by solution swelling, which not only results in unknown dopant concentration but can also change the properties of the material [221]. Therefore, in this study, fluorophores (i.e., DPA and perylene) and UCNPs were investigated as optical labels for microplastics. In order to identify the optimal conditions for fluorophores, the two candidates DPA and perylene were compared in terms of their absorption and emission, brightness, doping ratio and photostability. Based on the narrower absorption and emission bands, DPA was chosen to avoid an excitation at a different channel in the fluorescent microscope. UCNP, are a discussed as an alternative for fluorophores as they do not show

photobleaching [154,155] and allow for deep tissue imaging based on the NIR excitation [157–159]. Both labels were successfully embedded in a PS matrix and showed strong luminescent signals. Given the influence of the shape of the MP on the organism [135], it is a problem that most studies only work with commercially available round particles [135,160–162]. Therefore, one goal in this field is to produce microplastics that resemble those found in the environment, which is typically done using top-down approaches such as ball milling [168]. MP produced from PS was reported in a size range 5 µm to 200 µm with various production techniques and manufacturing times [160,167,171,172].

To reduce particle size and simplify production, NFs could be a good precursor as many polymers (e.g. PS, PMMA or PET) which could be found as microplastics in the environment, have been already been produced by electrospinning [99,134,181,182]. Since most studies investigating the toxicity of MPs are using PS [135], this polymer was chosen as a model substrate. The produced NFs were investigated by SEM and the homogenous distribution of the optical labels were confirmed by fluorescence microscopy. This verified that both particles and molecules can be used to stain PS-NFs without interfering with the electrospinning process. Furthermore, the stable embedding was proven by a leaching study, where only minimal loss of both DPA (0.0023 wt%) and UCNPs (0.2 wt%) was seen. Therefore, no unspecific binding of the dye to other cell organelles is expected and also the lanthanide or fluorides concentration are below critical concentrations [194–197]. In conclusion, both optical labels can be used for staining PS.

Subsequently, different methods to produce MP form the NFs were investigated, such as ball milling, cryo-milling, or grinding in solution with an UT to tailor the shape of the MP particles. In general, the particles produced by milling are irregular fragments with a rough surface. Cryo-Milling resulted in large fragments with a high standard deviation. Here, due to cooling of the milling system, refilling the vessel was not feasible. Further optimization is needed to benefit from the cooling. The best results could be obtained by ball milling, where the milling protocol and the chosen ball size play a key role. With a size of (4 ± 3) µm, these particles are in the smallest size range reported so far, do not require cryo-cooling, wet grinding media, and can be prepared in only about 2 h.

Fibrous MP, on the other hand, could be produced using an UT. With this, the structure of the fibers could be preserved while cutting them in smaller fragments. However, further studies are needed as the current particles are too long to be of biological interest. Longer shredding times, more efficient cooling or higher speeds should be investigated in the future.

Based on the interesting size of the particles produced by BM, which is similar to erythrocytes that can get stuck in mouse kidneys [176], DPA-labeled MP were applied to the MIPK model, followed by a histological study. Here, the good detectability in the stained tissue could be demonstrated. Furthermore, the particles stuck in smaller renal vessels and capillaries, which can impact on the kidney function and should be investigated further

This study demonstrated the principle of using NFs as MP precursors with optional doping of optical labels. Therefore, future studies should focus on investigating the effects on cells, tissues, or whole organisms and compare the results with spherical particles to investigate the effect of

particle shape. In addition, different types of plastics can be studied in the same way, which could provide insight into material effects. Here, currently a Master student is applying this model on poly (methyl methacrylate).
For multiplexing, UCNPs can be particularly beneficial because their emission can be tuned based on their lanthanide doping while keeping the excitation wavelength constant. They can therefore be used to color code, for example, different shapes, types or sizes of MPs. Finally, with a UCNPs doping MP can be quantified, which has not yet been achieved in a reliable manner [222]. As Yttrium or Ytterbium can be sensitively quantified by ICP-OES [223] and doping ratio is known, the mass of MP can be calculated from the amount of UNCPs found. An ongoing study is investigating the distribution of MP in mice. This can be used to better understand the uptake of MP and distribution mechanims, to identify tissues of higher risks, and to select cell lines of interest for cell culture experiments. However, at the time of submission of this thesis, the results have not been finalized, whereas this study could not be implemented in this thesis.

In summary, the work presented in this thesis underscores the significant potential of NFs in various fields ranging from biomedical applications to environmental science. Their ease of fabrication and modification makes them an interesting tool for future innovations. With continues research, NFs will undoubtedly play a key role in advancing scientific research and practical applications.

7 Summary

This thesis focuses on the development and use of nanofibers (NFs), highlighting their benefits such as simple production by electrospinning, their large surface-to-volume ratio and the possibility of chemical modifications. These properties make NFs suitable for various applications, including biosensors, medical devices, and environmental uses.

Point-of-care (POC) testing is an important tool in resource-limited settings aiming to meet the requirements of the WHO for being inexpensive, portable but still sensitive and reliable. Compared to common tests, nucleic acid testing (NAT) can enhance sensitivity and specificity significantly but involves multiple steps like nucleic acid (NA) extraction, amplification, and detection, necessitating new POC solutions. Therefore, different materials like particles and membranes developed for NA extraction and their integration in sample-to-answer (S2A) devices were reviewed. While emerging materials offer interesting solutions for example the protection of RNA or mild elution conditions, integration in S2A devices and automation especially in resource limited settings is a remaining challenge. Future work needs to address the integration of sample lysis, especially for complex matrices like whole blood, reduction of user-input and storage of on paper-based devices. With isothermal amplification methods and portable, battery-powered devices, NAT testing is expected to become a standard technique in the field of POC.

In this thesis zwitterionic NFs were developed to allow the extraction of NA under mild conditions. Based on an initial material study, hydrophilic nylon NFs were electrospun and doped with one cationic and one anionic polymer. An in-depth material study revealed an influence of the chemical composition and the morphology of the NFs, which need to be controlled during production. After optimization, NAs could be successfully adsorbed at a pH of 4.5 in the presence of 0.1 % Tween20 by electrostatic interactions. Elution was then triggered by a change to pH 10 and the addition of 50 mM sodium chloride, as NAs are electrostatically repulsed from the anionic NFs. The addition of high salt concentrations or charged detergents typically needed for the elution used from cationic materials was avoided.

Further research focused on the isolation form NA from biological samples like serum. A dilution of 1:150 allowed successful extraction, but further improvements are needed to enhance efficiency. Increasing the number of cationic binding sites by adjusting the doping ratio or adsorption pH showed potential for optimization. To achieve a sample-to-answer (S2A) device, NFs were integrated into a paper-based analytical device (µPAD). Within this flow-through set-up a good extraction efficiency could be maintained. Finally, recombinase polymerase amplification (RPA) was tested on filter paper as an isothermal amplification method. Future studies should combine the extraction of NAs from serum samples within the µPAD design and the amplification via RPA within one-test design to achieve a S2A device.

Microplastics (MPs) are present in the environment and human body, but their effects on organisms are still unknown. Current research focuses on investigating MP at the cellular level and within whole organisms and organs. However, commonly used commercial spherical particles do not represent the irregular fragments and fibrous particles found in the environment. This study aimed to produce true-to-life MP using NFs as a precursor.

They have a great potential as a one-dimensional nanomaterial and the ease of introducing several types of dopants. The shape of the particles can be adjusted depending on the production techniques. With ball milling irregular particles around 4 µm were obtained, while fibrous particles shredded with an Ultraturrax resulted in a length of 20 µm and must be further optimized.

As optical labels are often required in histological studies, DPA and UCNPs were successfully embedded in the NFs during electrospinning. A homogenous distribution and low leaching rates ensured the suitability of those optical labels. DPA labeled MP was then investigated with the *ex vivo* mouse isolated perfused kidney model, revealing a selective detection of the MPs within the tissue. As particles got stuck in smaller renal vessels and glomerular capillaries, future studies must focus on the impact of the shape of the MP. Based on those results, these systems can be further applied in biological assays, including cell, animal, or tissue studies and expanded towards different types of polymers as well.

8 Zusammenfassung

Die vorliegende Arbeit befasst sich mit der Entwicklung und der Anwendung von Nanofasern (NF), wobei ihre Vorteile wie die einfache Herstellung durch Elektrospinnen, ihr großes Oberflächen-Volumen-Verhältnis und die Möglichkeit der chemischen Modifizierung hervorzuheben sind. Aufgrund dieser Eigenschaften eignen sich NFs für verschiedene Bereiche, wie Biosensoren, medizinische Anwendungen und Umweltanalytik.

Point-of-Care (POC) Tests sind eine wichtige Methode in ressourcenbeschränkten Umgebungen, um die Anforderungen der WHO zu erfüllen, d. h. kostengünstig, portabel und dennoch sensitiv und zuverlässig zu sein. Im Vergleich zu herkömmlichen antikörperbasierten Tests, können über den Nachweis von Nukleinsäuren (NAT) die Messempfindlichkeit und Spezifität erheblich verbessern, erfordern jedoch mehrere Schritte wie die Extraktion der Nukleinsäure (NA), die Amplifikation und den Nachweis, was neue Lösungen für den POC-Bereich erforderlich macht. Daher wurden verschiedene für die NA-Extraktion entwickelte Materialien und ihre Integration in *sample-to-answer* (S2A) Geräte verglichen. Neu entwickelte Materialen bieten interessante Eigenschaften, wie zum Beispiel den Schutz von RNA vor Nukleasen oder milde Elutionsbedingungen, jedoch stellt deren Integration in S2A Test und deren Automatisierung eine Herausforderung dar. Künftige Arbeiten sollten sich mit der Integration des Probenausschlusses im Test-Design befassen, was insbesondere für komplexere Proben wie Vollblut relevant ist. Zudem müssen die Lagerbedingungen und Haltbarkeit von Tests untersucht werden und die Handhabung der Tests verbessert werden. Durch die Verwendung von isothermen Amplifizierungsmethoden, kann auf tragbare und batteriebetriebene Geräte zurückgegriffen werden. Aus diesem Grund wird erwartet, dass sich NAT-Tests in Zukunft zu einer Standard Diagnosemethode entwickeln wird.

In dieser Arbeit wurden daher zwitterionische NFs für die Extraktion von NA unter milden Bedingungen entwickelt. Auf Basis einer Materialstudie wurden hydrophile Nylon-NFs elektrogesponnen, die mit einem kationischen und einem anionischen Polymer dotiert waren. Aufgrund der Ergebnisse dieser Materialstudie müssen die chemische Zusammensetzung und die Morphologie der NFs streng kontrolliert werden. Nach Optimierung konnten die NAs bei einem pH-Wert von 4,5 in Anwesenheit von 0,1 % Tween20 durch elektrostatische Wechselwirkungen erfolgreich adsorbiert werden. Die Elution wurde dann durch eine Änderung des pH-Werts auf 10 und die Zugabe von 50 mM Natriumchlorid ausgelöst, da so die NAs elektrostatisch von den anionischen NFs abgestoßen werden. Damit konnte eine Zugabe von hohen Salzkonzentrationen oder geladenen Detergenzien, die normalerweise für die Elution von kationischen Materialien benötigt werden, vermieden werden.

Des Weiteren sollten NA aus biologischen Proben wie Serum isoliert werden. Eine Verdünnung von 1:150 ermöglichte eine erfolgreiche Extraktion, jedoch musste die Effizienz verbessert werden. Sowohl die Erhöhung der Anzahl der kationischen Bindungsstellen durch Anpassung des Dotierungsverhältnisses oder das Herabsetzen des Adsorptions-pH-Wertes zeigte Optimierungspotenzial. Für die Entwicklung eines S2A-Tests, wurden NFs in ein Mikrofluidik-Analysegerät auf Papierbasis (µPAD) integriert. Die gute Extraktionseffizienz der NFs konnte auch im Test Design nachgewiesen werden. Schließlich wurde die Rekombinase-Polymerase-Amplifikation (RPA) auf Filterpapier als isotherme Amplifikationsmethode getestet. Für die Fertigstellung des S2A-Tests, sollten zukünftige Studien die Extraktion von NAs aus Serumproben im µPAD-Design mit der Amplifikation mittels RPA kombinieren.

Mikroplastik (MP) ist in der Umwelt und im menschlichen Körper verbreitet, aber dessen Auswirkungen auf Organismen sind noch unbekannt. Die aktuelle Forschung konzentriert sich auf die Untersuchung von Mikroplastik auf zellulärer Ebene und im ganzen Organismen, sowie einzelnen Organen. Üblicherweise werden kugelförmigen Partikel verwendet, jedoch repräsentieren diese nicht die in der Umwelt vorkommenden unregelmäßigen Fragmente und faserigen Partikel. Ziel dieser Studie war die Herstellung von naturgetreuem MP unter Verwendung von NFs Ausgangsmaterial.
Diese haben als eindimensionales Nanomaterial großes Potenzial und lassen sich leicht mit verschiedenen Arten von Dotierstoffen modifizieren. Die Form der Partikel kann je nach Herstellungsverfahren angepasst werden. Durch das Vermahlen mit Kugelmühlen wurden unregelmäßige Partikel von etwa 4 µm produziert. Durch die Zerkleinerung mit einem Ultraturrax konnten fasrige Partikel gewonnen werden, deren Länge von 20 µm jedoch für eine biologische Anwendung zu groß ist.
Da in histologischen Studien häufig optische Markierungen erforderlich sind, wurden DPA und UCNPs während des Elektrospinnens erfolgreich in die NFs eingebettet. Die Eignung dieser optischen Marker konnte durch die homogene Verteilung in den Fasern und die geringe Auslaugung bewiesen werden. Das mit DPA markierte MP wurde dann in einem *ex vivo* Modell von isolierten, perfundierten Nieren der Maus untersucht, wobei das MP selektiv im Gewebe angeregt werden konnte. Da die Partikel in kleineren Nierengefäßen und glomerulären Kapillaren stecken blieben, müssen sich künftige Studien auf den Einfluss der Form des MP konzentrieren. Auf der Grundlage dieser Ergebnisse kann dieses System für weitere Anwendungen in biologischen Bereichen, einschließlich Zell-, Tier- oder Gewebestudien, eingesetzt und auch auf andere Arten von Polymeren ausgedehnt werden.

References

[1] M. N. Emaus, M. Varona, D. R. Eitzmann, S.-A. Hsieh, V. R. Zeger, J. L. Anderson, *TrAC, Trends Anal. Chem.* **2020**, *130*, 115985.
[2] Z. Li, Y. Bai, M. You, J. Hu, C. Yao, L. Cao, F. Xu, *Biosens. Bioelectron.* **2021**, *177*, 112952.
[3] R. Paul, E. Ostermann, Q. Wei, *Biosens. Bioelectron.* **2020**, *169*, 112592.
[4] F. Yang, G. Wang, W. Xu, N. Hong, *J. Virol. Methods* **2017**, *247*, 61.
[5] B. Shi, Y. K. Shin, A. A. Hassanali, S. J. Singer, *J. Phys. Chem. B* **2015**, *119*, 11030.
[6] S. Bag, S. Rauwolf, S. P. Schwaminger, W. Wenzel, S. Berensmeier, *LANGMUIR* **2021**, *37*, 5902.
[7] P. E. Vandeventer, J. S. Lin, T. J. Zwang, A. Nadim, M. S. Johal, A. Niemz, *J. Phys. Chem. B* **2012**, *116*, 5661.
[8] A. S. Ezeuko, M. O. Ojemaye, O. O. Okoh, A. I. Okoh, *Journal of Cleaner Production* **2022**, *381*, 135157.
[9] D. R. Eitzmann, M. Varona, J. L. Anderson, *Anal. Chem,* **2022**, *94*, 3677.
[10] O. Nacham, K. D. Clark, J. L. Anderson, *Anal. Chem.* **2016**, *88*, 7813.
[11] S.-E. Kim, M. van Tieu, S. Y. Hwang, M.-H. Lee, *Micromachines* **2020**, *11*, 302.
[12] H. Kettler, K. White, S. Hawkes, *Mapping the landscape of diagnostics for sexually transmitted infections: key findings and recommendations*, World Health Organization, Geneva **2004**.
[13] C.-W. Liu, H. Tsutsui, *SLAS Technology* **2023**, *28*, 302.
[14] N. Sritong, M. Sala de Medeiros, L. A. Basing, J. C. Linnes, *Lab Chip* **2023**, *23*, 888.
[15] Z. Li, X. Xu, D. Wang, X. Jiang, *TrAC, Trends Anal. Chem.* **2023**, *158*, 116871.
[16] J. Park, D. H. Han, J.-K. Park, *Lab Chip* **2020**, *20*, 1191.
[17] P. Jokela, A. E. Jääskeläinen, H. Jarva, T. Holma, M. J. Ahava, L. Mannonen, M. Lappalainen, S. Kurkela, R. Loginov, *Journal of clinical virology the official publication of the Pan American Society for Clinical Virology* **2020**, *131*, 104614.
[18] B. Koo, M. G. Kim, K. Lee, J. Y. Kim, S. Lee, S.-H. Kim, Y. Shin, *Sensors and Actuators B: Chemical* **2023**, *380*, 133382.
[19] R. Tang, M. Li, X. Yan, M. Xie, L. N. Liu, Z. Li, F. Xu, *Cellulose (London, England)* **2022**, *29*, 2479.
[20] K. Malpartida-Cardenas, J. Baum, A. Cunnington, P. Georgiou, J. Rodriguez-Manzano, *Analyst* **2023**, *148*, 3036.
[21] B. P. Sullivan, A. T. Bender, D. N. Ngyuen, J. Y. Zhang, J. D. Posner, *J. Chromatogr., B: Anal. Technol. Biomed. Life Sci.* **2021**, *1163*, 122494.
[22] L. Chen, J. M. Cabot, B. Paull, *Lab Chip* **2021**, *21*, 2565.
[23] A. T. Bender, B. P. Sullivan, J. Y. Zhang, D. C. Juergens, L. Lillis, D. S. Boyle, J. D. Posner, *Analyst* **2021**, *146*, 2851.
[24] S. Mirna Lorena, P. C. Cynthia, A. R. Maria Isabela, V. M. Pamela, R. H. Gabriela, B. Jorge, G. Mariano, *Sep. Purif. Rev.* **2023**, *52*, 193.
[25] Y. Duan, X. Zhang, Y. Li, X. Zhao, X. Zhao, L. Chen, C. Shi, C. Ma, X. Wang, *J. Pharm. Biomed. Anal.* **2023**, *224*, 115190.
[26] A. Jagannath, Y. Li, H. Cong, J. Hassan, G. Gonzalez, W. Wang, N. Zhang, M. D. Gilchrist, *ACS Appl. Mater. Interfaces* **2023**, *15*, 31159.
[27] X. Wang, C. Yan, X. Wang, X. Zhao, C. Shi, C. Ma, *Anal. Bioanal. Chem.* **2020**, *412*, 6927.
[28] S. Soltani, N. Khanian, T. S. Y. Choong, U. Rashid, *New J. Chem.* **2020**, *44*, 9581.
[29] W. Q. Brandão, J. C. Medina-Llamas, J. J. Alcaraz-Espinoza, A. E. Chávez-Guajardo, C. P. de Melo, *RSC Adv.* **2016**, *6*, 104566.
[30] A. J. Wieberneit, N. Wongkaew, A. J. Baeumner, *Adv. Mater. Interfaces* **2024**.

[31] J. Xu, J. Wang, Y. Wan, P. Cheng, Y. Geng, M. Xia, L. Zheng, Y. Tan, K. Liu, D. Wang, *Adv. Mater. Interfaces* **2022**, *9*, 2200613.
[32] T.-C. Ho, C.-C. Chang, H.-P. Chan, T.-W. Chung, C.-W. Shu, K.-P. Chuang, T.-H. Duh, M.-H. Yang, Y.-C. Tyan, *Molecules* **2022**, *27*.
[33] R. Tang, X. Yan, J. Hu, Y. Luo, J. P. Giesy, Y. Xie, H. Yin, *Cellulose* **2024**, *31*, 5115.
[34] A. Salazar, F. M. Ochoa-Corona, J. L. Talley, B. H. Noden, *Acta Trop.* **2022**, *225*, 106201.
[35] J.-H. Kang, Y. T. Kim, K. Lee, H.-M. Kim, K. G. Lee, J. Ahn, J. Lee, S. J. Lee, K.-B. Kim, *Nanoscale* **2020**, *12*, 5048.
[36] N. Ali, R. d. C. P. Rampazzo, A. D. T. Costa, M. A. Krieger, *Biomed. Res. Int.* **2017**, *2017*, 9306564.
[37] S. Berensmeier, *Appl. Microbio.l Biotechnol.* **2006**, *73*, 495.
[38] N. Capriotti, L. C. Amorós Morales, E. de Sousa, L. Juncal, M. L. Pidre, L. Traverso, M. F. López, M. L. Ferelli, G. Lavorato, C. Lillo, O. Vazquez Robaina, N. Mele, C. Vericat, P. Schilardi, A. F. Cabrera, S. Stewart, M. H. Fonticelli, P. Mendoza Zéliz, S. Ons, V. Romanowski, C. Rodríguez Torres, *Heliyon* **2024**, *10*, e25377.
[39] A. Szymczyk, M. Drozd, A. Kamińska, M. Matczuk, M. Trzaskowski, M. Mazurkiewicz-Pawlicka, R. Ziółkowski, E. Malinowska, *Int. J. Mol. Sci.* **2022**, *23*.
[40] H. Yue, J. M. Shin, T. Tegafaw, H. S. Han, K.-S. Chae, Y. Chang, G. H. Lee, *J. Nanopart. Res.* **2020**, *22*.
[41] M. Bae, J. Park, H. Seong, H. Lee, W. Choi, J. Noh, W. Kim, S. Shin, *Diagnostics* **2022**, *12*, 1995.
[42] G. Ramos-Mandujano, R. Salunke, S. Mfarrej, A. T. Rachmadi, S. Hala, J. Xu, F. S. Alofi, A. Khogeer, A. M. Hashem, N. A. M. Almontashiri, A. Alsomali, D. B. Shinde, S. Hamdan, P.-Y. Hong, A. Pain, M. Li, *Global chall.* **2021**, *5*, 2000068.
[43] S. Bowman, P. Roffey, D. McNevin, M. E. Gahan, *Aust. J. Forensic Sci.* **2016**, *48*, 407.
[44] T. H. Ali, A. M. Mandal, T. Heidelberg, R. S. D. Hussen, *RSC Adv.* **2022**, *12*, 13566.
[45] S. Tripathy, A. K. Chalana, A. Talukdar, P. V. Rajesh, A. Saha, G. Pramanik, S. Ghosh, *Analyst* **2021**, *147*, 165.
[46] C. P. Raptopoulou, *Materials* **2021**, *14*, 310.
[47] Y. Sun, H. Yu, S. Han, R. Ran, Y. Yang, Y. Tang, Y. Wang, W. Zhang, H. Tang, B. Fu, B. Fu, X. Weng, S.-M. Liu, H. Deng, S. Peng, X. Zhou, *Natl. Sci. Rev.* **2024**, *11*, nwae022.
[48] W. Pan, X. Wang, X. Ma, Y. Chu, S. Pang, Y. Chen, X. Guan, B. Zou, Y. Wu, G. Zhou, *ACS Appl. Mater. Interfaces* **2021**, *13*, 50309.
[49] N. Nasirpour, M. Mohammadpourfard, S. Zeinali Heris, *Chem. Eng. Res. Des.* **2020**, *160*, 264.
[50] H. Tateishi-Karimata, N. Sugimoto, *Biophys. Rev.* **2018**, *10*, 931.
[51] S. Paul, H. Moon, *Biomicrofluidics* **2021**, *15*, 34110.
[52] R. Carapito, S. C. Bernardo, M. M. Pereira, M. C. Neves, M. G. Freire, F. Sousa, *Sep. Purif. Technol.* **2023**, *315*, 123676.
[53] P. Pereira, A. Q. Pedro, M. C. Neves, J. C. Martins, I. Rodrigues, M. G. Freire, F. Sousa, *Life* **2021**, *11*.
[54] J. S. Park, N.-I. Goo, D.-E. Kim, *LANGMUIR* **2014**, *30*, 12587.
[55] T. Paul, P. Mohapatra, P. P. Mishra, *Appl. Surf. Sci.* **2022**, *577*, 151696.
[56] W. Y. Cui, H. J. Yoo, Y. G. Li, C. Baek, J. Min, *Biosens. Bioelectron.* **2022**, *199*, 113878.
[57] P. Thawornpan, S. Thanapongpichat, A. W. Tun, W. Jumpathong, L. de Jong, H. Buncherd, *Anal. Lett.* **2021**, *54*, 2037.
[58] T. H. Le Thang, W. Han, J. Shin, J. H. Shin, *Sens. Actuators, B* **2023**, *375*, 132948.

[59] P. Garneret, E. Coz, E. Martin, J.-C. Manuguerra, E. Brient-Litzler, V. Enouf, D. F. González Obando, J.-C. Olivo-Marin, F. Monti, S. van der Werf, J. Vanhomwegen, P. Tabeling, *PLOS ONE* **2021**, *16*, e0243712.
[60] J. Mei, D. Wang, Y. Zhang, D. Wu, J. Cui, M. Gan, P. Liu, *Adv. Sci.* **2023**, *10*, e2205217.
[61] K. Sun, X. Yang, Y. Wang, Q. Guan, W. Fu, C. Zhang, Q. Liu, W. An, Y. Zhao, W. Xing, D. Xu, *Microbiology spectrum* **2023**, *11*, e0517022.
[62] G. Miao, M. Guo, K. Li, X. Ye, M. G. Mauk, S. Ge, N. Xia, D. Yu, X. Qiu, *Chemosensors* **2022**, *10*, 271.
[63] Y. Shang, G. Xing, H. Lin, Y. Sun, S. Chen, J.-M. Lin, *Food Control* **2024**, *155*, 110047.
[64] W. Ouyang, J. Han, *Angewandte Chemie International Edition* **2020**, *59*, 10981.
[65] K. Dust, A. Hedley, K. Nichol, D. Stein, H. Adam, J. A. Karlowsky, J. Bullard, P. van Caeseele, D. C. Alexander, *J. Virol. Methods* **2020**, *285*, 113970.
[66] J. A. Lieberman, G. Pepper, S. N. Naccache, M.-L. Huang, K. R. Jerome, A. L. Greninger, *J. Clin. Microbiol.* **2020**, *58*.
[67] N. Kovačević, *Sample Preparation Techniques for Soil, Plant, and Animal Samples* **2016**.
[68] R. N. Deraney, L. Schneider, A. Tripathi, *Analyst* **2020**, *145*, 2412.
[69] C. H. Kim, J. Park, S. J. Kim, D.-H. Ko, S. H. Lee, S. J. Lee, J.-K. Park, M.-K. Lee, *Sens. Actuators, B* **2020**, *320*, 128346.
[70] S. I. Pearlman, M. Leelawong, K. A. Richardson, N. M. Adams, P. K. Russ, M. E. Pask, A. E. Wolfe, C. Wessely, F. R. Haselton, *ACS applied materials & interfaces* **2020**, *12*, 12457.
[71] S. Lu, Y. Yang, S. Cui, A. Li, C. Qian, X. Li, *Biosensors* **2024**, *14*.
[72] I. Seder, D.-M. Kim, S.-H. Hwang, H. Sung, D.-E. Kim, S.-J. Kim, *Sensors and Actuators B: Chemical* **2021**, *349*, 130788.
[73] D. Zhang, R. Gao, S. Huang, Y. Huang, J. Zhang, X. Su, S. Zhang, S. Ge, J. Zhang, N. Xia, *Sensors and Actuators B: Chemical* **2023**, *390*, 133939.
[74] D. Xu, X. Jiang, T. Zou, G. Miao, Q. Fu, F. Xiang, L. Feng, X. Ye, L. Zhang, X. Qiu, *Microfluid. Nanofluid.* **2022**, *26*, 69.
[75] S. Hu, Y. Jie, K. Jin, Y. Zhang, T. Guo, Q. Huang, Q. Mei, F. Ma, H. Ma, *Biosensors* **2022**, *12*, 324.
[76] J. Yin, Z. Zou, Z. Hu, S. Zhang, F. Zhang, B. Wang, S. Lv, Y. Mu, *Lab Chip* **2020**, *20*, 979.
[77] H. Huang, D. Long, Y. Lin, C. Dong, W. Huang, M. Zhang, L. Wan, H. Gou, T. Chen, F. Li, *Journal of clinical virology the official publication of the Pan American Society for Clinical Virology* **2024**, *173*, 105688.
[78] Y. Fang, Y. Wang, L. Zhu, H. Liu, X. Su, Y. Liu, Z. Chen, H. Chen, N. He, *Chinese Chemical Letters* **2023**, *34*, 108092.
[79] D. E. Gaddes, P.-W. Lee, A. Y. Trick, P. Athamanolap, C. M. O'Keefe, C. Puleo, K. Hsieh, T.-H. Wang, *Analytical chemistry* **2020**, *92*, 13254.
[80] A. Y. Trick, H. T. Ngo, A. H. Nambiar, M. M. Morakis, F.-E. Chen, L. Chen, K. Hsieh, T.-H. Wang, *Lab Chip* **2022**, *22*, 945.
[81] Z. Li, S. Zhang, J. Zhang, L. Avery, D. Banach, H. Zhao, C. Liu, *Advanced Science* **2024**, *11*, e2310066.
[82] Y. Peng, R. Hu, S. Xue, Y. He, L. Tian, Z. Pang, Y. He, Y. Dong, Y. Shi, S. Wang, B. Hong, K. Liu, R. Wang, L. Song, H. Fan, M. Li, Y. Tong, *Analytica chimica acta* **2024**, *1311*, 342720.
[83] Y. Huang, Z. Gao, C. Ma, Y. Sun, Y. Huang, C. Jia, J. Zhao, S. Feng, *Analyst* **2023**, *148*, 2758.

[84] P. Changtor, P. Rodriguez-Mateos, K. Buddhachat, W. Wattanachaiyingcharoen, A. Iles, S. Kerdphon, N. Yimtragool, N. Pamme, *Biosensors & bioelectronics* **2024**, *250*, 116051.
[85] P. Rodriguez-Mateos, B. Ngamsom, C. Walter, C. E. Dyer, J. Gitaka, A. Iles, N. Pamme, *Analytica chimica acta* **2021**, *1177*, 338758.
[86] N. Zhang, C. Yue, X. Zhan, Z. Cheng, C. Li, Y. Du, F. Tian, *Anal Bioanal Chem* **2023**, *415*, 6561.
[87] A. Y. Trick, J. H. Melendez, F.-E. Chen, L. Chen, A. Onzia, A. Zawedde, E. Nakku-Joloba, P. Kyambadde, E. Mande, J. Matovu, M. Atuheirwe, R. Kwizera, E. A. Gilliams, Y.-H. Hsieh, C. A. Gaydos, Y. C. Manabe, M. M. Hamill, T.-H. Wang, *Science translational medicine* **2021**, *13*.
[88] T. Peng, L. Dong, X. Feng, Y. Yang, X. Wang, C. Niu, Z. Liang, W. Qu, Q. Zou, X. Dai, M. Li, X. Fang, *Talanta* **2023**, *258*, 124462.
[89] A. Niemz, T. M. Ferguson, D. S. Boyle, *Trends Biotechnol.* **2011**, *29*, 240.
[90] T. J. Moehling, G. Choi, L. C. Dugan, M. Salit, R. J. Meagher, *Expert Rev. Mol. Diagn.* **2021**, *21*, 43.
[91] J. R. Choi, R. Tang, S. Wang, W. A. B. Wan Abas, B. Pingguan-Murphy, F. Xu, *Biosens. Bioelectron.* **2015**, *74*, 427.
[92] Y. Liu, L. Zhan, Z. Qin, J. Sackrison, J. C. Bischof, *ACS nano* **2021**, *15*, 3593.
[93] P. P. Nelson, B. A. Rath, P. C. Fragkou, E. Antalis, S. Tsiodras, C. Skevaki, *Front. Cell. Infect.* **2020**, *10*, 181.
[94] T. He, J. Li, L. Liu, S. Ge, M. Yan, H. Liu, J. Yu, *RSC Adv.* **2020**, *10*, 25808.
[95] M. A. Dineva, L. MahiLum-Tapay, H. Lee, *Analyst* **2007**, *132*, 1193.
[96] X. Wang, L. Xing, Y. Shu, X. Chen, J. Wang, *Anal. Chim. Acta.* **2014**, *837*, 64.
[97] S. Agarwal, A. Greiner, J. H. Wendorff, *Prog. Polym. Sci.* **2013**, *38*, 963.
[98] L. Persano, A. Camposeo, C. Tekmen, D. Pisignano, *Macromol. Mater. Eng.* **2013**, *298*, 504.
[99] J. Xue, T. Wu, Y. Dai, Y. Xia, *Chem. Rev.* **2019**, *119*, 5298.
[100] N. Aliheidari, N. Aliahmad, M. Agarwal, H. Dalir, *Sensors* **2019**, *19*.
[101] S. Chigome, G. Darko, N. Torto, *Analyst* **2011**, *136*, 2879.
[102] J. Płotka-Wasylka, N. Szczepańska, M. de La Guardia, J. Namieśnik, *TrAC, Trends Anal. Chem.* **2016**, *77*, 23.
[103] E. M. Reyes-Gallardo, R. Lucena, S. Cárdenas, *TrAC, Trends Anal. Chem.* **2016**, *84*, 3.
[104] L. Matlock-Colangelo, N. W. Colangelo, C. Fenzl, M. W. Frey, A. J. Baeumner, *Sensors* **2016**, *16*.
[105] W. Q. Brandão, J. C. Medina-Llamas, J. J. Alcaraz-Espinoza, A. E. Chávez-Guajardo, C. P. de Melo, *RSC Adv.* **2016**, *6*, 104566.
[106] L. Zheng, H. S. Sundaram, Z. Wei, C. Li, Z. Yuan, *React. Funct. Polym.* **2017**, *118*, 51.
[107] L. D. Blackman, P. A. Gunatillake, P. Cass, K. E. S. Locock, *Chem. Soc. Rev.* **2019**, *48*, 757.
[108] A. R. Esfahani, Z. Zhang, Y. Y. L. Sip, L. Zhai, A. A. Sadmani, *J. Water Process Eng.* **2020**, *37*, 101438.
[109] A. Chunder, S. Sarkar, Y. Yu, L. Zhai, *Colloids Surf. B Biointerfaces* **2007**, *58*, 172.
[110] D. W. Fox, D.-X. Antony, Y. Y. L. Sip, J. Fnu, A. Rahmani, T. Jurca, L. Zhai, *Mater. Today Commun.* **2022**, *33*, 104535.
[111] X. Wang, B. Ding, G. Sun, M. Wang, J. Yu, *Prog. Mater. Sci.* **2013**, *58*, 1173.
[112] N. Hussain, S. Ullah, M. N. Sarwar, M. Hashmi, M. Khatri, T. Yamaguchi, Z. Khatri, I. S. Kim, *Fibers Polym.* **2020**, *21*, 2780.
[113] S. Kundu, R. S. Gill, R. F. Saraf, *J. Phys. Chem. C* **2011**, *115*, 15845.

[114] B. Kim, H. Park, S.-H. Lee, W. M. Sigmund, *Mater. Lett.* **2005**, *59*, 829.
[115] M. Bandeira, B. S. Chee, R. Frassini, M. Nugent, M. Giovanela, M. Roesch-Ely, J. S. Da Crespo, D. M. Devine, *Materials* **2021**, *14*, 2889.
[116] X. Wang, B. Ding, G. Sun, M. Wang, J. Yu, *Prog. Mater. Sci.* **2013**, *58*, 1173.
[117] P. B. Gahan, *EPMA J.* **2010**, *1*, 503.
[118] M. Leeman, J. Choi, S. Hansson, M. U. Storm, L. Nilsson, *Anal. Bioanal. Chem.* **2018**, *410*, 4867.
[119] B. A. Newcomb, P. V. Gulgunje, Y. Liu, K. Gupta, M. G. Kamath, C. Pramanik, S. Ghoshal, H. G. Chae, S. Kumar, *Polym. Eng. Sci.* **2016**, *56*, 361.
[120] S. R. Shukla, A. M. Harad, D. Mahato, *J. Appl. Polym. Sci.* **2006**, *100*, 186.
[121] T. Ozer, C. McMahon, C. S. Henry, *Rev. Anal. Chem.* **2020**, *13*, 85.
[122] A. T. Singh, D. Lantigua, A. Meka, S. Taing, M. Pandher, G. Camci-Unal, *Sensors (Basel, Switzerland)* **2018**, *18*, 2838.
[123] Y. Chen, Y. Liu, Y. Shi, J. Ping, J. Wu, H. Chen, *TrAC, Trends Anal. Chem.* **2020**, *127*, 115912.
[124] M. Tan, C. Liao, L. Liang, X. Yi, Z. Zhou, G. Wei, *Front. cell. infect. microbiol.* **2022**, *12*, 1019071.
[125] E. A. Pumford, J. Lu, I. Spaczai, M. E. Prasetyo, E. M. Zheng, H. Zhang, D. T. Kamei, *Biosens. Bioelectron.* **2020**, *170*, 112674.
[126] Y. Bai, J. Ji, F. Ji, S. Wu, Y. Tian, B. Jin, Z. Li, *Talanta* **2022**, *240*, 123209.
[127] B. A. Rohrman, R. R. Richards-Kortum, *Lab Chip* **2012**, *12*, 3082.
[128] H. Ahn, B. S. Batule, Y. Seok, M.-G. Kim, *Anal. Chem.* **2018**, *90*, 10211.
[129] C. Schrader, A. Schielke, L. Ellerbroek, R. Johne, *J. Appl. Microbiol.* **2012**, *113*, 1014.
[130] B. N. Dickhaus, R. Priefer, *Colloids Surf. A* **2016**, *488*, 15.
[131] A. Salis, M. Boström, L. Medda, F. Cugia, B. Barse, D. F. Parsons, B. W. Ninham, M. Monduzzi, *LANGMUIR* **2011**, *27*, 11597.
[132] R. Geyer, J. R. Jambeck, K. L. Law, *Sci. Adv.* **2017**, *3*, e1700782.
[133] N. P. Ivleva, A. C. Wiesheu, R. Niessner, *Angewandte Chemie (International ed. in English)* **2017**, *56*, 1720.
[134] A. A. Koelmans, N. H. Mohamed Nor, E. Hermsen, M. Kooi, S. M. Mintenig, J. de France, *Water research* **2019**, *155*, 410.
[135] U. Rozman, G. Kalčíková, *J. Hazard. Mater.* **2022**, *424*, 127529.
[136] S. Kefer, O. Miesbauer, H.-C. Langowski, *Polymers* **2021**, *13*.
[137] A. Vdovchenko, M. Resmini, *International journal of molecular sciences* **2024**, *25*.
[138] R. W. Chia, J.-Y. Lee, J. Jang, H. Kim, K. D. Kwon, *J Soils Sediments* **2022**, *22*, 2690.
[139] B. Toussaint, B. Raffael, A. Angers-Loustau, D. Gilliland, V. Kestens, M. Petrillo, I. M. Rio-Echevarria, G. van den Eede, *Food Addit Contam Part A Chem Anal Control Expo Risk Assess* **2019**, *36*, 639.
[140] A. A. Mamun, T. A. E. Prasetya, I. R. Dewi, M. Ahmad, *Sci. Total Environ.* **2023**, *858*, 159834.
[141] H. A. Leslie, M. J. M. van Velzen, S. H. Brandsma, A. D. Vethaak, J. J. Garcia-Vallejo, M. H. Lamoree, *Environ. Int.* **2022**, *163*, 107199.
[142] P. Schwabl, S. Köppel, P. Königshofer, T. Bucsics, M. Trauner, T. Reiberger, B. Liebmann, *Ann. Intern. Med.* **2019**, *171*, 453.
[143] N. S. Roslan, Y. Y. Lee, Y. S. Ibrahim, S. Tuan Anuar, K. M. K. K. Yusof, L. A. Lai, T. Brentnall, *J. Glob. Health* **2024**, *14*, 4179.
[144] P. M. Anger, E. von der Esch, T. Baumann, M. Elsner, R. Niessner, N. P. Ivleva, *TrAC, Trends Anal. Chem.* **2018**, *109*, 214.
[145] W. Cowger, A. Gray, S. H. Christiansen, H. DeFrond, A. D. Deshpande, L. Hemabessiere, E. Lee, L. Mill, K. Munno, B. E. Ossmann, M. Pittroff, C. Rochman, G. Sarau, S. Tarby, S. Primpke, *Appl. Spectrosc.* **2020**, *74*, 989.

[146] D. Ho, S. Liu, H. Wei, K. G. Karthikeyan, *Microchem. J.* **2024**, *197*, 109708.
[147] E. G. Karakolis, B. Nguyen, J. B. You, C. M. Rochman, D. Sinton, *Environ. Sci. Technol. Lett.* **2019**, *6*, 334.
[148] P. Das, S. Ganguly, S. Margel, A. Gedanken, *LANGMUIR* **2021**, *37*, 3508.
[149] A. S. Keller, J. Jimenez-Martinez, D. M. Mitrano, *Environ. Sci. Technol.* **2020**, *54*, 911.
[150] Y. Liu, J. Li, B. V. Parakhonskiy, R. Hoogenboom, A. Skirtach, S. de Neve, *J. Hazard. Mater.* **2024**, *462*, 132785.
[151] N. Yakovenko, B. Amouroux, M. Albignac, F. Collin, C. Roux, A.-F. Mingotaud, P. Roblin, C. Coudret, A. ter Halle, *Environ. Sci.: Nano* **2022**, *9*, 2453.
[152] M. Al-Sid-Cheikh, S. J. Rowland, R. Kaegi, T. B. Henry, M.-A. Cormier, R. C. Thompson, *Commun. Mater.* **2020**, *1*.
[153] J. R. Lakowicz, *Principles of fluorescence spectroscopy*, Springer, New York, NY **2006**.
[154] A. P. Demchenko, *Methods Appl. Fluoresc.* **2020**, *8*, 22001.
[155] M. Bettinelli, L. Carlos, X. Liu, *Physics Today* **2015**, *68*, 38.
[156] F. Li, L. Tu, Y. Zhang, D. Huang, X. Liu, X. Zhang, J. Du, R. Fan, C. Yang, K. W. Krämer, J. Marques-Hueso, G. Chen, *Nat. Photon.* **2024**, *18*, 440.
[157] A. Douplik, G. Saiko, I. Schelkanova, V. V. Tuchin.
[158] P. N. Prasad, *Introduction to biophotonics*, Wiley-Interscience, Hoboken NJ **2003**.
[159] B. C. Wilson, S. L. Jacques, *IEEE J. Quantum Electron.* **1990**, *26*, 2186.
[160] L. Eitzen, S. Paul, U. Braun, K. Altmann, M. Jekel, A. S. Ruhl, *Environ. Res.* **2019**, *168*, 490.
[161] A. K. Sarkar, A. E. Rubin, I. Zucker, *Environ. Sci. Technol.* **2021**, *55*, 10491.
[162] D. Choi, J. Bang, T. Kim, Y. Oh, Y. Hwang, J. Hong, *J. Hazard. Mater.* **2020**, *400*, 123308.
[163] M. Cole, *Sci. Rep.* **2016**, *6*, 34519.
[164] A. Villacorta, C. Cazorla-Ares, V. Fuentes-Cebrian, I. H. Valido, L. Vela, F. Carrillo-Navarrete, M. Morataya-Reyes, K. Mejia-Carmona, S. Pastor, A. Velázquez, J. Arribas Arranz, R. Marcos, M. López-Mesas, A. Hernández, *J. Hazard. Mater.* **2024**, *476*, 135134.
[165] A. Arenas-Vivo, F. R. Beltrán, V. Alcázar, M. U. de La Orden, J. Martinez Urreaga, *Mater. Today Commun.* **2017**, *12*, 125.
[166] F. Bertelà, C. Battocchio, G. Iucci, S. Ceschin, D. Di Lernia, F. Mariani, A. Di Giulio, M. Muzzi, I. Venditti, *Polymers* **2023**, *15*.
[167] E. von der Esch, M. Lanzinger, A. J. Kohles, C. Schwaferts, J. Weisser, T. Hofmann, K. Glas, M. Elsner, N. P. Ivleva, *Front. Chem.* **2020**, *8*, 169.
[168] S. Kefer, O. Miesbauer, H.-C. Langowski, *Polymers* **2021**, *13*, 2881.
[169] S. Reynaud, A. Aynard, B. Grassl, J. Gigault, *Curr. Opin. Colloid Interface Sci.* **2022**, *57*, 101528.
[170] P. Heinrich, L. Hanslik, N. Kämmer, T. Braunbeck, *Environ Sci Pollut Res* **2020**, *27*, 22292.
[171] B. Hrovat, E. Uurasjärvi, M. Viitala, A. F. Del Pino, M. Mänttäri, N. Papamatthaiakis, A. Haapala, K. Peiponen, M. Roussey, A. Koistinen, *Sci. Total Environ.* **2024**, *925*, 171821.
[172] J. Schmidt, M. Plata, S. Tröger, W. Peukert, *Powder Technol.* **2012**, *228*, 84.
[173] X. Dong, X. Liu, Q. Hou, Z. Wang, *Sci. Total Environ.* **2023**, *855*, 158686.
[174] V. Stock, L. Böhmert, E. Lisicki, R. Block, J. Cara-Carmona, L. K. Pack, R. Selb, D. Lichtenstein, L. Voss, C. J. Henderson, E. Zabinsky, H. Sieg, A. Braeuning, A. Lampen, *Arch. Toxicol.* **2019**, *93*, 1817.
[175] H. Haller, K. de Groot, F. Bahlmann, M. Elger, D. Fliser, *Kidney Int.* **2005**, *68*, 1932.

[176] H.-J. Schurek, *A laboratory manual of kidney perfusion techniques*, MV Wissenschaft, Münster **2017**.
[177] F. Schweda, C. Wagner, B. K. Krämer, J. Schnermann, A. Kurtz, *Am. J. Physiol. Renal Physiol.* **2003**, *284*, F770-7.
[178] A. Schroter, S. Märkl, N. Weitzel, T. Hirsch, *Adv. Funct. Mater.* **2022**, *32*, 2113065.
[179] A. Dong, X. Ye, J. Chen, Y. Kang, T. Gordon, J. M. Kikkawa, C. B. Murray, *J. Am. Chem. Soc.* **2011**, *133*, 998.
[180] A. Haider, S. Haider, I.-K. Kang, *Arab. J. Chem.* **2018**, *11*, 1165.
[181] S. Piperno, L. Lozzi, R. Rastelli, M. Passacantando, S. Santucci, *Applied Surface Science* **2006**, *252*, 5583.
[182] Y. Ko, J. P. Hinestroza, T. Uyar, *ACS Appl. Polym. Mater.* **2023**, *5*, 7298.
[183] D. Ho, S. Liu, H. Wei, K. G. Karthikeyan, *Microchem. J.* **2024**, *197*, 109708.
[184] G. George, Z. Luo, *CNANO* **2020**, *16*, 321.
[185] M. Taniguchi, J. S. Lindsey, *Photochem. Photobiol.* **2018**, *94*, 290.
[186] L. Cheng, C. Wang, Z. Liu, *Nanoscale* **2013**, *5*, 23.
[187] A. Satpathy, T.-Y. Su, W.-T. Huang, R.-S. Liu, *J. Chin. Chem. Soc.* **2023**, *70*, 992.
[188] F. Wang, X. Liu, *J. Am. Chem. Soc.* **2008**, *130*, 5642.
[189] M. Buchner, U. Ngoensawat, M. Schenck, C. Fenzl, N. Wongkaew, L. Matlock-Colangelo, T. Hirsch, A. Duerkop, A. J. Baeumner, *J. Mater. Chem. C* **2017**, *5*, 9712.
[190] M. Haase, H. Schäfer, *Angew. Chem., Int. Ed.* **2011**, *50*, 5808.
[191] B. Chen, F. Wang, *Acc. Chem. Res.* **2020**, *53*, 358.
[192] L. M. Wiesholler, C. Genslein, A. Schroter, T. Hirsch, *Anal. Chem.* **2018**, *90*, 14247.
[193] V. Patravale, P. Dandekar, R. Jain, in *Nanoparticulate Drug Delivery*, Elsevier **2012**, p. 87.
[194] S. Hirano, K. T. Suzuki, *Environ. Health Perspect.* **1996**, *104 Suppl 1*, 85.
[195] V. Bastos, P. Oskoei, E. Andresen, M. I. Saleh, B. Rühle, U. Resch-Genger, H. Oliveira, *Sci. Rep.* **2022**, *12*, 3770.
[196] H. Oliveira, A. Bednarkiewicz, A. Falk, E. Fröhlich, D. Lisjak, A. Prina-Mello, S. Resch, C. Schimpel, I. V. Vrček, E. Wysokińska, H. H. Gorris, *Adv. Healthc. Mater.* **2019**, *8*, e1801233.
[197] S. Guth, S. Hüser, A. Roth, G. Degen, P. Diel, K. Edlund, G. Eisenbrand, K.-H. Engel, B. Epe, T. Grune, V. Heinz, T. Henle, H.-U. Humpf, H. Jäger, H.-G. Joost, S. E. Kulling, A. Lampen, A. Mally, R. Marchan, D. Marko, E. Mühle, M. A. Nitsche, E. Röhrdanz, R. Stadler, C. van Thriel, S. Vieths, R. F. Vogel, E. Wascher, C. Watzl, U. Nöthlings, J. G. Hengstler, *Arch. Toxicol.* **2020**, *94*, 1375.
[198] T. Rojac, M. Kosec, B. Malič, J. Holc, *J. Eur. Ceram. Soc.* **2006**, *26*, 3711.
[199] J. Rios, A. Restrepo, A. Zuleta, F. Bolívar, J. Castaño, E. Correa, F. Echeverria, *Metals* **2021**, *11*, 1621.
[200] A. F. Fuentes, L. Takacs, *J Mater Sci* **2013**, *48*, 598.
[201] Y. Deng, Y. Zhang, B. Lemos, H. Ren, *Sci. Rep.* **2017**, *7*, 46687.
[202] Y. Lu, Y. Zhang, Y. Deng, W. Jiang, Y. Zhao, J. Geng, L. Ding, H. Ren, *Environ. Sci. Technol.* **2016**, *50*, 4054.
[203] T. Luo, Y. Zhang, C. Wang, X. Wang, J. Zhou, M. Shen, Y. Zhao, Z. Fu, Y. Jin, *Environ. Pollut.* **2019**, *255*, 113122.
[204] X. Xie, T. Deng, J. Duan, J. Xie, J. Yuan, M. Chen, *Ecotoxicol. Environ. Saf.* **2020**, *190*, 110133.
[205] J. L. Shamshina, R. S. Stein, N. Abidi, *Green Chem.* **2021**, *23*, 9646.
[206] J. Chen, W. Wang, H. Liu, X. Xu, J. Xia, *Environ. Pollut. Bioavailab.* **2021**, *33*, 227.
[207] A. Tirkey, L. S. B. Upadhyay, *Mar. Pollut. Bull.* **2021**, *170*, 112604.
[208] J.-L. Xu, X. Lin, J. J. Wang, A. A. Gowen, *Sci. Total Environ.* **2022**, *851*, 158111.

[209] D. Choi, J. Bang, T. Kim, Y. Oh, Y. Hwang, J. Hong, *J. Hazard. Mater.* **2020**, *400*, 123308.
[210] P. M. Andrews, S. B. Bates, *Anat. Rec.* **1984**, *210*, 1.
[211] J. M. Austyn, S. Gordon, *Eur. J. Immunol.* **1981**, *11*, 805.
[212] L. Liu, G.-P. Shi, *Cardiovasc. Res.* **2012**, *94*, 3.
[213] Y. Hou, R. Qiao, F. Fang, X. Wang, C. Dong, K. Liu, C. Liu, Z. Liu, H. Lei, F. Wang, M. Gao, *ACS nano* **2013**, *7*, 330.
[214] R. S. Ajee, P. S. Roy, S. Dey, S. Sundaresan, *J Nanopart Res* **2024**, *26*, 1.
[215] M. Simsek, K. Hoecherl, M. Schlosser, A. J. Baeumner, N. Wongkaew, *ACS Appl. Mater. Interfaces* **2020**, *12*, 39533.
[216] S. N. Mobarez, N. Wongkaew, M. Simsek, A. J. Baeumner, A. Duerkop, *Chemosensors* **2020**, *8*, 99.
[217] N. Wongkaew, M. Simsek, J. Heider, J. Wegener, A. J. Baeumner, S. Schreml, J. A. Stolwijk, *ACS Appl. Bio Mater.* **2020**, *3*, 4912.
[218] Y. Bai, J. Ji, F. Ji, S. Wu, Y. Tian, B. Jin, Z. Li, *Talanta* **2022**, *240*, 123209.
[219] S. M. Lee, H. K. Balakrishnan, E. H. Doeven, D. Yuan, R. M. Guijt, *Biosens.* **2023**, *13*.
[220] T. Tian, Y. Bi, X. Xu, Z. Zhu, C. Yang, *Anal. Methods* **2018**, *10*, 3567.
[221] E. Kim, J. Lee, D. Kim, K. E. Lee, S. S. Han, N. Lim, J. Kang, C. G. Park, K. Kim, *Chem. Commun.* **2009**, https://pubs.rsc.org/en/content/articlelanding/2009/cc/b823110a.
[222] Y. Deng, Y. Zhang, B. Lemos, H. Ren, *Sci Rep* **2017**, *7*, 46687.
[223] B. Zawisza, K. Pytlakowska, B. Feist, M. Polowniak, A. Kita, R. Sitko, *J. Anal. At. Spectrom.* **2011**, *26*, 2373.

Curriculum Vitae

Personal Data

Name	Alissa Wieberneit
Address	Humboldtstr. 60a, 93053 Regensburg
E-Mail	wieberneit@outlook.de
Date of Birth	28.01.1997, Starnberg

Academical Education

01/2021 - 02/2025	**PhD. Studies** *University of Regensburg, Department of Analytical Chemistry, Chemo- and Biosensors* Topic: "Development of Nanofibers for Applications in the field of Point of Care and Environmental Studies"
10/2018 - 11/2020	**Studies of Chemistry (Master of Science)** *University of Regensburg, Department of Analytical Chemistry, Chemo- and Biosensors* Topic: "Nanofiber-Based Isolation of Nucleic Acids"
10/2015 - 09/2018	**Studies of Chemistry (Bachelor of Science)** *University of Regensburg, Department of Analytical Chemistry, Chemo- and Biosensors* Topic: "C14 "
09/2007 - 06/2015	**Advanced School-Leaving Certificate** *Christoph-Probst Gymnasium Gilching*

Professional Experience

01/2024	**Research Stay** *Fraunhofer Institute IZI-BB in Potsdam*
11/2022	**Research Stay** *KMUTT University in Bangkok, Thailand*
2020 - 2024	Supervision of Teaching Students in Demonstration Lectures
03/2020	**10. Spring School of Industrial Analytical Chemistry** *GdCh, Aalen*
10/2017 - 02/2020	**URA-Lab Regensburg, Hr. Dr. Robert Schupfner** Commissioned Analysis (Part Time Job, University of Regensburg)
09/2014	Trial Study of Chemistry at the TU Munich
07/2014	Student Internship at Roche Diagnostics GmbH in Penzberg
07/2012	Student Internship at Max Planck Institute in Munich in Biochemistry

Further Education and Training

06/2024	Workshop: Kontakte aufbauen und sich bekannt machen
05/2024	Workshop: Professional Communications
04/2024	NaWik course: Presentation and Media Skills
2022	Quality Management Course (final presentation in food safety)
06/2022	Workshop: Leadership cases
06/2022	Workshop: Leadership skills

Publication and Presentations

Publication

Wieberneit, A. J.; Wongkaew, N.; Baeumner, A. J. Novel Electrospun Zwitterionic Nanofibers for Point‐Of‐Care Nucleic Acid Isolation Strategies Under Mild Conditions. *Adv. Mater.Interfaces* **2024. DOI:** 10.1002/admi.202400329.

Presentations

Oral Presentations

- 2024, Pittcon, San Diego, USA
  "Zwitterionic Nanofibers for High-Performance in-Line Nucleic Acid Extraction in microfluidic Paper-Based Devices for Point-of-Care Applications"
- 2024, Analytica Conference, Munich, Germany, invited talk
  "Nucleic Acid Extraction Through Zwitterionic Nanofibers Integrated in Flow Through Micro-Paper-Based Devices"
- 2023, Life Science Seminar, Regensburg, Germany
  "Nanofibers for Bioanalytical Applications"

Poster Presentations

- 2021, 3rd European BioSensor Symposium, online at TH Wildau
  "Electrospun cationic nanofibers for nucleic acid extraction in paper-based analytical devices"
- 2022, Analytica Conference, Munich, Germany
  "Zwitterionic Nanofibers for Nucleic Acid Extraction in Paper-Based Analytical Devices"
- 2023, Anakon, Vienna, Austria
  "Zwitterionic Nanofibers for Nucleic Acid Extraction in Paper-Based Analytical Devices"

Science Communication

- 2024 March, FameLab regional heat, 1st place
  "Spinning-Man: Into the (Nano-)Fiber-Verse"
- 2024, April, NACHT SCHAFFT WISSEN 2024
  "Entwicklung von Nanofasern für medizinische Schnelltests"
- 2024 June, Uni goes Downtwon
  "Schnelltests 2.0: Den PCR-Test aufs Papier gebracht"
- 2024 June, FameLab Germany Finals, 2nd place
  "Spinning-Man: Into the (Nano-)Fiber-Verse"
- 2024 July, Tag der Chemie, University of Regensburg
  Initiation, organization, and co-host of the 1st ChemSlam